UNIVERSITÉ DU QUÉBEC

THÈSE PRÉSENTÉE À L'UNIVERSITÉ DU QUÉBEC À CHICOUTIMI COMME EXIGENCE PARTIELLE DU DOCTORAT EN INGÉNIERIE

PAR

LADAN FOROUGHI MOBARAKEH

DEVELOPMENT OF NANO-STRUCTURED ICEPHOBIC SURFACES BASED ON PLASMA POLYMERIZATION

DÉVELOPPEMENT DE SURFACES GLACIOPHOBES NANO-STRUCTURÉES BASÉ SUR LA POLYMÉRISATION PAR PLASMA

February 2014

ABSTRACT

Accumulated ice on exposed surfaces leads to operational difficulties and extensive maintenance for power transmission lines, antennas, aircraft, ships, and ground transportation vehicles.

In the present study, the low pressure plasma polymerized Hexamethyldisiloxane (PP-HMDSO) film is deposited on aluminum surfaces to create a superhydrophobic coating with icephobic properties. Prior to the deposition of this low surface energy coating, aluminum surfaces were anodized or immersed in boiling water to make micro/nano structured surfaces.

Plasma parameters were optimized in order to find the best optimum conditions for having high static contact angle and low contact angle hysteresis. Hence, the Grey-based Taguchi method was used as one of the Design of Experiment (DOE) techniques. The stability of coatings was studied under accelerated aging conditions such as UV degradation, immersion in distilled water and different pH solutions, and several icing/de-icing cycles. It was observed that the PP-HMDSO coatings are quite stable against UV exposure and immersion in distilled water. However, the icephobicity of the PP-HMDSO coating deposited on the anodized aluminum decreased after fifteen icing/de-icing cycles.

The stability of the developed coating was improved against several icing/de-icing cycles by increasing the deposition time of plasma polymerized coating from 15 to 25 minutes. The results showed that increasing the deposition time of plasma polymerization leads to decrease of the ice adhesion strength of coatings on anodized aluminum while it has no significant effect on the PP-HMDSO coating deposited on a water-treated aluminum surface. Finally, the superhydrophobic PP-HMDSO coating also provides anti-corrosion protection for the aluminum substrate.

RÉSUMÉ

L'accumulation de glace sur les surfaces exposées conduit à des difficultés opérationnelles et des efforts de maintenance élevés pour les lignes de transport d'électricité, les antennes, les avions, les bateaux et les véhicules de transport terrestre.

Dans ce travail, le dépôt de Hexaméthyldisiloxane polymérisé par plasma à basse pression (HMDSO-PP) a été réalisé pour créer des revêtements avec des propriétés superhydrophobes/glaciophobes sur la surface de l'aluminium. Avant de réaliser le revêtement à faible énergie de surface, les surfaces d'aluminium ont été anodisées ou immergées dans de l'eau bouillante pour produire des surfaces micro/nano structurées.

Les paramètres du plasma ont été optimisés pour trouver les conditions optimales afin d'obtenir un angle de contact élevé et une faible hystérésis de l'angle de contact. Pour ce faire, la méthode Taguchi-Grey, a été utilisée comme l'une des techniques de conception expérimentale (DOE). La stabilité des revêtements a également été étudiée dans des conditions de vieillissement accéléré tels que la dégradation par UV, l'immersion dans de l'eau distillée, et les solutions avec différents pH, et l'effet de plusieurs cycles de glaçage/de- glaçage. Les résultats obtenus ont montrés que les revêtements PP-HMDSO ont de bonnes stabilités après l'exposition aux rayons UV et après l'immersion dans de l'eau distillée. Toutefois, la propriété de glaciophobe du revêtement PP-HMDSO déposé sur l'aluminium anodisé a été diminuée après quinze cycles de glaçage/de- glaçage.

L'étude de l'effet du temps de dépôt de PP-HMDSO ont montré que l'augmentation du temps de dépôt conduit à une diminution de la force d'adhérence de la glace sur un revêtement de PP-HMDSO déposé sur l'aluminium anodisé alors qu'il n'a pas d'effet significatif sur le revêtement PP-HMDSO déposé sur la surface d'aluminium traitée dans l'eau bouillant. Ainsi, le revêtement PP-HMDSO superhydrophobe a également fourni une protection contre la corrosion au substrat d'aluminium.

TABLE OF CONTENTS

ACKNOWLEDGMENTS

This work has been carried out within the framework of the NSERC/Hydro-Quebec/UQAC Industrial Chair on Atmospheric Icing of Power Network Equipment (CIGELE) and the Canada Research Chair on Engineering of Power Network Atmospheric Icing (INGIVRE) at the University of Quebec at Chicoutimi.

I would like to take this opportunity to express my most sincere gratitude to all of my professors during my academic education. I would especially like to convey my deepest gratitude to my director of studies, Professor Masoud Farzaneh, for his continued support, supervision, scientific knowledge, and patience during the entire project.

I am also grateful to Dr Reza Jafari as co-director of this work; I would like to express my appreciation and respect to him for his scientific and generous support.

I am also grateful to Dr. Gelareh Momen for her valuable advice and useful discussions and help. I would like to thank all the CIGELE and INGIVRE researchers, technicians, and secretaries, for their co-operation, moral as well as technical support, and encouragement; I would like to name specially Pierre Camirand, Claude Damours, Xavier Bouchard and Denis Masson. I would also like to thank Mrs Harriette Mostert for her valued efforts and editorial help.

I want to extend my warmest thanks to my parents for all the love, support, advice and encouragement they have given me. I am especially grateful to them for teaching me to

be ambitious and for believing in me throughout my life. Finally, I would like to thank to my husband Hamid: for being so loving, supporting, patient, and understanding during this study.

LIST OF FIGURES

LIST OF TABLES

CHAPTER I

INTRODUCTION

CHAPTER I

INTRODUCTION

I-1- Research problem description

In the word's cold climates, ice accumulation on aircraft and aerospace components, transport vehicles, electrical fittings, and connectors creates many problems. For example, the January 1998 ice storm in a vast area of North America caused massive damage to the electrical infrastructure, leading to widespread long-term power outages [1–4]. Hence, developing techniques to reduce ice accumulation on structures is receiving special attention. One solution to this problem is producing a weak ice adhesion coating, called icephobic coating on the outdoor surface structure [5]. Many research initiatives are underway to develop a superhydrophobic and hydrophobic coating with icephobic properties [6–9].

In general, the superhydrophobicity of a surface is the result of a combination of low surface free energy and surface roughness [10]. The superhydrophobic coating with icephobic properties should have a low adhesion to ice, and it must ease the removal of ice from the surface.

Plasma technology is one of the proven methods used to create superhydrophobic surfaces. Plasma technology takes advantage of highly reactive plasma species to modify the functionality of various substrates. It is one of the most common surface treatment technologies most common being used for surface activation, cleaning, adhesion improvement, anti-corrosion coatings, and biomedical coatings. The plasma polymerization process serves to deposit the coating by using the active species created by the plasma. The plasma polymerization method is economically and industrially attractive for the following reasons: it is typically an environmentally friendly, short and energy-efficient process which can be used to deposit a thin polymer film by using a low quantity of reagents [11].

The selection of the precursor in a plasma polymerization method is the primary effective parameter in creating a low surface energy material coating. The most popular precursors, which are used for the fabrication of a hydrophobic/superhydrophobic coating by using plasma polymerization methods, are organosilicon and fluorocarbon precursors. Fluorocarbon polymers are well known for their low surface energy especially attributed to CF_2 and CF_3 groups. These polymers are changed into a broad range of elements to produce custom tailored films because of their biocompatibility, low friction coefficient, the chemical composition, and the degree of cross-linking [12]. As well, organosilicon

monomers are a suitable choice for further studies due to their usual liquid state, volatility, safe handling, availability, and low cost [12]. Hexamethyldisiloxane (HMDSO), a safe and easy to handle organosilicon precursor, has been extensively employed for plasma polymer layer deposition in many applications.

A wide variety of plasma processing parameters, such as input power, monomer flow rate, distance between substrate and monomer inlet as well as deposition time and pressure can directly affect the chemical and physical characteristics of the plasma's thin film. In most studies, influential parameters have been investigated separately and kept constant individually, without attempting to show their synergistic or antagonistic effects. So, it is not an easy task to determine the optimal parameters without performing a tremendous number of experiments. However, a systematic approach using factorial experimental design can be used to simplify the experimental burden. Therefore, an inexpensive and easy-to-operate experimental design to study the interactive impact of various factors on a given surface is important and necessary. The Grey-based Taguchi method, one of the Design of Experiment methods (DOE), can be used to solve complicated interrelations between multiple performance characteristics [13].

The durability and stability of the coatings are important factors in the lifetime of a coating under extreme environmental conditions. Many experimental studies created superhydrophobic coatings by different methods, but few examine the durability of these coatings under simulated environmental conditions such as UV degradation, rainwater and ice-accumulation. UV-degradation is an important aging process when coatings are

exposed to atmospheric weathering conditions. Rainwater is another environmental problem, with a normal pH of 4- 6, that needs to be simulated the outdoor conditions and also to compare the effect of natural and basic solutions, the coating is immersed in various pH solutions. In addition, the coating is immersed in distilled water for many hours in order to study the durability of a superhydrophobic coating. Finally, the stability of the coating after several icing/de-icing cycles is considered as an important factor in cold regions.

I-2- Objective

The aim of our research is to create a stable icephobic coating by using low pressure plasma polymerization of a HMDSO coating deposited on aluminum surfaces. The effect of different plasma parameters will simultaneously be optimized in order to obtain maximum contact angle and minimum contact angle hysteresis. In the present work, the stability of plasma polymer thin film has been surveyed under accelerated aging conditions, which are UV exposure, immersion in various pH solutions, and several icing/de-icing cycles.

Thus, the specific objectives of this research are defined as follows:

- Creating the micro/nano structured roughness of an aluminum surface by using two industrial methods: anodization and immersion in boiling water (boehmitage);
- Selecting the suitable monomer in order to create a superhydrophobic surface;
- Minimizing the number of experiments for optimization of plasma processing parameters in order to have the highest contact angle and the lowest contact angle hysteresis by using the Grey-based Taguchi method as a DOE method;

- Studying the physical and chemical characterization of plasma polymerized coatings;
- Studying the stability of plasma polymerized coatings under accelerated aging conditions (several icing/de-icing cycles, UV-degradation and immersion in various pH solutions);
- Improving the stability of plasma polymerized coatings;
- Studying the corrosion resistance of superhydrophobic surfaces.

I-3-Statement of Originality

As will be presented later in this thesis, in the literature review, the superhydrophobic surfaces with icephobic properties has been achieved by using different techniques. The low pressure plasma polymerization method is an environment-friendly technique that has many advantages such as good adhesion to all substrates, as well as mechanical, chemical and thermal stability. To the best of our knowledge there have been no experiments done on the fabrication of icephobic coating using a low pressure plasma polymerization technique with high durability under various outdoor conditions, such as UV degradation, immersion in various pH solutions, and especially after successive icing/deicing cycles. The research work in this Ph.D. thesis was carried at the CIGELE (the Industrial Chair on Atmospheric Icing of Power Network Equipment) and INGIVRE (the Canada Research Chair on Engineering of Power Network Atmospheric Icing) laboratories à l'université du Québec à Chicoutimi.

I-4- Overview of thesis

The thesis is divided into seven chapters as follows:

- Chapter one provides a brief introduction to the problem of ice accumulation and a solution to this problem. It also summarizes the objectives of the thesis and includes a brief overview of it.
- Chapter two presents an overview of surface wettability, superhydrophobic surfaces, and their application for anti-icing coatings. It also provides a literature review on the effect of plasma process parameters on wettability of plasma polymerized coatings and their stability under accelerated aging conditions.
- Chapter three takes a closer look at the set-up of the plasma reactor used in this study; DOE method and characterization techniques in order to analyze the plasma polymerized thin films. The surface analytical techniques such as contact angle measurement, Fourier transform infrared spectroscopy (FT-IR), X-ray photoelectron spectroscopy (XPS), Atomic force microscopy (AFM), Scanning electron microscopy (SEM), and Ellipsometry are introduced. As well, the QUV accelerated weathering instrument, wind tunnel, centrifugal instrument, and Electrochemical test are also explained.
- Chapter four describes the initial steps of the surface treatment methods as well as how the plasma process parameters (input power, deposition time, monomer flow rate, and distance from monomer flow inlet) are simultaneously optimized by using the Grey-based Taguchi method. It also describes how the optimum plasma parameters are obtained in order to have high contact angle and low contact angle hysteresis.
- In chapter five, the stability of the plasma polymer coatings under the optimum conditions given in the previous chapter is discussed in terms of UV degradation, immersion in various pH solutions and several icing/de-icing cycles. The physical-chemical

characteristics (wettability, surface morphology, and chemical surface composition) of plasma polymerized HMDSO deposited are also studied.

- In chapter six, the effect of deposition time of plasma polymerization on the stability of the surface under accelerated aging conditions is studied; the results are compared with the results obtained in chapter five. As well, the corrosion resistance of the developed surfaces is studied by an electrochemical test.
- In chapter seven, the thesis is concluded and some recommendations are given for future work.

CHAPTER II

REVIEW OF BACKGROUND LITERATURE

CHAPTER II

REVIEW OF BACKGROUND LITERATURE

Introduction

This chapter presents a brief overview of wettability in addition to the concept of superhydrophobicity and its applications. Then, it focuses on the anti-icing application of a superhydrophobic coating developed through different techniques. Afterwards, the plasma treatment and the plasma polymerization method to develop thin films are introduced. As well, a review of the recent research on the influences of plasma process parameters in the development of hydrophobic and superhydrophobic surfaces is presented. Finally, a literature review about the stability of different coatings under accelerated aging conditions such as UV degradation, immersion in various pH solutions, and corrosion resistance is presented.

II-1- Wettability and superhydrophobicity

The wettability of the surface is evaluated by measuring the contact angle. This contact angle is a result of the interface/surface tensions (surface free energies) between liquid and solid, which are surrounded by vapor, (Figure II.1). It has been shown that the maximum contact angle attainable on a flat surface by lowering the surface energy cannot exceed 120° [14]. The contact angle is measured according to Young's equation, Equation II.1, for flat, rigid, and homogeneous surfaces. In conformity with this equation, the contact angle depends on the surface energies of the involved interfaces. These surface energies come from the solid, liquid, and solid/liquid interfaces [15].

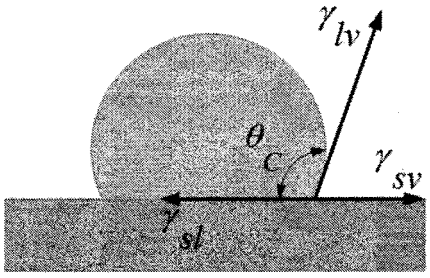

Figure II.1: The interfaces and contact angle of a water droplet.

$$Cos\ \theta_C = \frac{\gamma_{sv} - \gamma_{sl}}{\gamma_{lv}} \qquad \text{(II.1)}$$

Where,

- γ_{sv}: Surface energy of solid/vapor (N/m)

- γ_{sl}: Surface energy of solid/liquid (N/m)

- γ_{lv}: Surface energy of liquid/vapor (N/m)

- θ_C: Contact angle between solid/liquid (°)

Superhydrophobic surfaces are defined as a surface with a contact angle greater than 150°. Furthermore, the self-cleaning property of a superhydrophobic surface is referred to as the lotus effect since water droplets do not wet the surface and easily roll off to remove dirt and debris (see Figure II.2) [16].

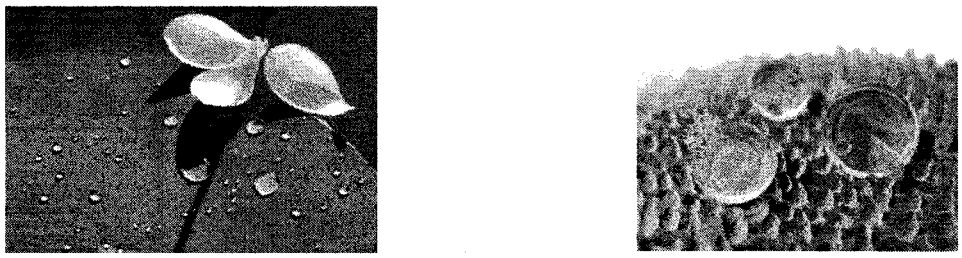

Figure II.2: The photos of water droplet on the lotus leaves [17].

Superhydrophobic surfaces can be generated by two main approaches: (i) either the creation of a rough surface from low surface energy materials or (ii) the creation of a rough surface followed by the application of a low surface energy material coating [18,19].

Contact angle hysteresis is defined with regards to dynamic contact angles, i.e. contact angles related to moving liquid fronts [20]. For a droplet moving along a solid surface, the contact angle at the front of the drop is an advancing angle and at the back, a receding angle. The difference between an advancing and a receding angle is known as contact angle hysteresis.

To measure the contact angle on the surface has deliberately been made rough, the effect of roughness on the solid/liquid interface should be taken into account. Many studies have tried to find a relationship between surface chemical energy, roughness, and contact angle; however two main regimes exist are generally accepted in all studies namely the Wenzel regime and the Cassie- Baxter regime (Figures II.3a-b).

Figure II.3: Schematic of a) Wenzel regime and b) Cassie-Baxter regime.

In the Wenzel regime, the liquid drop is in contact with the whole surface of the substrate, penetrating into the interstices among surface projections. The contact angle is expected to increase as the surface roughness also increases. The Wenzel regime is defined by Equation II.2 for the contact angle on a rough surface:

$$\text{Cos}\,\theta^* = r.\cos\theta_C \qquad \text{(II.2)}$$

Where

- θ^*: Apparent contact angle (°)

- r : Roughness factor

- θ_C : Contact angle of flat surface (°)

The roughness factor is defined by the actual surface area divided by the projected surface area. Therefore, the surface roughness is more than 1. The Wenzel model predicts that a hydrophobic surface with increasing roughness becomes even more hydrophobic, while a hydrophilic surface with increasing roughness becomes more hydrophilic [21]. On the other hand, Wenzel-type surfaces are generally characterized by a high contact angle and contact angle hysteresis, and water droplets have been stuck onto its surface because the texture hinders the motion and points to a large force of adhesion.

In the Cassie-Baxter's model [22], the water drop is facing a composite of substrate projections and the air trapped between them, which allows the water to freely roll off (self-cleaning behavior). The contact angle values in this model are determined by the fractions of solid and air facing the drop, as in Equation II.3:

$$\cos\theta^* = f.(cos\theta + 1) - 1 \qquad \text{(II.3)}$$

Where:

- θ^*: Apparent contact angle (°)
- f : Surface fraction (the ratio of surface top-post to projected surface)
- θ : Contact angle of flat surface (°)

Generally, Cassie-Baxter-type surfaces are characterized by high contact angle and very low contact angle hysteresis. The low value of f shows the existence of trapped air

between projections along the rough surface that leads to water droplets' rolling off the surface because of the low adhesion force.

Many different methods have been developed to fabricate superhydrophobic surfaces [6,23–30]. These surfaces have a number of practical applications in various areas such as cleaning coatings [31], biomedical [10], anti-icing [30,32,33], anti-fouling [34,35] and anti-corrosion [32], anti-sticking surfaces [36], anti-contamination of glass surfaces such as windows in buildings and windshields in vehicles [37]. Several studies showed a good correlation between hydrophobicity, especially superhydrophobicity and icephobicity of surfaces [7,30,32,38–43]. Hence, the fabrication of hydrophobic and superhydrophobic surfaces has much promise in anti-icing application.

II-2- Icephobicity

In cold climate regions, ice and snow accumulation on power transmission and distribution line conductors can lead to either mechanical failure or insulator flashover. This accumulation may cause power outages with major socio-economic consequences, as was the case with ice storms in Canada during 1998 and 2007 (see Figure II.4).

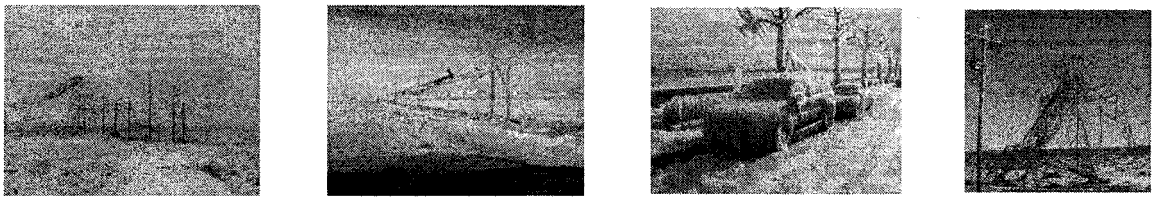

Figure II.4: Ice storms 1998 and 2007, Canada [44].

Over the past decades, different methods have been developed to reduce ice adhesion on exposed surfaces. In general, the two different strategies adopted to reduce ice deposits on overhead transmission lines are de-icing methods and anti-icing methods [5].

De-icing methods are used in order to shed the ice sleeve when a critical amount of ice has accumulated on a conductor. The aim of de-icing methods is to remove ice accumulations by using techniques such as freezing point depressants (salt, chemical sprays, etc.) for highways, de-icing fluids (e.g. ethylene and propylene glycols) for aircraft, mechanical vibration of cables, Joule heating of the conductors, and electrolysis. Most of these techniques require a great deal of energy and resources. In addition, these techniques sometimes may involve surveillance of lines and on-site intervention. When ice has already accumulated on a surface, these de-icing methods are employed [5].

The second strategy, anti-icing, is applied to prevent ice adhesion and accumulation on exposed surfaces at subzero temperatures. These methods must be implemented before the formation of ice by producing coatings that weaken ice adhesion. This coating acts directly at the interface between the ice and the exposed surface. It consists of preventing the freezing of super-cooled water droplets upon impact with the protected surface and using a combination of different methods in order to limit ice accretion [5]. Anti-icing methods are sought after because they can avoid some of the expenses and environmental costs of de-icing.

To prevent the growth of ice, it is necessary to understand how it forms under

atmospheric conditions. According to ISO-12494 [45], atmospheric icing is traditionally classified into two different formation processes, namely precipitation icing and in-cloud icing. The physical properties and the appearance of the accreted ice will vary widely according to the variation in meteorological conditions during ice growth. Tables II.1 and II.2 and Figure II.5 give the typical properties and major meteorological parameters controlling ice accretion.

Table II.1, Typical properties of accreted atmospheric ice [45]

Type of ice	Density (kg/m^3)	Adhesion and cohesion	General appearance	
			Color	Shape
Glaze	900	Strong	Transparent	Evenly distributed/ icicles
Wet snow	300-600	Weak (forming) Strong (frozen)	White	Evenly distributed/ Eccentric
Hard rime	600-900	Strong	Opaque	Eccentric/ Pointing windward
Soft rime	200-600	Low to medium	White	Eccentric/ Pointing windward

Table II.2, Meteorological parameters of accreted atmospheric ice [45]

Type of ice	Air T(°C)	Wind speed (m/s)	Droplet size	Water content in air	Typical storm duration
Precipitation icing					
Glaze (freezing rain or drizzle)	-10 to 0	Any	Large	Medium	Hours
Wet snow	0-3	any	Flakes	Very high	Hours
In-cloud icing					
Glaze	See Figure II.5		Medium	High	Hours
Hard rime			Medium	Medium	Days
Soft rime			Small	Low	Days

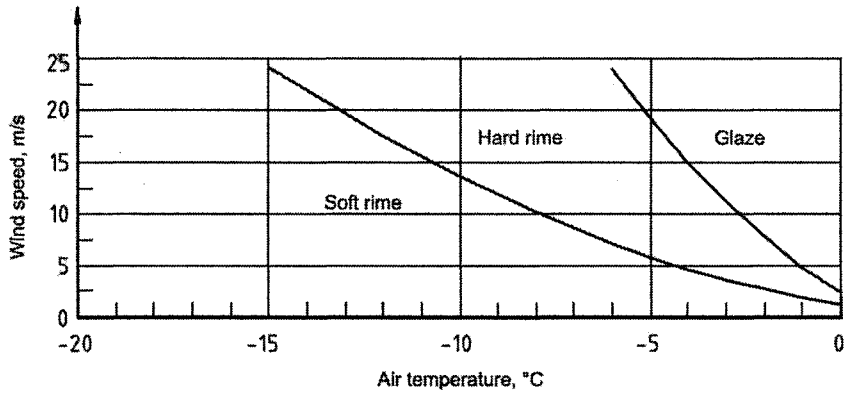

Figure II.5, Type of accreted ice as a function of wind speed and temperature [45]

When these types of atmospheric ice are compared, glaze ice is denser and exerts greater static/dynamic forces to the equipment. Also it conducts electricity more easily and is more dangerous for the performance power network components [45].

Several attempts have been made at CIGELE to produce hydrophobic and superhydrophobic surfaces in order to reduce ice adhesion strength. Methods listed in Table II.3, include spin-coating, dip-coating, spray-coating, self-assembly, sputtering plasma, and electrochemical deposition.

Table II.3: Summary of some of CIGELE research work for creating icephobic coating.

Technique	Material	Results	Ref
Spin-coating Plasma sputtering	Metalic nanopaticles Teflon	CA > 150 ° CAH < 10 ° ARF = 4 – 8.1	Safaee et. al. [39]
Spin coating Dip- coating Plasma sputtering	ZnO or TiO2 Fluoroalkyl-silane Teflon	CA = 163° - 165 ° CAH = 2° - 4° ARF = 3.44	Noormohammed et. al. [46]
Dip-coating Spin-coating	Fluoropolymer Silicone rubber	CA = 150°-153° CAH = 4.5°-7° ARF = 3.5-4.4	Farhadi et. al. [8]
Self-assembly	Silicone rubber	CA = 143°-147 ° DFT = 12-13	Arianpour et. al. [9]
Plasma Sputtering	Teflon	CA = 165 ° CAH = 3° ARF = 3.5	Jafari et. al. [47]
Electrochemical deposition	Teflon	CA = 130° -150° ARF = 2.5-4.88	Menini et. al. [6,48]
Dip-coating Spin-coating Spray coating	Organosilane TiO_2-Zonyl	CA = 153°-150° CAH = 5.7°-80° ARF = 3.5-4.4	Kulinich et. al. [49]
Spin Coating	Silicone rubber	CA = 160° CAH = 7° CALT = 125° (at -10°C) DFT = More than 10 min	Momen et. al. [24]
Sol-gel plasma enhanced chemical vapor deposition	Methanolic ZnO C_2F_6 and Teflon	CA = 164 ° CAH = 2.5 °	Sarkar et. al. [50]

CA: Contact angle
CAH: Contact angle hysteresis
ARF: Adhesion reduction factor
CALT: Contact angle at Low Temperature
DFT: Delay freezing time

The anti-icing coating can also delay the freezing time [51–53]. *Guo* et al. [51] compared the delayed freezing time (at temperature -10°C) of different rough surfaces coated with ZnO nanohairs. They found that freezing time for the surface with a micro/nano structure (contact angle ~ 150 °) is around 7220 seconds. Freezing time is

approximately 1740 seconds for the nano structured surface (contact angle ~ 120°). For the surface with a micro structure and also the smooth surface (contact angle ~ 90°), the delay freezing times are 30.5 seconds and 1260 seconds respectively (Figure II.6). The results showed that the combination of both nano structure and microstructure leads to an increased the ratio of trapped air; thus the drop was greatly suspended. On a nanostructure surface, the water-condensed drops cannot be suspended, due to the lack of a microstructure. When a microstructure surface and a smooth surface are compared, water-condensed drops on the microstructure may collapse more easily than on the smooth surface due to intrinsic contact states.

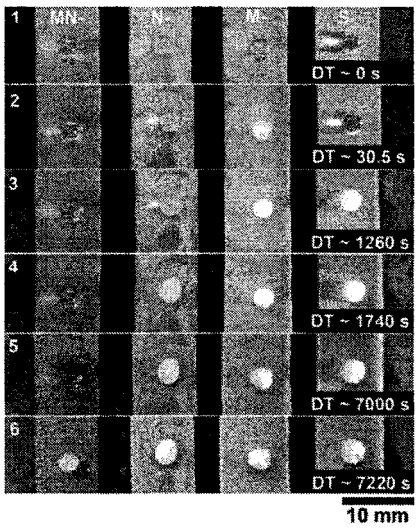

Figure II.6: In situ observation of ice formation on different structured surfaces at –10 ° C with freezing delay times (MN: micro/nano-structured surface, N: nano-structured surface, M: micro-structured surface and S: smooth surface) [51].

In addition, other studies have shown that superhydrophobic surfaces with low contact angle hysteresis can keep their hydrophobic properties at low temperatures [54]. They showed that the superhydrophobic properties of the surface have been kept at working temperatures varying from -10°C to 17.5°C, as shown in Figure II.7. This property is due to the surface micro/nano scale roughness and the hydrophobicity of stearic acid.

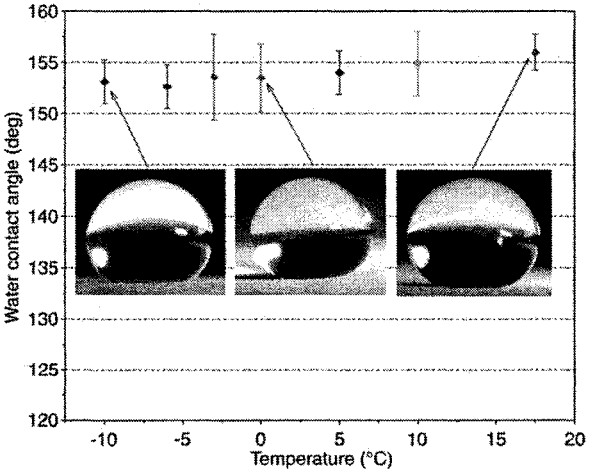

Figure II.7: Variations of contact angle of a superhydrophobic aluminum surface at different temperatures [54].

Nevertheless, a few studies did not agree with this hypothesis [55,56]. *Chen* et al. [55] have shown that hydrophilic and hydrophobic surfaces have a lower ice adhesion strength than superhydrophobic and superhydrophilic surfaces (see Figure II.8). They investigated a correlation between the ice adhesion strength and the area fraction of air in contact with a liquid. Their results showed that ice adhesion strength increases linearly with the increases of the area fraction of air in contact with a liquid.

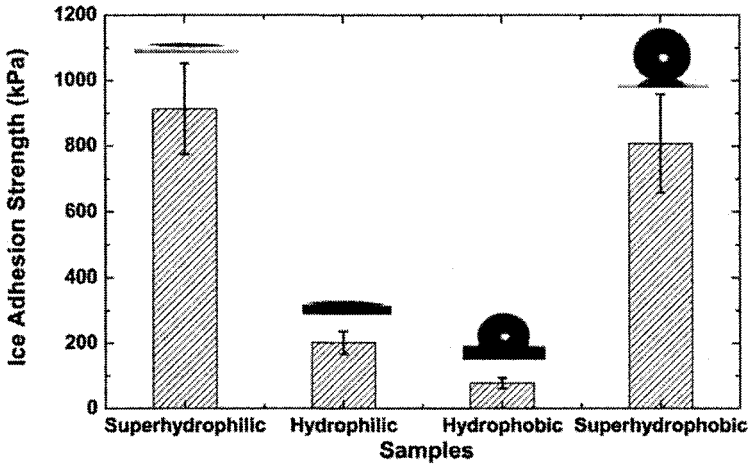

Figure II.8: Average ice adhesion strength on four different silicon wafer surfaces (superhydrophilic to superhydrophobic) measured at -15 °C [55].

In order to investigate the relation between icephobicity and hydrophobicity, the following factors should be considered: the deposition of specific functional groups of a low surface energy material coating, the method of accumulating ice on the surface, the type of ice, and the morphology of the surface. The deposition of low surface energy materials leads to the creation of a hydrophobic coating, but the effect of specific functional groups can lead to improve hydrophobic characteristics. *Hare* et al. [57] showed that the surface energy of hydro/fluorocarbon groups decreases in the following manner: $-CH_3 > -CH_2 > -CF_2 > -CF_3$. Also, the increase of methyl groups on structures of organosilicon precursor causes them to gain more hydrophobic properties. In most of the research studies, the accumulation of ice was performed in a wind tunnel in order to simulate real atmospheric ice conditions [7]. While in other cases, the delay time of water frozen on a surface was studied [55]. *Sarshar* et al. [53] showed that the superhydrophobic surfaces can also lead to the delay of ice formation.

It is to be noted that by changing the aerodynamic conditions of the closed-loop low-temperature wind tunnel, different types of ice can be accumulated. Therefore, between these types of atmospheric ice (glaze ice, hard and soft rime ice), glaze ice is denser and exerts stronger static/dynamic forces on the equipment [39,46].

Finally, the relation between the roughness of the coating and the diameter of liquid droplets can have an effect on how ice adheres to a surface. *Jung* et al. [56] showed that superhydrophobic surfaces may not necessarily offer the best choice for icephobic applications. Nanometer scale smooth surfaces showed much better icephobic properties under the studied controlled conditions [56].

II-3- Plasma treatment

Plasma describes the state of (partially) ionized gases composed of electrons, ions, photons, and various neutral species at different levels of excitation and it also is sometimes referred to as the fourth state of matter [58]. Plasma technology is a suitable method for surface treatment. It can tailor polymers in different forms in order to modify their surface properties without changing their intrinsic bulk properties. Moreover, it is dry and clean, without any significant ecological concerns.

Plasma systems usually operate in the range of low frequency (40- 450 kHz), radio frequency (13.56 MHz or 27.12 MHz), and microwave (915 MHz or 2.45 GHz) [59]. Generally, plasma polymerization is categorized according to the pressure in which the process is carried out: (1) low pressure plasma polymerization (the pressure is lower than

atmospheric pressure, usually in the range of a few Pascal) and (2) atmospheric pressure plasma polymerization. However, each has its own advantages and disadvantages. Plasma parameters are easier to control in low-pressure situations than in normal atmospheric pressure. One of the main attractions of low pressure plasma technology regards the lower amounts of processed gases involved, which are better for the environment [60]. Also, it can generate more homogeneous films with fewer impurities [32]. On the other hand, atmospheric pressure plasma reactors require less energy and offer shorter process times compared to low-pressure plasma [59].

As shown in Figure II.9, plasma technology can be used for various surface modifications such as:

- Etching and cleaning of surface layers
- Chemical surface functionalization
- Deposition of solid films (plasma polymerization)

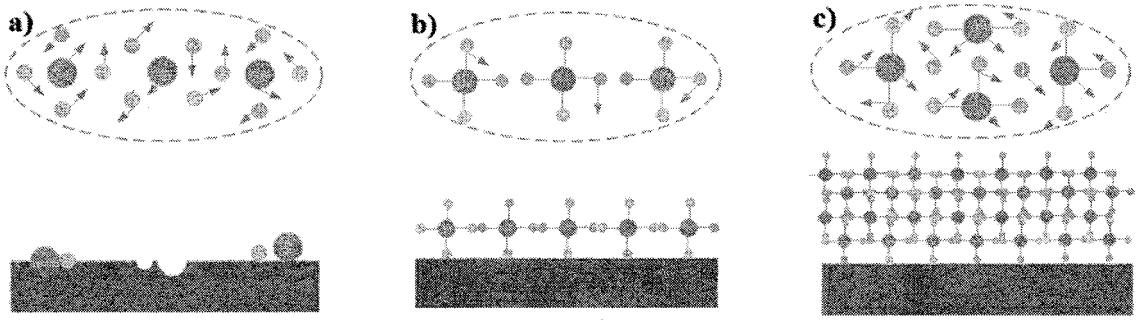

Figure II.9: Schematic of plasma surface modifications a) etching and cleaning, b) functionalizing and c) deposition of a thin film.

II-4- Plasma polymerization

Plasma polymerization involves thin film deposition, a technique for fabricating thin polymer coating from almost any organic or inorganic precursor in order to create hydrophilic/hydrophobic surfaces [11,12,61]. Plasma polymerization offers a number of advantages over other polymerization methods. The most significant advantage of plasma polymerization is its ability to produce polymer films of organic compounds that do not polymerize under normal chemical polymerization conditions. Nearly all monomers, even saturated hydrocarbons and organic compounds without a polymerizable structure such as a double bond, can be polymerized with this technique. A second advantage is the ease of application of the polymers as coatings versus conventional coating processes. While coating a substrate with conventional polymers requires a number of steps, plasma polymerization essentially accomplishes all these in a single step. This leads to a cleaner synthesis and coating process, since no solvent is needed during the polymer preparation; no cleaning of the resultant polymer is needed either.

In this process, the growth of low molecular weight molecules (monomers) into high molecular weight molecules (polymers) occurs with the assistance of plasma energy, which involves activated electrons, ions, and radicals [11]. In low-pressure plasma polymerization, generally, the liquid precursor is vaporized in an evaporator pumped into the vacuum chamber. The excited electrons created in the glow discharge ionize the monomer molecules. The monomer molecules break apart (fractionate) to create free electrons, ions, exited molecules, and radicals. The radicals adsorb, condense, and

polymerize on the substrate, as shown in Figure II.10. The electrons and ions crosslink, or create a chemical bond, with already deposited molecules, creating a harder and denser coating [62].

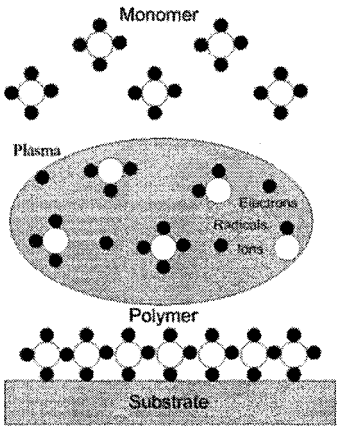

Figure II.10: Plasma polymerization process.

The important advantages of depositing thin films via low pressure plasma polymerization are [11,12,61]:

- The precursor used does not need to contain the type of functional groups normally associated with conventional polymerization.
- Deposition is achieved without the use of solvents (environmentally benign process).
- Such films are often highly coherent and adherent to a variety of substrates, including glass and metal surfaces.
- Less time is needed for the processes involved, such as coating, curing, loading and/or unloading, and part transfer.

- The thickness of plasma polymerization films can be easily varied from 1nm to several mm's.
- Plasma polymerization films can be deposited directly onto an activated substrate without breaking vacuum.
- The deposited film has good corrosion resistance.
- Through careful control of the plasma polymerization parameters, plasma polymerization films can be tailored to contain specific functional groups.

Plasma polymerization is a specific type of plasma chemistry, and many factors can affect the chemistry and morphology properties of the resulting polymer. The most important plasma process parameters are deposition time, input power, monomer flow rate, type of carrier gas, distance from the precursor injection point, and type of both precursor and carrier gas. In the following section, the effect of these plasma process parameters on the surface wettability, surface roughness and/or surface chemical composition is discussed.

II-4-1- Influence of precursor chemistry

The choice of monomer is of primary importance in order to create the superhydrophobic coating. The most popular precursors, which are used for the fabrication of hydrophobic coatings by plasma polymerization, are organosilicon precursors and fluorocarbon precursors.

The plasma polymerized fluorocarbon precursor displays several advantages, including low coefficient of friction, low surface tension, good thermal stability, good

biocompatibility, and chemical resistance [12]. A vast number of publications have investigated types of fluorocarbon precursors with different chain lengths, saturated and unsaturated, linear and cyclic structures, all factor that can affect the water repellency of a coating [63–74].

Organosilicon monomers have many advantages, such as stability at elevated temperature, availability, liquid state, safe handling, and low cost. Due to this assets, many studies have preferred the plasma polymerization of different organosilicon precursors in order to create a hydrophobic coating [41,75–82].

Kale et al. [83,84] compared the effect of two monomers, Hexamethyldisiloxane (HMDSO) and Tetraethylorthosilicate (TEOS), on the wettability of nylon 66 fabrics. They showed that the contact angles of HMDSO plasma-treated fabrics are higher than those treated with TEOS plasma. The higher contact angle values achieved in the case of HMDSO monomer may be attributed to its higher organic nature when compared to TEOS. The molecular structure of these monomers is presented in Figure II.11.

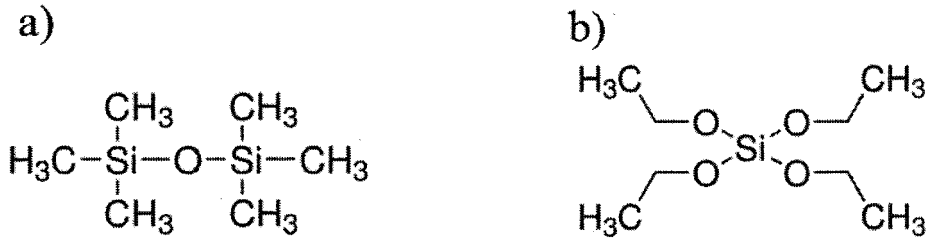

Figure II.11: Chemical structure of (a) Hexamethyldisiloxane and b) Tetraethylorthosilicate.

According to *Ji* et al. [41], the use of Toluene in atmospheric pressure plasma polymerization HMDSO improves the hydrophobicity of a coating. They showed that the contact angle of untreated glass, which is about 50°, was increased to 135° after depositing the plasma polymerized HMDSO coating; with the plasma polymerized HMDSO/Toluene thin film it showed a superhydrophobic surface (contact angle ~ 150°, Figure II.12). The bulky non-polar aromatic ring of Toluene could cause the superhydrophobic property. The SEM and AFM analysis also showed that the granules created by HMDSO/toluene coating. Futhermore, the surface roughness are broader than these of the HMDSO coatings and the surface roughness of the HMDSO/Toluene film (116nm) is higher than that of HMDSO coating (70nm) [41]

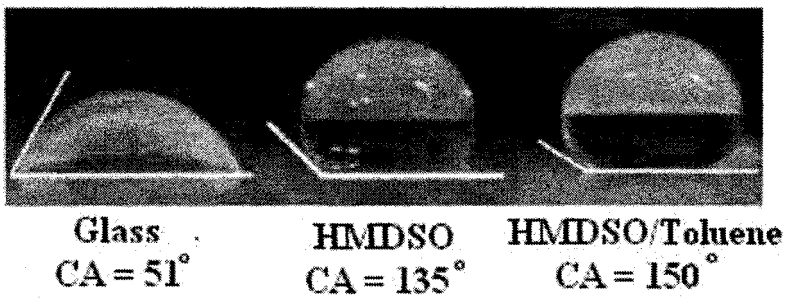

Figure II.12: Image of CA of (from left to right) untreated glass, HMDSO plasma-treated glass, and toluene/HMDSO plasma- treated glass [41].

A comparison of fluorocarbon precursor with different saturated and unsaturated, linear and cyclic structures has been carried out by *Zhang* et al. [65]. They came to the conclusion that in order to break the π band in cyclic unsaturated structure, lower bond energy (2.74eV) than C-F (5.35eV) and C-C (3.61ev) is needed. The applied precursors are

shown in Figure II.13. Similarly, *Mukhopadhyay et al.* [63] also showed that the presence of the aromatic ring led to an increase of the coating deposition rate and hydrophobicity.

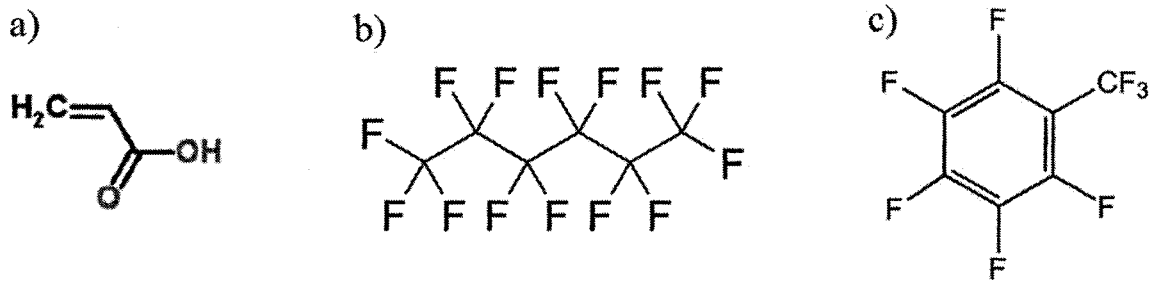

Figure II.13: Molecular structure of a) Acrylic acid (unsaturated), b) Perfluorohexane (linear saturated) and c) Octafluorotoluene (cyclic unsaturated) [65].

The effect of the increase of the lengths of perfluoroalkyl groups (C_nF_{2n+1}) on increasing the contact angle has been observed by *Hozumi* et al. [66] and *Takai* et al. [67]. It has been shown that increasing the length of monomer led to an increase in the concentration of fluorine groups and, consequently, resulted in a higher contact angle (Figure II.14) [66].

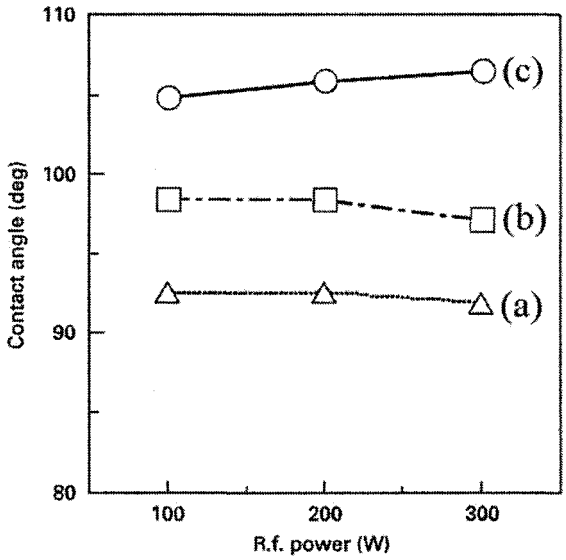

Figure II.14: R.F. Variation of contact angles for the different plasma precursors deposited a) FAS-3, b) FAS-13, and c) FAS-17 [66].

II-4-2- Influence of input power on wettability

One of the most important plasma operating parameters is input plasma power. This parameter allows control over precursor fragmentation in the plasma and the physic-chemical properties of the deposited film, considering that low input power results in decreased fragmentation of precursor as well as an increase in the linear structure of the coating. Nevertheless, for high input power, the high fragmentation of precursor led to an increase in both the cross-linked structure and the roughness of the coating. At the same time, it led to a decrease in desired groups. Many studies showed the effect of plasma polymerization power on the contact angle of the resulting coating [85,86].

Hegemann et al. [79] investigated plasma polymerized HMDSO films on polycarbonate (PC) substrates in an effort to generate hydrophobic surfaces. Their results

showed that a low plasma power input yielded the low fragmentation and high linearization of the monomer. As a result, and due to an increase of methyl groups' content, a hydrophobic coating was created. In addition, they showed that the content of methyl groups was reduced through stronger fragmentation of the HMDSO molecules by increasing the power input. The end result was improved mechanical stability.

Siliprandi et al. [85] showed the decrease of the degree of polymerization and formation implies growth in itself (oligomer-like layer) at low input power. As well, the smooth structure was deposited in ultra-low fragmentation conditions. As a result, the contact angle increased when input power was reduced as shown in Table II.4.

Table II.4: Contact angle measurements for the low pressure deposition process at different power inputs [85].

Input power (W)	Advancing angle (°)	Receding angle (°)
5	125	79
15	105	80
40	103	79

Behnisch et al. [78] studied the contact angle of plasma polymerization of Hexamethyldisilazane (HMDSN) and Hexamethyldisiloxane (HMDSO) on biodegradable polymer foil surface in a radio frequency glow discharge. They mentioned that a high contact angle is obtained at a low power value with high concentrations of monomer (contact angle 97 ° ± 2 for HMDSN and 103 ° ± 4 for HMDSO).

According to the measurements carried out by *Zanini* et al. [75], a decrease in the

ratio of Si-CH_3 bonds to CH_X bonds (low hydrophobic properties) is obtained by mounting the plasma power of HMDSO coating in a low pressure radio frequency plasma reactor. These results showed that by escalating the input plasma power from 20 W to 100 W, the contact angle is decreased from 104° to 89°.

On the contrary, some studies demonstrated that the increasing the input power leads to an increase in hydrophobic properties of plasma polymerized coating. *Palaskar* et al. [86] reported the creation of superhydrophobic coating (contact angle ~ 150.1 °) at a high input power of atmospheric plasma polymerized HMDSO coating. They showed that by increasing the input power, the greater fragmentation of a monomer provides better chances of polymerization. Moreover, the results of surface morphology by a Scanning electron microscopy (SEM) analysis showed that by heightening the discharge power, the deposition coating rate was faster.

II-4-3- Influence of deposition time on wettability

Several studies have shown that deposition time is an important parameter in controlling the thickness of the coating as well as the deposition rate. However, increasing the deposition time can increase the presence of hydrophobic functions [31,43,63,64,74–77,87,88].

Kale et al. [31] showed that by increasing the deposition time in the same plasma conditions, the chemical nature of the deposited polymer is similar and consequently, the variation of contact angle remains constant.

Grimoldi et al. [77] investigated the chemical structure, morphological structure, and hydrophobic characteristic of the plasma polymerization of HMDSO. Figure II.15 shows the results of surface morphology of different surfaces at different deposition times of a HMDSO film by Atomic Force microscopy (AFM) analysis. It reveals that the surface roughness (rms) of an untreated silicon wafer was around 0.118 nm, but at a low deposition time, the surface roughness (rms) reached 0.22 nm. However, at a high deposition time, surface roughness increased to 0.305 nm [77]. These results demonstrate that by increasing deposition time up to 5 minutes, surface roughness is increased.

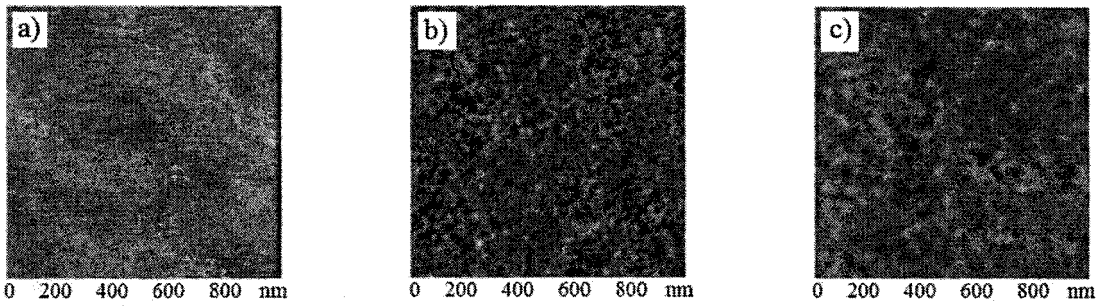

Figure II.15: AFM Images of a) untreated silicon wafer, b) PP-HMDSO coating deposited at 30 sec deposition and c) PP-HMDSO film at 5 min deposition [77].

Moreover, these results also show that water repellency was improved when deposition time was increased and after that, it reached saturation values (Figure II.16) [77].

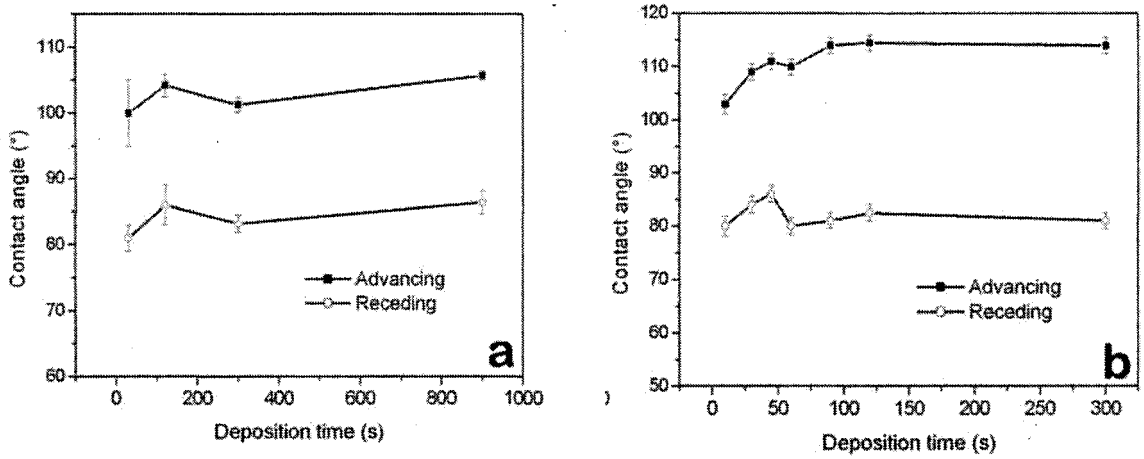

Figure II.16: Advancing and receding contact angle of PP-HMDSO film at different deposition times on a) wafer silicon b) polyethylene [77].

Prat et al. [64] studied the effect of treatment time of atmospheric pressure plasma polymerization of Hexafluoropropylene (HFP) and Tetrafluoroethylene (TFE) on wettability of a commercial poly(vinyl chloride) surface. Their results showed that the contact angles increased significantly in the first 3 minutes of plasma treatment. As treatment continued, the thickness of the layer increased but the degree of hydrophobicity of the surface was unchanged, as shown in Figure II.17.

Zanini et al. [75,76] studied the effect of deposition time on the contact angle of Hexamethyldisiloxane (HMDSO) coating in a low pressure plasma reactor with capacitive-coupled radio frequency (RF) (13.56 MHz). They found that increasing deposition time increases the ratio of Si–O–Si bonds to Si–CH_3 bonds; however the carbon content decreases. Their results indicated that hydrophobicity was reduced by increasing deposition time.

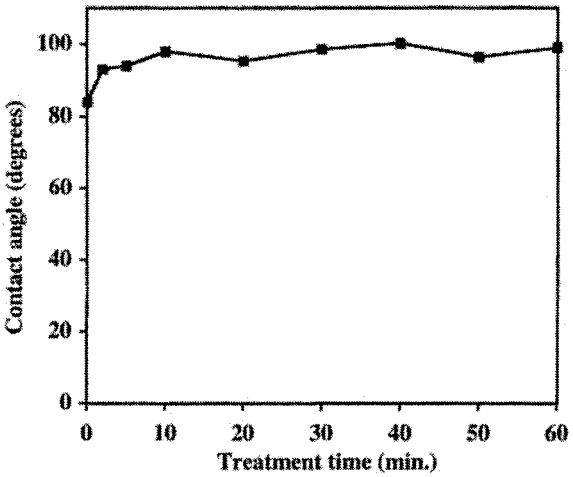

Figure II.17: Contact angle of PP-Hexafluoropropylene coating on poly(vinyl chloride) tube as a function of deposition time [64].

II-4-4- Influence of monomer flow on wettability

The monomer flow rate is another parameter that can affect the wettability of a coating. By increasing the monomer flow rate, the concentration of methyl groups can also increase. However, it may lead to coating delaminate [31,89].

Kale et al. [31] observed the effect of monomer flow on wettability of atmospheric pressure plasma polymerized Hexamethyldisiloxane coating on cotton fabrics. They found that by increasing the monomer concentration, the surface energy changed smoothly.

According to the results of *Morent* et al. [89], the contact angle of atmospheric pressure plasma polymerized Hexamethyldisiloxane increased from 99° to 108° by accelerating the concentration monomer flow from 1.3 to 3 ppm. They showed that by further increasing the concentration of monomer flow to 4 ppm, the contact angle remained

constant. Figure II.18 depicts that the FT-IR peaked due to Si–C and CH_3 vibrations (1260, 2960 cm^{-1} as methyl group functions) are considerably increased by augmenting the monomer flow.

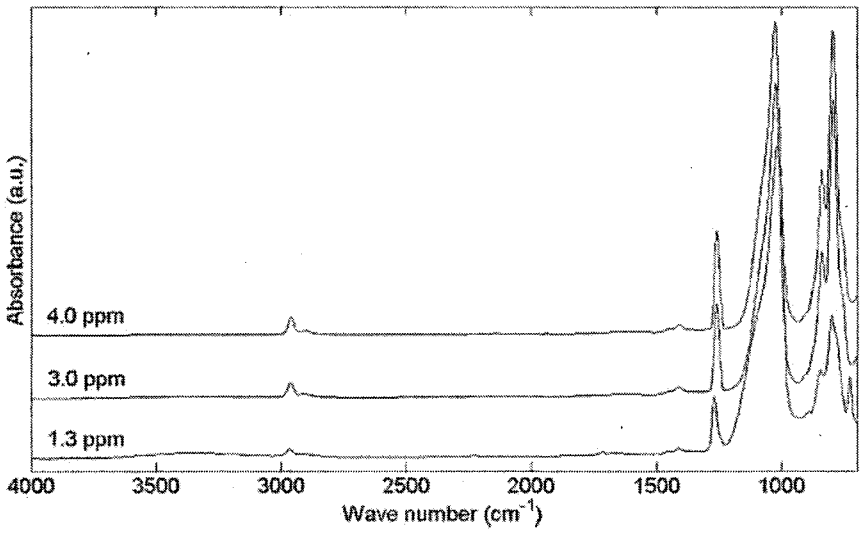

Figure II.18: FT-IR spectra of PP-HMDSO films deposited with different monomer concentrations (discharge power 9.5 W, film thickness 700 nm) [89].

II-4-5- Influence of distance from monomer inlet on wettability

The substrate position related to the plasma discharge and monomer inlet can affect the hydrophobicity of plasma-polymerized films. Inside the glow discharges, all radicals contribute through the activation growth mechanism triggered by positive ion bombardment, leading to high deposition rates. Instead, after glow discharge, ions soon disappear and the radical distribution also changes to favorite groups which have a longer half-life [73,90].

Intranuovo et al. [73] studied the plasma polymerization of Hexafluoropropylene oxide (C_3F_6O, HFPO) in glow and in afterglow discharge in a radio frequency (RF) reactor. Based on Figure II.19, the SEM image of coatings deposited at a distance near the gas inlet are flat; however, by increasing the distance, the surface morphology is changed so that it resembles "stone roses". The effect of distance on the hydrophobicity of their coatings is shown in Figure II.20. These results demonstrated that the increase in the distance between substrate and inlet gas leads to an increase in the hydrophobicity of a surface.

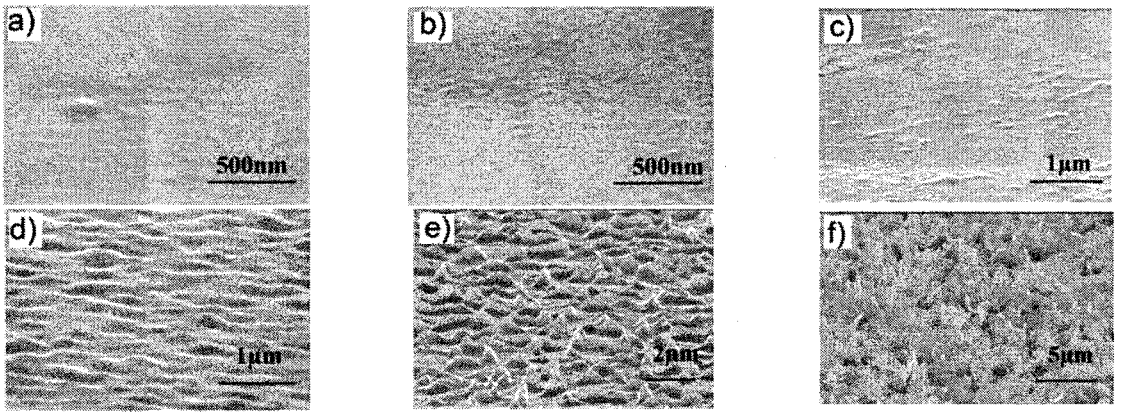

Figure II.19: SEM images of the coatings at a) 1, b) 3, c) 5, d) 8, e) 11, and f) 18 cm from the gas inlet [73].

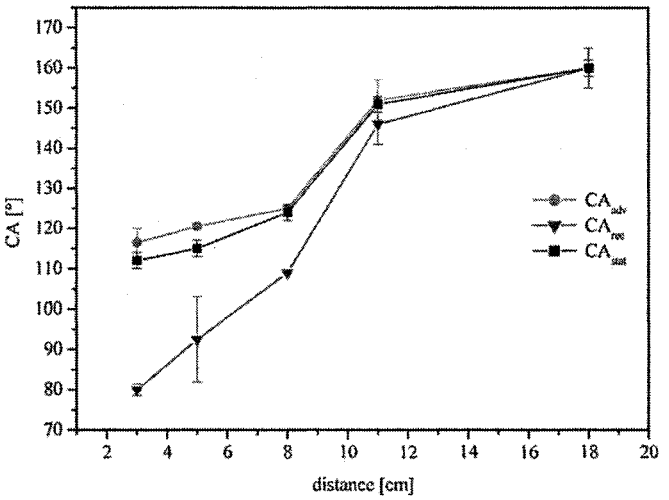

Figure II.20: Static, advancing, and receding contact angle vs. axial position of samples from the gas inlet [73].

Butoi et al. [91] studied the effect of distance from a RF coil on the structure of a plasma polymerized Hexafluoropropylene oxide film. Their results showed that at a short distance, a cross-linked and amorphous film was obtained, while at a greater distance a linear and higher degree of order film was obtained. *Yajima* et al. [90] also showed that the greater the distance from the copper coil leads to an increase of hydrophobicity.

II-4-6- Influence of pre-treatment and different carrier gas

The surface pre-treatment is often necessary for surface activation prior to coating, and it also can clean the surface contamination. Different types of carrier gases can be used in plasma to create a chemical surface functionalization, etching, and plasma polymerization. Each of these predominant reactions depends on the gas feed, the operation parameters, and the chemical nature of the substrate. Likewise, it can improve the adhesion between the surface and deposited films. The effect of pre-treatment and the type of carrier

gas on the plasma polymer film properties, especially hydrophobicity, has been investigated by several groups [66,67,71,72,79,81,82,92,93].

Different plasma pre-treatments on polycarbonate surfaces have been carried out by *Hegemann* et al. to enhance the adhesion of the surface coating [79]. Figure II.21 illustrates AFM topography of the surface pretreated by different carrier gases such as Ar, O_2, N_2 or He, prior to the HMDSO deposition on the polymer substrate. The pretreatment by O_2 and Ar produced a higher surface roughness (Rms = 29 nm and 26 nm, respectively) than other gases. However, the untreated surface roughness decreased after pretreatment. These results indicate that the pretreatment of O_2 and Ar increases the probability of removing the outermost of the surface.

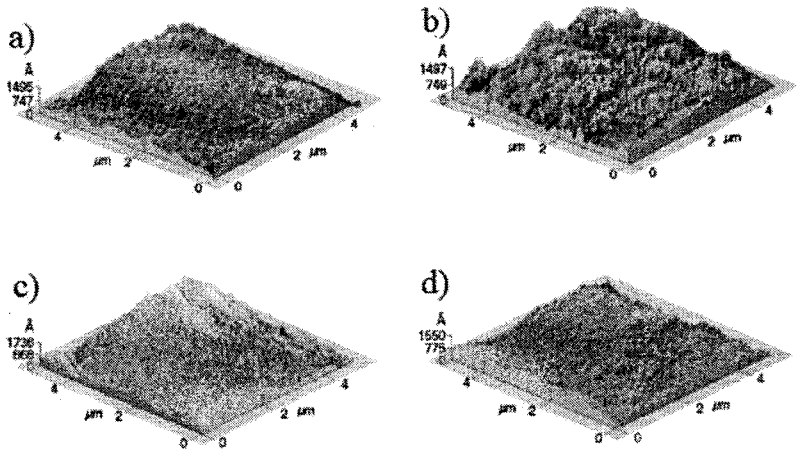

Figure II.21: AFM topography of different pre-treatments (a) O_2 plasma treatment, (b) Ar plasma treatment, (c) N_2 plasma treatment, and (d) He plasma treatment [79]

Several authors studied the effect of oxygen plasma to clean and/or etch the surface in order to create a hydrophilic surface [66,67,82,92,94]. *Hirotsu* et al. [82] fabricated a hydrophobic coating on poly (L-lactic acid)/poly (butylene succinate) by the following process: (1) plasma etching with O_2, followed by (2) plasma polymerization Hexamethyldisiloxane (HMDSO) and/or Hexamethyldisilazane (HMDSN) coating. The contact angle of the untreated surface was around 75 ° (Figure II.22A). The contact angle of PP-HMDSO on the surface without any pre-treatment was about 106°-108° (Figure II.22C). Only by plasma etching with O_2, the contact angle decreased to 48° and the surface had a hydrophilic characteristic (see Figure II.22B). However, the PP-HMDSO coating deposited on the etched surface became more hydrophobic, and the contact angle increased to 134° (Figure II.22D).

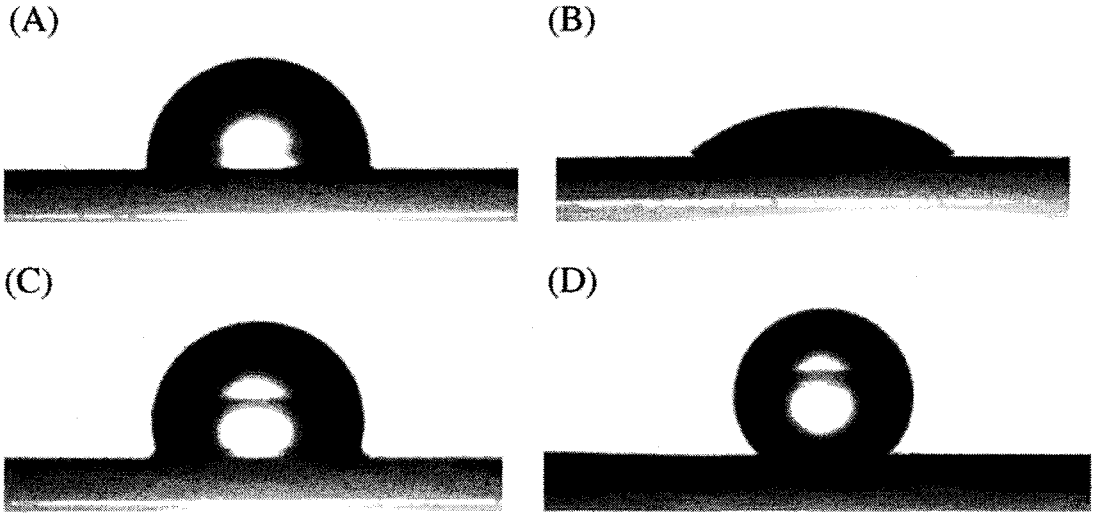

Figure II.22: Contact angle of (A) untreated Poly(L-lactic acid)/poly(butylene succinate) surface, (B) the O_2 plasma etched surface, (C) the HMDSO plasma polymer coated surface, (D) PP-HMDSO film deposited on O_2 plasma etched surface [82].

The effect of the type of carrier gas on surface morphology, chemical composition, and hydrophobicity of plasma polymerization of Allylpentafluorobenzene (APFB) coating has been studied by *Zhang* et al. [72]. The results indicated that the influence of Argon in intensive defluorination of the coating gave rise to the highest F/C = 0.53 (at power 5W), while oxygen gave rise to the lowest value F/C = 0.41 (at power 5W). The roughness of the PP-APFB coating without any carrier gases was reported around 1.5 nm. According to Figure II.23, the surface roughness of PP-APFB coating with Ar as a carrier gas increased to 3.5nm while for the other carrier gases (He, N_2, O_2) a smoother surface was observed. Additionally, the hydrophobic properties of the coating increased according to the following order of the gases used: $O_2 < N_2 < H_2 < Ar$.

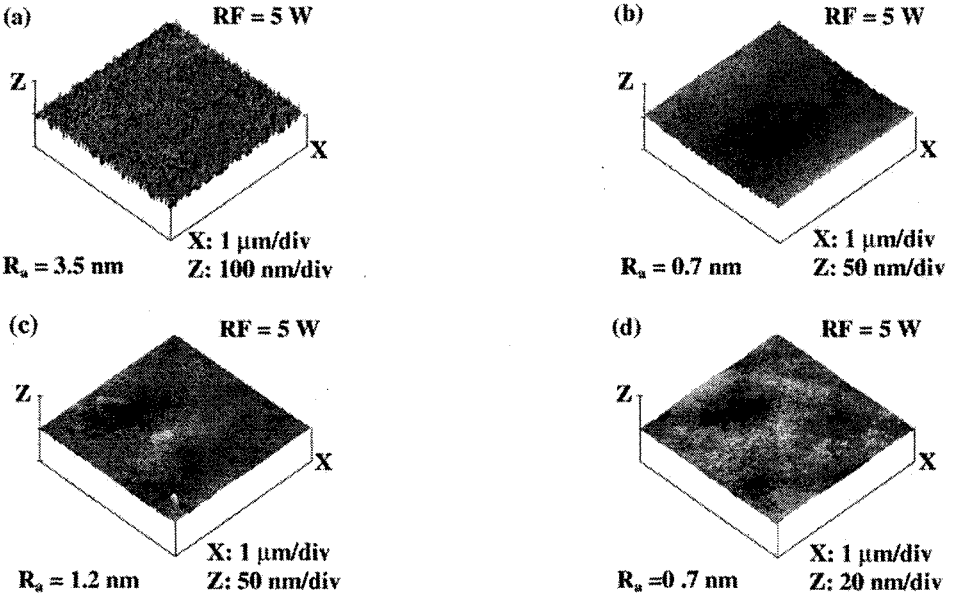

Figure II.23: AFM images of the plasma polymerized APFB coating at RF power of 100 W with the carrier gas of a) Ar, b) He, c) N_2, and d) O_2 [72].

II.5-Stability

The preparation of a stable coating is a critical topic for many industrial applications. A number of research groups studied the stability of hydrophobic and superhydrophobic coatings under different conditions, such as UV exposure [76,95–99] and immersion in various pH solutions [95,97,100–102], distilled water [103–105], as well as corrosive solution [100,101,106].

II-5-1-UV degradation

Sunlight is a major cause of damage to a number of materials, including plastics, textiles, coatings, and other organic materials. The type of damage, such as loss of physical properties, chalking, cracking, peeling, fading, and color change varies depending on the material sensitivity and the spectrum of sunlight [76,95–99]. The electromagnetic energy from sunlight is normally divided into ultraviolet, visible light and infrared energy. Ultraviolet (UV) light has been recognized as the main cause of damage. In order to simulate the outdoor sunlight, *Zanini* et al. [76] studied the effect of PP-HMDSO coating in a solar-box. This equipment is a solar simulated environment equipped with a UV radiation 1500W Xenon lamp, where four periods of 672 hours exposure under different conditions of temperature and relative humidity were carried out. Their result showed that the contact angle of the treated sample under simulated aging decreased from 122° to 55°. The decreased hydrophobic characteristics observed for the treated sample could be derived from chemical and/or physical surface modification due to the temperature and humidity

conditions during the aging process.

Isimjan et al. [97] studied the effect of an extra-layer of SiO_2 nano-particles on steel coated by three layer of TiO_2 (TiO_2*3) nano-particles under UV exposure (mercury lamp, 315–400 nm, 100 mW/cm^2). Figure II.24 shown that the contact angle of a TiO_2*3 surface before UV exposure is around 175°, but after 275 minutes of UV exposure, the contact angle decreases to around 0°. By using one to three layers of SiO_2 nano-particles on the TiO_2*3 surface, the contact angle decreases from 155° to 140°. Moreover, all of the SiO_2 nano-particle coated surfaces maintain their superhydrophobicity after 275 minutes of UV exposure.

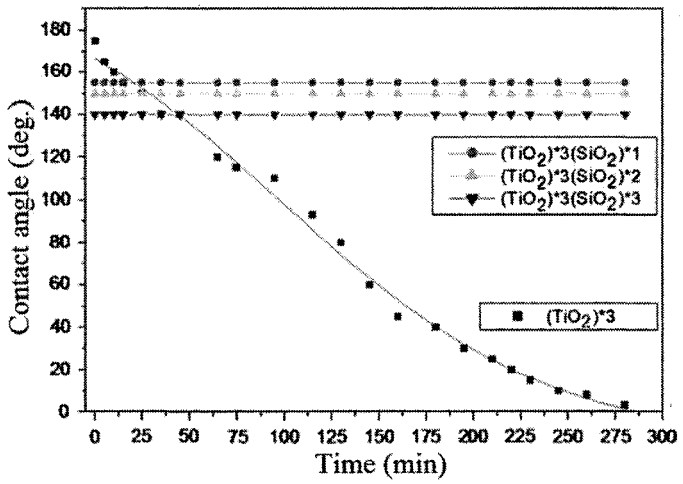

Figure II.24: Contact angles of three different layers of SiO_2 on top of a superhydrophobic TiO_2 coated sample after a certain period of UV exposure [97].

II-5-2- Effect of different pH

In order to simulate the influence of rainwater on a superhydrophobic coating, the surfaces are immersed in various pH solutions [95,97,100–105]. *Momen* et al. [95] studied the stability of the surfaces spray-coated with silicone rubber/ZnO/SiO_2 composites after immersion in different pHs (4, 6, 7 and 10) in order to simulate rainwater conditions. Their results showed that the contact angle of this coating before immersion in the solution is 162°, with a contact angle hysteresis around 7.2°. After 240 hours of immersion in different pH solutions, as shown in Figure II.25, the contact angle slightly decreased (around 145°). The researchers concluded that the surfaces keep their superhydrophobic properties after immersion in pH solutions, except for the sample immersed in tap water, due to ionic contamination.

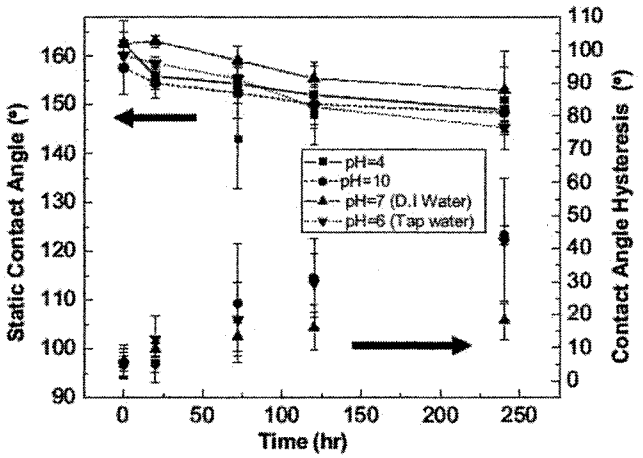

Figure II.25: Contact angle values as a function of time immersion in various pHs [95].

Touzin et al. [105] showed the reduction of hydrophobic properties of plasma-

polymerized fluorocarbon coatings on stainless steel (from 105° to 58°) after four weeks of immersion in distilled water. The XPS results, as shown in Figure II.26, indicated that the reduction of fluorine concentration after four weeks of immersion in water led to a decrease of the contact angle.

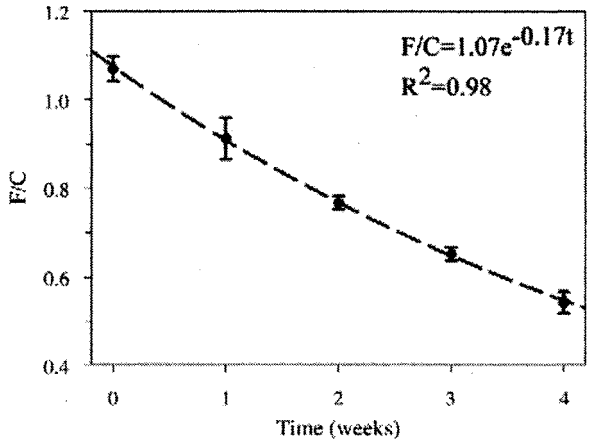

Figure II.26: X-ray photoelectron spectroscopy F/C ratio of plasma-polymerized fluorocarbon coatings deposited on stainless steel as a function of immersion time in distilled water [105].

Furthermore, the topography of these surfaces was analyzed by AFM analysis before and after each week. The results show (Figure II.27) that the roughness of the surface before immersion in water was around 0.8 nm. After one week of immersion, the roughness increased to 2.5 nm and the presence of protrusions on the surface was observed. The roughness started to decrease from 0.9 to 0.6 after four weeks. Smooth and homogeneous surfaces were revealed after four weeks of aging. The mechanism explaining the protrusions could be as follows: water progressively infiltrates the polymeric coating at localized small defects, thus creating the protrusions (which could be bubbles, week 1).

Eventually the water therein dissolves as the coating becomes more hydrophilic: the protrusions smear (week 2) and finally disappear after 3 weeks.

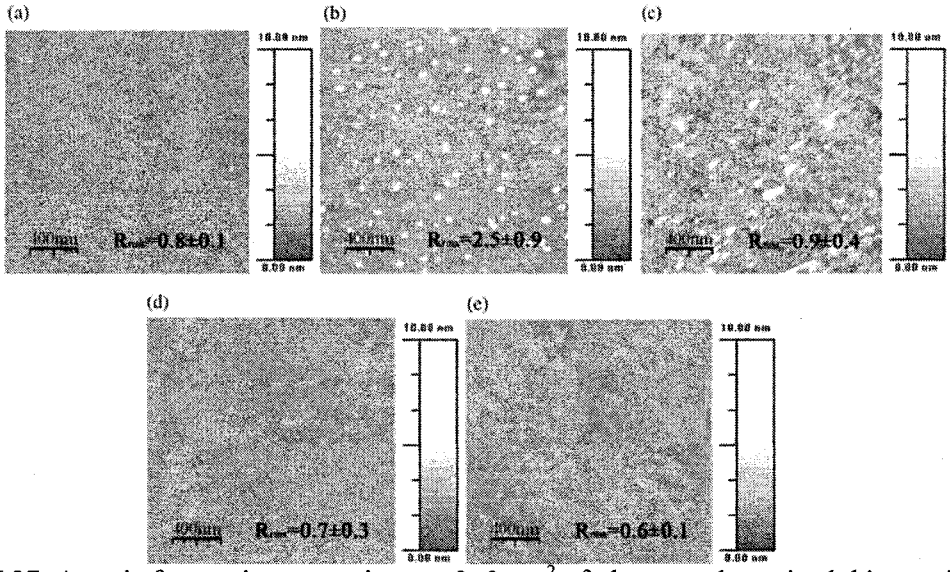

Figure II.27: Atomic force microscopy images 2×2 μm^2 of plasma-polymerized thin coating after: (a) 0 week, (b) 1 week, (c) 2 weeks, (d) 3 weeks and (e) 4 weeks of ageing in D.I. water [105].

II-5-3- Corrosion resistance

Aluminum and its alloy are also widely used in aerospace, marine applications, automotive applications, and so on for their low density, favorable mechanical properties, and resistance to corrosion. Aluminum and its alloys have a natural corrosion protection from the oxide layer, but if exposed to certain substances such as salt, acid, corrosive gases (SO_2), etc., it may corrode. Corrosion in aluminum structure is significant and becomes costly. For example, in 2013, the cost of corrosion related to the aircraft industry in North America will be around 13 billion dollars [107]. Nowadays, the protective corrosion of

metal special aluminum is an important topic in research. Several studies showed that superhydrophobic coatings lead to an increase in the corrosion resistance of surfaces [100,101,106,108].

Yin et al. [106] showed that anodized aluminum could inhibit the corrosion of an aluminum surface up to 61%, while this resistance increased to 96% by depositing a superhydrophobic coating on the surface. As shown in Figure II.28, the corrosion potential of an untreated surface is around -650 mV. By anodizing the surface, this value increases to -620 mV. The corrosion potential of a superhydrophobic coating leads to a positive shift of -400 mV. Furthermore, their results show that a superhydrophobic coating can lead to at most a 300% reduction in the corrosion current density of an aluminum surface compared to an untreated aluminum surface.

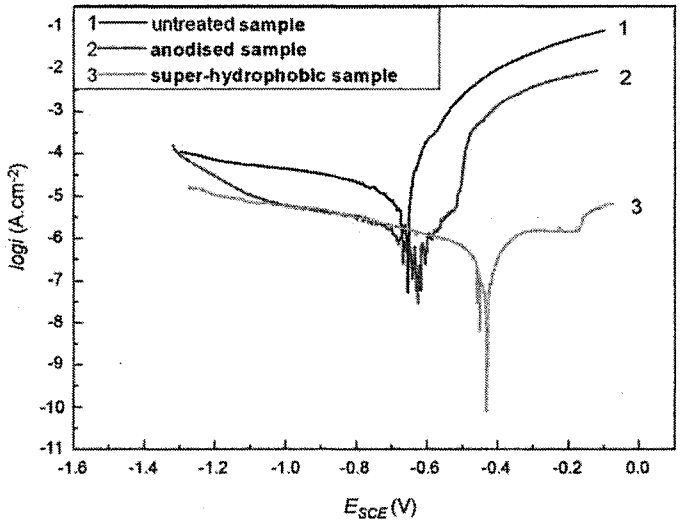

Figure II.28: Potentiodynamic polarization curves of untreated, anodized and super hydrophobic samples for 24 h in sterile seawater at 2mV/s [106].

Ishizaki et al. [100] also showed that the corrosion current density of a superhydrophobic surface was decreased by more than one order of magnitude as compared to that of the uncoated one. These results indicate that the superhydrophobic film has good corrosion resistance.

II-6-Conclusion

We presented a review of the principles on wettability and superhydrophobicity. Literature reviews of new research on icephobic properties of superhydrophobic and hydrophobic coating were presented. The definition of plasma, surface modification by plasma treatment and its advantages were summarized. The effect of plasma processing parameters on the physical-chemical characteristic of a thin film was discussed. From this review, the following can be concluded:

- The input plasma power is one of the key parameters for controlling the fragmentation of precursor in order to deposit the special function on a surface;

- The distance from the monomer inlet or glow discharge with the substrate had a significant effect on the morphology and wettability of a surface;

- Deposition time was considered an effective parameter that controls the thickness of a coating;

- Monomer flow rate can also control the hydrophobicity while it increases the monomer concentration.

Finally, a brief study was done on the stability of superhydrophobic coatings under accelerated aging conditions such as UV degradation, immersion in different pH solutions to simulate rainwater conditions and exposure to an environment.

CHAPTER III

EXPERIMENTAL APPROACH

CHAPTER III

EXPERIMENTAL APPROACH

Introduction

In order to achieve our objective, i.e. the creation of a superhydrophobic surface with icephobic properties, the following steps were taken: 1) anodization of an aluminum surface or immersion in boiling water to obtain a micro/nanostructure, and 2) deposition of a HMDSO-based coating using low pressure plasma polymerization. The Grey-based Taguchi method was used to optimize plasma process parameters in order to obtain a maximum contact angle and a minimum contact angle hysteresis. This chapter deals with the most important techniques that have been used in this work to create surface roughness, low surface energy materials deposition, design of experiment, and physico-chemical characterization of the thin films. To investigate the icephobicity of these coatings, the wind tunnel and centrifugal instrument were introduced. The accelerated UV tester and

different pH solutions were employed in order to understand the durability of the coatings. The corrosion resistance of coating is evaluated using Biologic SP-300 under control of EC-Lab® software.

III-1- Thin film deposition process

The aluminum alloy 6061 coupons (5 cm × 3 cm × 0.15 cm) obtained from Rio Tinto Alcan (Mg 1.0, Si 0.6, Cu 0.28, Cr 0.05, Zn 0.1, Fe 0.25 and Mn 0.15, all in wt %), one of the most common aluminum alloys for aircraft and aerospace components, transport and electrical fittings and connectors, was used as a substrate [109]. Each of these surfaces was cleaned with acetone and distilled water, each for 5 minutes in ultrasonic bath water.

III-1-1- Preparation of micro/nanostructure roughness

As mentioned before, surface roughness and low surface energy material are the dominant factors for superhydrophobicity. Here, anodization methods and immersion in boiling water are used to create the micro/nanostructure roughness on the surface.

III-1-1-1-Anodization method

Anodization is a common electrochemical technology that is used to create an artificial porous oxide layer [110]. This layer is also known as aluminum oxide (Al_2O_3) or Alumina. This layer has several important properties, such as the ability to improve corrosion resistance, abrasion resistance, paint adhesion, and adhesive bonding

characteristics [111]. In an anodizing process, the aluminum workpiece is an anode (positive electrode) and any electronic conductor is a cathode (negative electrode). When the circuit is closed, electrons are withdrawn from the metal at the positive terminal, allowing ions at the metal surface to react with water to form an oxide layer on the metal. The electrons return to the bath at the cathode where they react with hydrogen ions to make hydrogen gas. The following reactions take place during anodization:

✓ At the anode electrode:

$$Al \rightarrow Al^{3+} + 3e^{-} \quad \text{(III.1)}$$

$$2Al^{3+} + 3O^{-} \rightarrow Al_2O_3 \quad \text{(III.2)}$$

$$2Al^{3+} + 3OH^{-} \rightarrow Al_2O_3 \quad \text{(III.3)}$$

✓ At the cathode electrode:

$$2H^{+} + 2e^{-} \rightarrow H_2 \quad \text{(III.4)}$$

✓ The overall process is as follows:

$$2Al + 3H_2O \rightarrow Al_2O_3 + 3H_2 \quad \text{(III.5)}$$

The anodization process was carried out on the coupons of aluminum in the laboratory as described in Figure III.1. The aluminum to be anodized (d) is immersed in phosphoric acid (10%wt, certified grade from LabMat Company) (e) as an electrolyte at a

fixed temperature of 18°C [24]. The temperature was kept constant by the water circulation system (b). In fact, cracks and bursts of the oxide film are generated if porous alumina is formed without temperature control. The process parameters, such as voltage and time, were changed in order to study the variation in wettability. In this study, the voltage was changed from 30 to 70 V for 30 to 90 minutes.

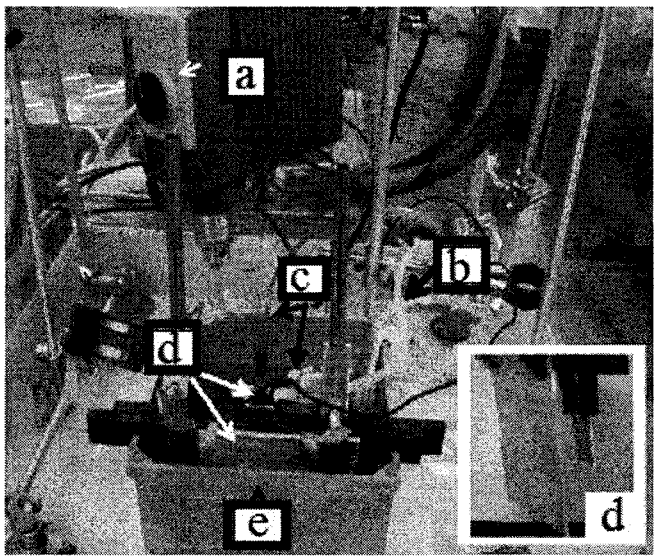

Figure III.1. The anodization set-up, a) Mechanical stirrer, b) Cooling system, c) Connection to power supply, d) Electrodes, and e) Bath.

III-1-1-2- Immersion in boiling water

The aluminum alloy 6061 surface was treated in boiling water. Three reactions can occur within this of temperature. Up to 70°C, aluminum hydroxide (Bayerite- ($Al(OH)_3$)) can be obtained; between 70°C to 350°C, aluminum hydroxide boehmite (AlO(OH)); and above 350°C, aluminum oxide Al_2O_3 [112,113]. In addition to developing the nano-

structure roughness [114], this process also improves the corrosion resistance of an aluminum alloy surface [112,113,115]. In this study, the aluminum coupons were immersed in boiling water for different immersion times, from 3 to 60 minutes (see Figure III.2).

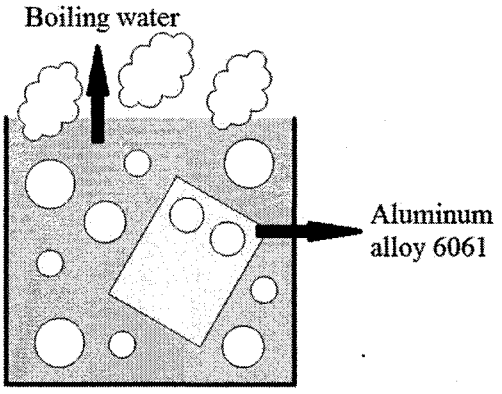

Figure III.2: Schematic of the immersion of aluminum alloy in boiling water.

III-1-2- Plasma polymerization process

Hexamethyldisiloxane [HMDSO, whose chemical formula is $(CH_3)_3$-Si-O-Si-$(CH_3)_3$], was used as an organosilicon precursor with 98% purity from Aldrich. The physical characteristics of this monomer are shown in Table III.1.

Table III.1: Physical characteristic of Hexamethyldisiloxane [116].

Molecular weight	162.38 g/mol
Density	0.764 g/ml at 20 °C
Boiling point	101 °C
Melting point	-59 °C
Flash point	0 °C

The RF plasma polymerization process was carried out in an inductively coupled radio frequency (13.56 MHz) system (HICP-600SB PECVD; Plasmionique Inc) (Figures III.3a-b). After the plasma chamber was evacuated at a pressure of 2×10^{-6} torr, argon gas was introduced. Prior to plasma polymerization of HMDSO (PP-HMDSO), the aluminum alloy surfaces were pre-cleaned and pre-activated for five minutes inside of the plasma reactor. The plasma power in the cleaning stage was 100 W, argon flow rate was set to 50 sccm, and the pressure was 2.66 Pa. This process results in further cleaning and removal of organic contaminations from the surface and increases the adhesion between the coating and the surfaces [117].

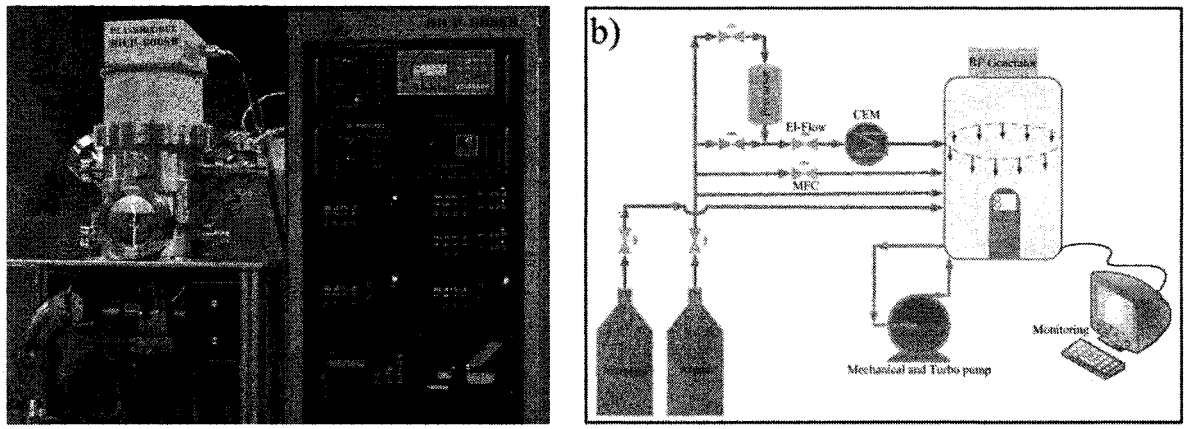

Figure III.3: a) Inductively coupled plasma reactor (CIGELE), b) Schematic of plasma reactor.

After plasma pre-treatment, plasma polymerization was carried out. The HMDSO was mixed with argon as a carrier gas and was subsequently heated at 125 °C in the Controlled Evaporator Mixer (CEM). The inlet flow rate of the carrier gas to the system and the monomer in liquid phase were controlled by a mass flow controller (MFC) and an

EL-Flow (digital mass flow meter and controller), respectively.

In this study, four controlling plasma polymerization parameters were varied: input power from 60 to 120 W, distances between substrate and monomer inlet from 8 to 17 cm, deposition time from 5 to 25 min, and monomer liquid flow rate from 10 to 20 g/hr. The pressure of the reactor and the flow rate of argon gas were fixed at 8 Pa and 20 sccm. Note that the substrate temperature was set at room temperature for all of the experiments.

III-2- Design of Experiment (DOE) technique

The design of experiment (DOE) was used to optimize the effect of the factors in order to make the fewest possible experiments. The Taguchi method is a generally accepted methodology for contemporary experiment design. It utilizes a well-balanced experimental design (allowing a limited number of experimental runs) named orthogonal array design and signal-to-noise ratio (S/N ratio), which serve the objective function to be maximized within the experimental domain. Taguchi uses logarithmic functions to determine the signal-to-noise ratios that optimize the response. In this method, signal-to-noise ratio (S/N) is used to represent a response or quality characteristic based on the largest required S/N and minimal noise factors. The S/N ratio for each response is computed by the following three formulas [117,118]:

• For the nominal best response

$$\frac{S}{N} = -10\, log\left(\frac{1}{nS}\sum_{i=1}^{n} y_i^2\right) \qquad \text{(III.6)}$$

• For the larger-the-better response

$$\frac{S}{N} = -10\ log\left(\frac{1}{n}\sum_{i=1}^{n}\frac{1}{y_i^2}\right) \quad \text{(III.7)}$$

• For the smaller-the-better response

$$\frac{S}{N} = -10\ log\left(\frac{1}{n}\sum_{i=1}^{n}y_i^2\right) \quad \text{(III.8)}$$

Where

- S is the standard deviation,

- y_i is the measured property,

- n is the number of samples in each test trial.

The following method is used for the optimization of a single performance characteristic. However, the Grey relational analysis can be applied to optimize the multiple performance characteristics. The experimental results are firstly normalized between zero and one by this method [119]. The optimal parametric combination is obtained at the highest Grey relational grade value. The optimal factor setting for maximizing the overall Grey relational grade can be performed by the Taguchi method [120]. The Grey relational coefficient ξ_{ij} for the i^{th} performance characteristic in the j^{th} experiment can be expressed as:

$$\xi_{ij} = \frac{min_i min_j|x_i^o - x_{ij}| + \xi\ max_i max_j|x_i^o - x_{ij}|}{|x_i^o - x_{ij}| + \xi\ max_i max_j|x_i^o - x_{ij}|} \quad \text{(III.9)}$$

Where

- x_i^o is the ideal normalized response for the i^{th} performance characteristic ($x_i^o = 1$);

- $\min_i \min_j |x_i^o - x_{ij}|$ is the smallest value of x_{ij};

- $\max_i \max_j |x_i^o - x_{ij}|$ is the largest value of x_{ij};

- ξ is the distinguishing coefficient defined in the range $0 < \xi < 1$.

The overall Grey relational grade is determined by averaging the Grey relational coefficients corresponding to the selected responses [119].

Where,

$$\gamma_j = \frac{1}{m}\sum_{i=1}^{m} \xi_{ij} \qquad \text{(III.10)}$$

- γ_j is the grey relational grade for the jth experiment;

- m is the number of performance characteristics.

In this study, each experiment was repeated three times. The error bars correspond to standard deviation of the mean value of responses.

III-3- Analytical methods

Several physical and chemical characterization techniques were used in this research

work, such as water repellency, surface morphology, surface chemical composition, durability of coating under UV exposure, ice-releasing, immersion in various pH and corrosion.

III-3-1- Wettability

Wettability is a very important parameter of a solid surface. The hydrophobicity/hydrophilicity of a solid surface is usually expressed in terms of wettability, which can be quantified by contact angle measurements. The contact angle is the result of interface/surface tensions (surface free energies) between a liquid and solid surrounded by vapor. The two kinds of contact angle are static contact angle and dynamic contact angle. Measurements of contact angles and sliding angles were carried out by using a Kruss DSA 100 goniometer and a Groz instrument, respectively (see Figures III.4a-b).

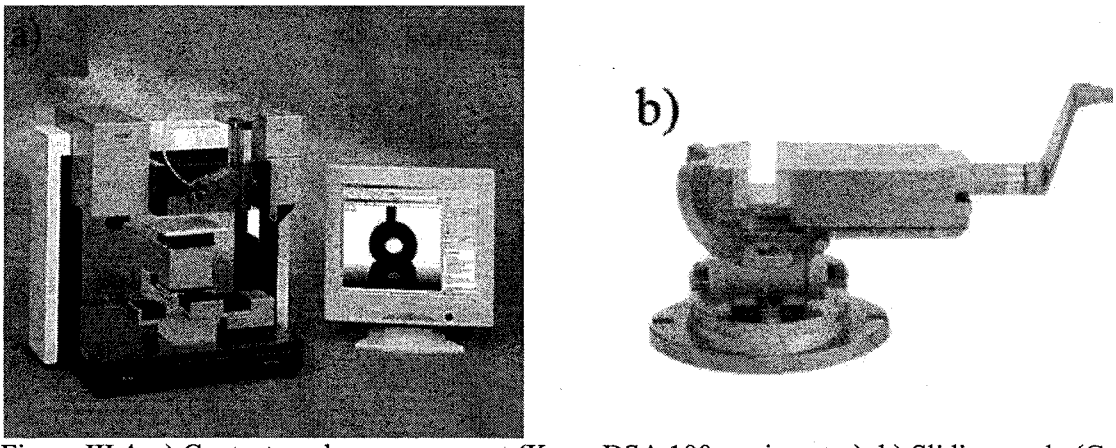

Figure III.4: a) Contact angle measurement (Kruss DSA 100 goniometer), b) Sliding angle (Groz instrument).

III-3-1-1-Static contact angle measurement

Static contact angles are acquired by fitting the symmetric water drops using the Laplace–Young method, which is theoretically considered the most accurate, because it takes into account distorted drop shapes due to liquid weight [25]. The needle disperses the distillated water drop on the surface, and this image is recorded by a video camera. In this study, the distilled water drop volume of 4 μl is used for an average of at least five contact angle values measured over an extended area of the surface.

III-3-1-2- Dynamic contact angle measurement

The dynamic contact angle is defined as a contact angle related to moving liquid fronts [32]. In this study, the contact angle hysteresis and sliding angle were measured as dynamic contact angles.

III-3-1-2-1-Contact angle hysteresis

In the present study, two methods are used to measure the contact angle hysteresis. In the first method, a 4μl water drop is deposited on the surface. The volume of the drop is dynamically increased to 7μl at a rate of 6 μl/min. The advancing angle refers to the maximum angle associated with added volume (see Figure III.5a). Likewise, by withdrawing the liquid drop volume from 7μl to 4 μl, the smallest possible angle upon removing volume is defined as a receding angle (see Figure III.5b). Contact angle hysteresis is defined as the difference between the advancing and the receding contact

angles [121].

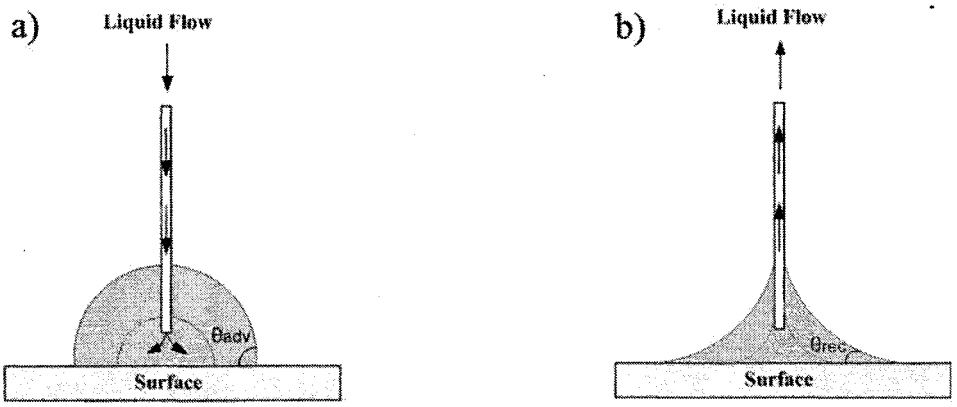

Figure III.5: Schematic diagram showing the a) advancing contact angle and b) receding contact angle in the first method.

In the second method, the advancing and receding contact angles were measured by holding the 4 μl water drop with a stationary needle in contact with the surface. The substrate was moved slowly in one direction by using a micrometric screw. The contact angle at the front of the drop is the advancing angle, and the receding angle occurs at the back of the drop (see Figure III.6). The difference between the advancing and the receding angle is called contact angle hysteresis [122].

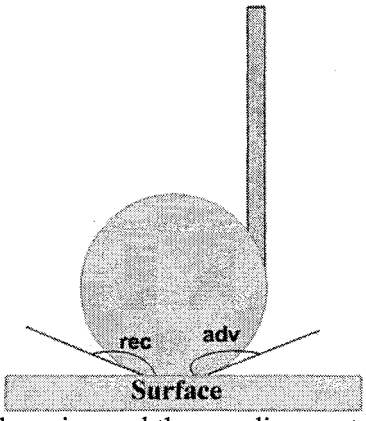

Figure III.6: Schematic of the advancing and the receding contact angles in the second method.

III-3-1-2-2-Sliding angle (SA)

Sliding angle or roll-off angle is another dynamic contact angle obtained by measuring the angle of the sample surface and the horizontal plane at which the liquid drop starts to slide off the surface due to gravity [123,124]. In this study, the Groz instrument has been used to measure the sliding angle. The slope of the surface from the horizontal plate was increased until the water droplet started to incline downward on the surface.

III-3-2- Surface morphology

The surface morphology of coatings was imaged with a Scanning Electron Microscope (SEM, JEOL JSM 6480 LV), an LEO field emission scanning electron microscope (FESEM) and an Atomic Force Microscope (AFM) (Digital Nanoscope IIIa by digital instruments).

III-3-2-1-Atomic force microscopy (AFM)

Atomic force microscopy (AFM) was used to study the surface morphology. The samples were analyzed with a Digital Nanoscope IIIa (see Figures III.7). AFM images were taken in tapping mode at a temperature of 22 °C with an oscillating silicon nitride probe. This technique provided us with three-dimensional images of the surface topography. Furthermore, AFM presented us with detailed topographical information such as root mean square surface roughness (rms), surface skewness (which describes the symmetry and the asymmetry of the coating roughness), and surface kurtosis (which indicates a spiky or bumpy surface). In this study, AFM images were reported for different scales from 1×1 (μm^2) to 10×10 (μm^2) with a scan rate ranging from 0.5 to 1 Hz.

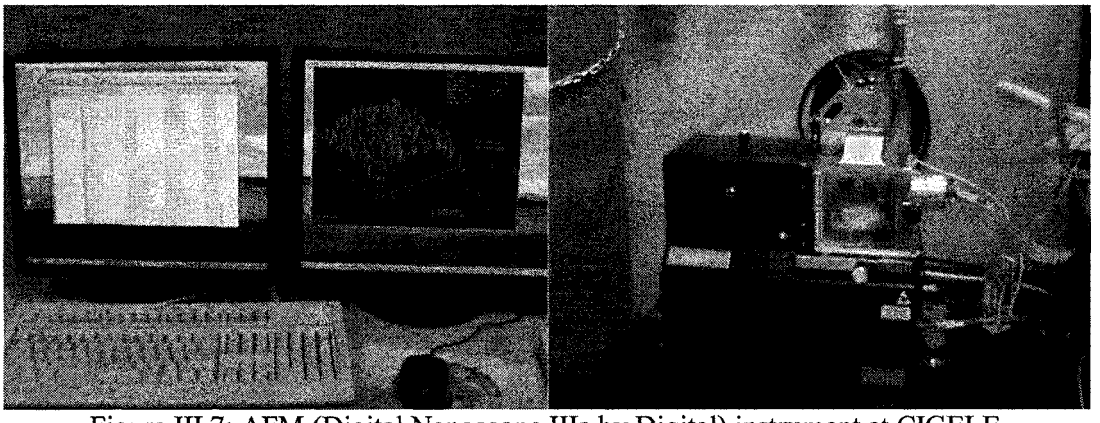

Figure III.7: AFM (Digital Nanoscope IIIa by Digital) instrument at CIGELE

III-3-2-2- Scanning electron microscopy (SEM)

The scanning electron microscope (SEM, JEOL JSM 6480 LV) and an LEO field

emission scanning electron microscope (FESEM) were used in this work to study the surface morphology of the plasma treated substrate (see Figure III.8).

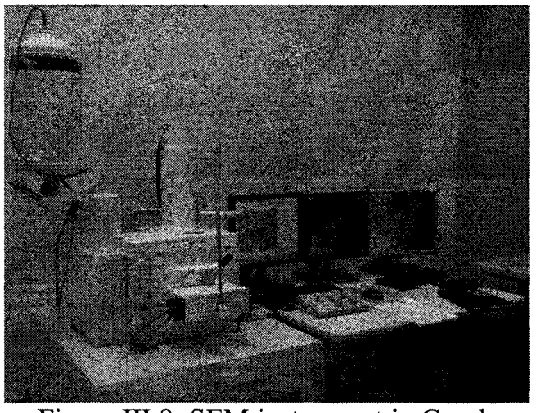

Figure III.8: SEM instrument in Cural.

III-3-3- Surface chemical composition

Fourier-Transform Infrared spectrometry (FT-IR) and X-ray Photoelectron Spectroscopy (XPS) are the techniques used to obtain chemical characterization.

III-3-3-1- Fourier transform infrared spectroscopy (FT-IR)

FT-IR technique is the most popular technique for characterizing the chemical composition of a coating. During an analysis by FT-IR, a sample is subjected to electromagnetic radiation in the infrared region of the spectrum. The wavelengths absorbed by the sample depend upon the nature of the chemical groups present.

In this study, the chemical structure of the deposited films was studied in detail by

using Fourier transform infrared spectroscopy (Perkin-Elmer, Spectrum One) (see Figure III.9). The reflected beam was collected for 24 scans at a resolution of 4 cm^{-1} and in the range of 400-4000 cm^{-1}.

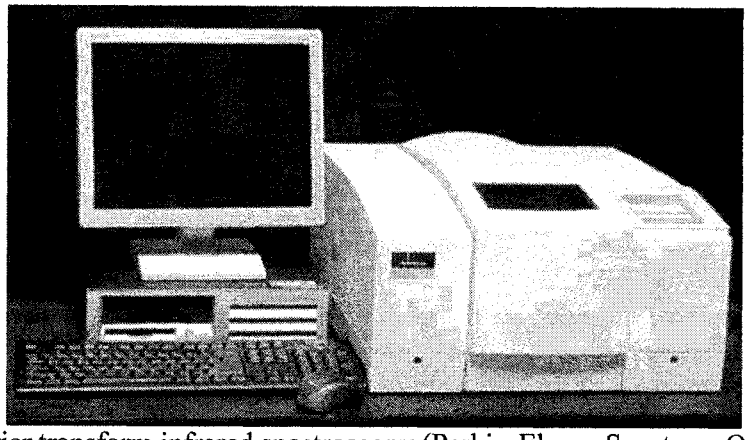

Figure III.9: Fourier transform infrared spectroscopy (Perkin-Elmer, Spectrum One) instrument of UQAC.

III-3-3-2- X-ray photoelectron spectroscopy (XPS)

The surface chemical structure was also examined by X-ray photoelectron spectroscopy (XPS) with a VG ESCALAB 3 Mk II surface analytical instrument (see Figure III.10). The Mg K achromatic X-ray source was operated at 216 W (12 kV, 18 mA). The inelastic background was subtracted using Shirley's method. The analyzed surface area was 2 × 3 mm^2 with a depth of 6-10 nm.

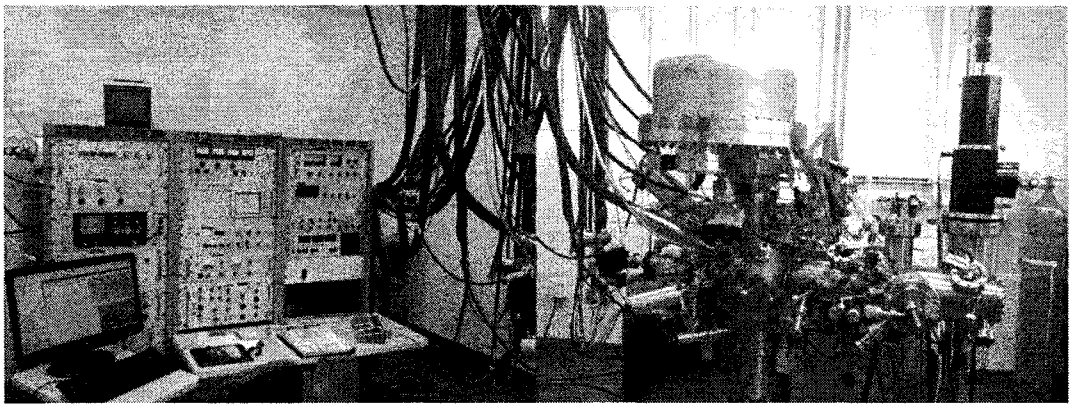

Figure III.10: XPS VG ESCALAB 3 Mk II instruments, Ecole polytechnique.

III-3-4- Coating thickness measurement (Ellipsometry)

The thickness was measured by RC2 ellipsometry from J.A. Woollam Co. This is a dual ellipsometry compensator equipped with QTH/D2 lamps and a CCD detector. The angles of incidence were 45, 55, 65, 75 degrees and the wavelength range was 190 to 1000 nm.

III-3-5- Ice adhesion test

The icephobic properties of the developed surfaces were studied by ice accumulation in the icing wind tunnel and ice detachment in a centrifugal instrument.

III-3-5-1-Icing wind tunnel

The atmospheric ice (glaze) was accumulated by spraying super-cooled micro-droplets of water on the substrates that were placed in the wind tunnel (Figure III.11a) and mounted on the end of a supporting beam (see Figure III.11b). The parameters for wind

tunnel tests have been summarized in Table III.2 [125].

Table III.2: Conditions of accumulated ice in the wind tunnel.

Air pressure	100 ± 0.1 kPa
Water pressure	325 ± 0.1 kPa
Temperature	-10 ± 0.8 °C
Velocity	10 ± 0.1 m/sec
Droplet size	67 μm

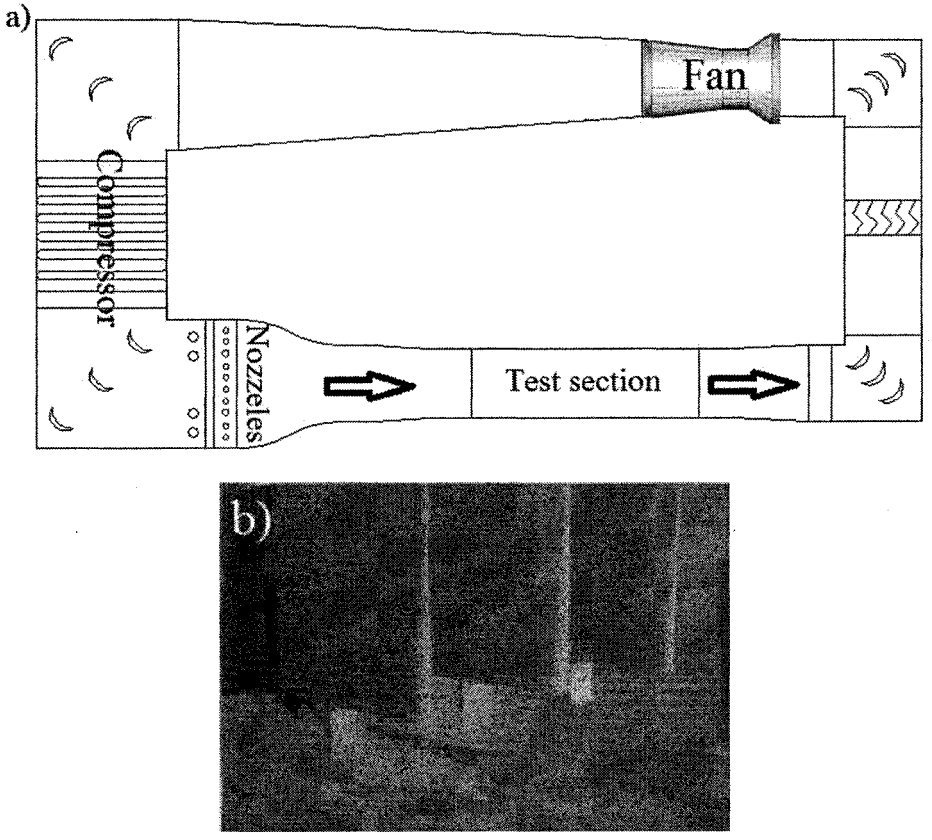

Figure III.11: a) Schematic of the wind tunnel test at CIGELE and b) A view of sample beams in the tunnel

III-3-5-2- Centrifugal instrument

After ice accumulation, samples underwent an ice adhesion strength test at a temperature of -10 °C by a centrifuge instrument (see Figure III.12) in order to compare the treated and untreated aluminum samples. Ice covered surface were placed on the beams within a centrifugal instrument. The beams were rotated by increasing speed from 0 to 5500 rpm. By noting the rotation speed at the ice detachment, the ice adhesion force was calculated.

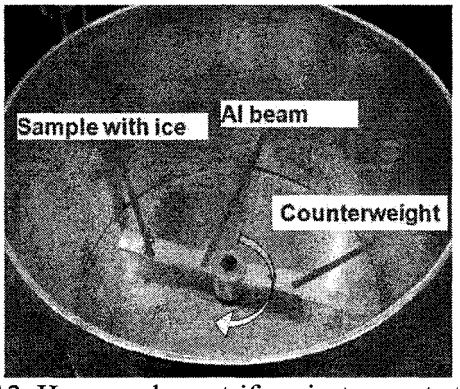

Figure III.12: Homemade centrifuge instrument at CIGELE.

The ice adhesion force is calculated from:

$$F = mr\omega^2 \qquad \text{(III.11)}$$

Where

- m is the ice mass (kg),
- r is the beam radius (m),

- ω is the rotation speed (rad/s).

The shear stress (kPa) is then calculated as:

$$\tau = F/A \quad \text{(III.12)}$$

Where

- A is the iced surface area (m^2),
- F is ice adhesion strength (N).

The adhesion reduction factors (ARF) were computed to reduce the bias caused by potential experimental errors. ARF is the ratio of ice shear stresses of untreated aluminum to treated aluminum.

$$ARF = \tau_{(\text{aluminum without coating})}/\tau_{(\text{aluminum with coating})} \quad \text{(III.13)}$$

It was mentioned that the Centrifuge adhesion test has many advantages. The process is simple and it is performed inexpensively, and timely; it is repeatable with standard deviation 25%. The centrifuge adhesion test is also more representative of accreted atmospheric ice and has a real time data collection. Finally, it can be adapted to the flat surface for exposure to environmental elements and repeat testing [126].

III-3-6- QUV accelerated weathering Tester

Sunlight is an important factor in the damage of material surfaces. Ultraviolet (UV)

light has been recognized as the cause of most of this damage. For this reason, the accelerated UV weathering test is used to simulate damaging outdoor conditions in a controlled laboratory environment (see Figure III.13). The substrate with polymeric coating was exposed to a UVA-340 fluorescent lamp. The test cycle was 8-hours with 0.89W/m^2 irradiance and a temperature of 60°C in the QUV accelerated weathering tester (ASTM G154).

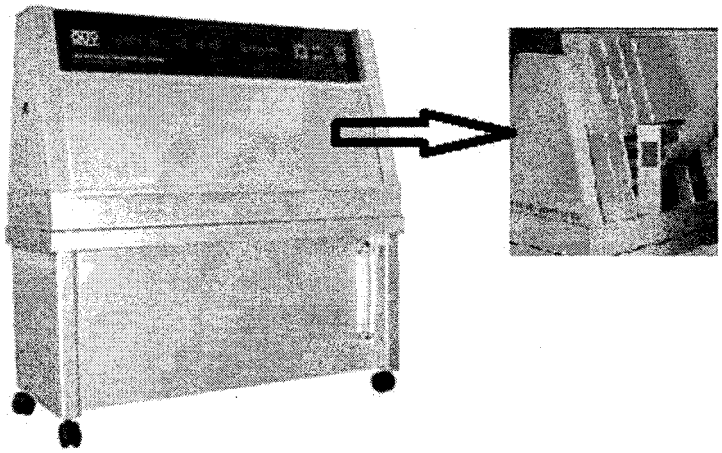

Figure III.13: QUV accelerated weathering instrument.

The annual mean of UV radiant exposure (295-385 nm) in a site north of Ottawa in Canada was estimated at 172 MJ/m^2 for one year, based on several years of data gathering [127]. Also, the irradiance from a narrow wavelength band (340nm) to a wider wavelength range (295-385nm) can be converted as follows:

$$10\ \text{kJ/m}^2\ (\text{at } 340\ \text{nm}) \cong 1\ \text{MJ/m}^2\ (\text{at } 295\text{-}385\ \text{nm}) \qquad \text{(III.14)}$$

Therefore, the required number of hours of UV exposure in the mentioned apparatus equal to one year of natural exposure can be calculated as follows [128]:

$$1720000\ J/m^2\ (\text{at } 340nm) = 0.89\ W/m^2\ (\text{at } 340nm) \times \text{Time (sec)} \quad \text{(III.15)}$$

$$\text{Time (sec)} \approx 1933200\ \text{sec} \approx 537\ \text{hr} \quad \text{(III.16)}$$

Then, 537 hours of exposure to the artificial UV instrument is equal to one year of sunlight exposure.

III-3-7- Electrochemical test (Corrosion)

Metal corrosion is an electrochemical reaction that involves oxidation of the anode into a positive ion, which is released from the solid metal. Potentiodynamic polarization is one of the electrochemical techniques for studying the corrosion behaviors of corrosion potential, corrosion current, and resistance polarization.

A plot of log (I_{corr}) versus E_{corr}, known as a Tafel plot, has been used to determine corrosion parameters (see Figure III.14). The slopes of this diagram are determined as the cathodic slope (β_c) and the anodic slope (β_a). The cathodic slope contains information concerning the kinetics of the reduction reaction occurring for a particular system. The particular features of the anodic slope depend strongly on the metal electrolyte system.

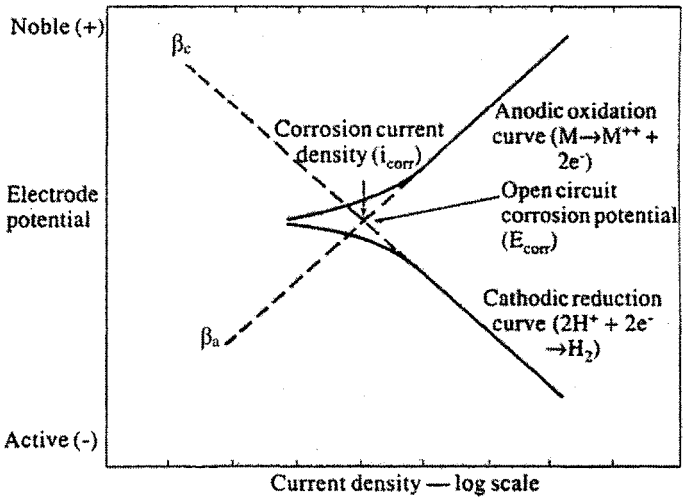

Figure III.14: Tafel plot for anodic and catholic slopes [129].

Polarization resistance is defined as the slope of the potential-current density (DE/Di) curve at the free corrosion potential, yielding the polarization resistance (Rp) that can be related (for reactions under activation control) to the corrosion current by the Stern-Geary equation [129]:

$$R_P = \frac{1}{(2.3 i_{corr})} \left(\frac{\beta_a \beta_c}{\beta_a + \beta_c} \right) \qquad \text{(III.17)}$$

Where

- R_p: Polarization resistance (Ω)
- I_{corr}: Current density (A)
- β_c: The cathodic Tafel slope
- β_a: The anodic Tafel slope

Electrochemical experiments were conducted by using a Biologic SP-300 under control of EC-Lab® software (see Figures III.15a-b). A set of three electrodes were used for the electrochemical measurements, in which the working electrode was the sample, the reference was a saturated calomel electrode (SCE), and the auxiliary was a platinum electrode. The electrolyte solution, 3.5 wt. % NaCl, was prepared by dissolving 35g of NaCl in a 1L glass flask [ASTM 47].

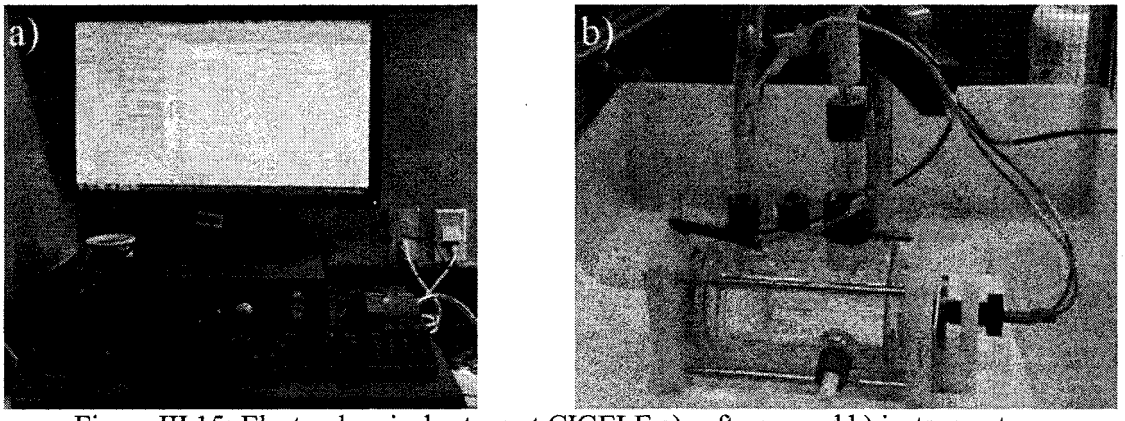

Figure III.15: Electrochemical set-up at CIGELE a) software and b) instrument

Prior to each experiment, samples were immersed in the electrolyte solution for 24 hours. The open circuit potential (OCP) was used to record the potential for 15 minutes. Potentiodynamic polarization experiments were carried out at the scan rate of 10 mV/s from -250 to +250 (mV) through an open circuit potential. The corrosion data of three surfaces, which are untreated aluminum, anodized aluminum, and plasma polymerized HMDSO coating on an anodized aluminum, were determined by the Tafel plot and a resistance polarization curve.

CHAPTER IV

PLASMA POLYMERIZED HMDSO COATING

CHAPTER IV

PLASMA POLYMERIZED HMDSO COATING

Introduction

Plasma polymerization is a suitable technique for depositing a thin film with widespread applications in the domains of biomedicine [130], biofouling [131], anti-corrosion [132] and anti-icing [133]. In this part of the study, a superhydrophobic coating is developed by using the plasma polymerization method. Two different methods, anodization and boehmite, are used to create the roughness of the surface on Al substrate. The effect of anodization parameters such as voltage and time, and the influence of immersion time in boiling water are studied over the superhydrophobic behaviour (high contact angle and low contact angle hysteresis). PP-HMDSO coating is deposited in a plasma reactor as described previously. In order to study the effect of plasma processing parameters simultaneously, the Grey-based Taguchi method is used (as a DOE technique). These parameters have been

optimized to achieve the highest possible contact angle and the lowest possible contact angle hysteresis.

IV-1- Creation of surface roughness

As mentioned before, anodization and boehmite methods were used to create surface roughness at a micro/nano-metric scale on the surface of aluminum alloys 6061. The presence of a rough micro-nanostructure on the aluminum surfaces is investigated by applying SEM and AFM analyses. In addition, the effects of various parameters of these two surface treatment methods on the wettability of the PP-HMDSO coating are studied by measuring the static and dynamic contact angles.

IV-1-1- Anodization process

In order to optimize the anodization parameters, the voltage is varied from 30 V to 70 V for the duration of 30 to 90 minutes, while the temperature during the anodization of aluminum alloy is kept constant at 18°C. In other words, each parameter has been varied individually.

The effect of anodization time on the contact angle of the PP-HMDSO coating deposited on an anodized aluminum surface at 50V was shown in Figure IV.1a. At 30 minutes anodization time, the contact angle of 139 ± 3 ° is attained. By increasing the anodization time to 90 minutes, the contact angle increases up to 158 ± 3 °. These results show that the contact angle of the surface varies on the anodization time. Figure IV.1b

shows the effect of the voltage at 90 minutes, which is the time of anodization. These results show slight improvement of the contact angle at 50 V; however, there is no significant variation in the contact angle values when voltages vary from 30 V to 70V.

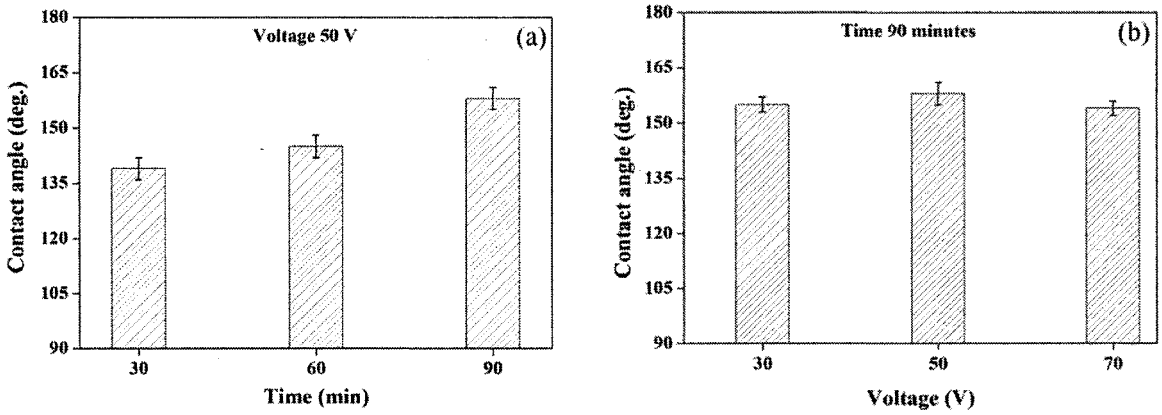

Figure IV.1: Contact angle of the PP-HMDSO coating deposited on an anodized aluminum surface as a function of a) anodization time and b) anodization voltage.

Several works done at CIGELE have shown that a high contact angle of different coatings can be obtained at voltage 50 V for the duration 90 minutes [6,7,24]. Therefore, based on our results and the previous works done at CIGELE, the optimum condition of anodization was fixed at the voltage 50V and the temperature 18 °C for 90 minutes.

The SEM image of the anodized aluminum surface at 50 V and 90 minutes is depicted in Figure IV.2. It exhibits the presence of a pores with a diameter of about 80-160 nm as a "hexagonal bird's nest" structure separated by thinner pore walls.

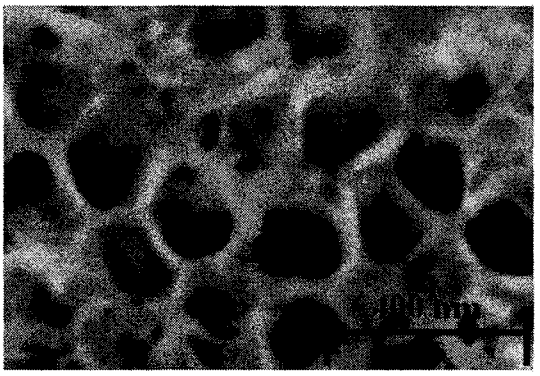

Figure IV.2: SEM image of the anodized aluminum surface.

IV-1-2- Boiling water treatment

The aluminum alloy surface is treated with boiling water to develop nano-pore structure films. This method is called boehmitage (formation of boehmite, $Al_2O_3 \cdot H_2O(s)$), and is used industrially to improve the corrosion properties of aluminum [112,134]. The results of the contact angle measurement of aluminum immersed in boiling water shows that the surface has hydrophilic properties due to the presence of polar components [135,136]. Also, the porosity and morphology of the substrate are changed by different immersion times [25,114,137].

The evaluation of contact angle and contact angle hysteresis of the PP-HMDSO coatings deposited on water treated aluminum as a function of immersion time in boiling water is depicted in Figures IV.3a-b. The contact angle of the PP-HMDSO coating deposited on untreated aluminum is around 115°. The PP-HMDSO coating on a surface immersed in boiling water shows superhydrophobic properties for an immersion of 3 to 60 minutes. A contact angle around 161 ± 2 ° is attained for 3 to 35 minute immersion times.

For immersions of more than 60 minutes, the contact angle decreases to 132 ± 2° (see Figure IV.3a). The contact angle hysteresis decreases when the immersion time goes up from 3 to 5 minutes. Immersion times above 5 minutes lead to an increase of the contact angle hysteresis (see Figure IV.3b). As our objective is to have a high contact angle and a low contact angle hysteresis, the immersion time of 5 minutes is determined to be optimal.

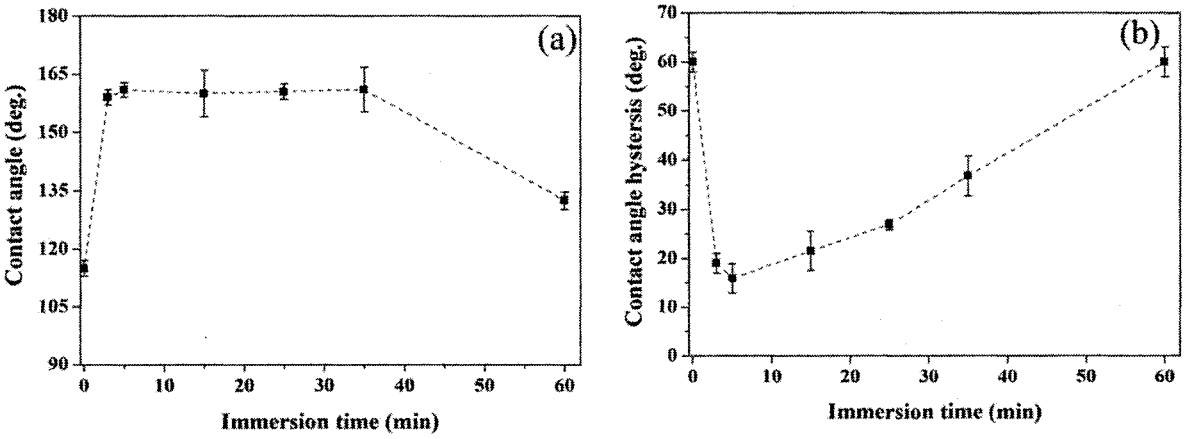

Figure IV.3: Variation of a) contact angle and b) contact angle hysteresis of the PP-HMDSO coating deposited on water-treated aluminum surfaces versus different immersion times in boiling water.

IV-2- Process of plasma polymerized HMDSO coating

Plasma pre-treatment can be used to clean and activate the surface thus improving the adhesion between the substrate and the thin film coating [66,138–140]. The effect of argon plasma pre-treatment on the water treated and anodized aluminum surfaces before the PP-HMDSO coating is presented in Figures IV.4a-b.

According to Figure IV.4a, the contact angle of the PP-HMDSO coating deposited on

a water treated aluminum surface without any pretreatment is about 143°. However, by using the argon pre-treatment before PP-HMDSO coating the surface, the contact angle increased to about 161°. Furthermore, the contact angle of the PP-HMDSO coating deposited on an anodized aluminum surface without pre-treatment is 145° while this value increased up to 158° with pre-treatment, as shown in Figure IV.4b. In fact, the argon plasma pre-treatment before the deposition of a HMDSO coating may activate the surface as well increase the adhesion of coating on the surface [130, 133].

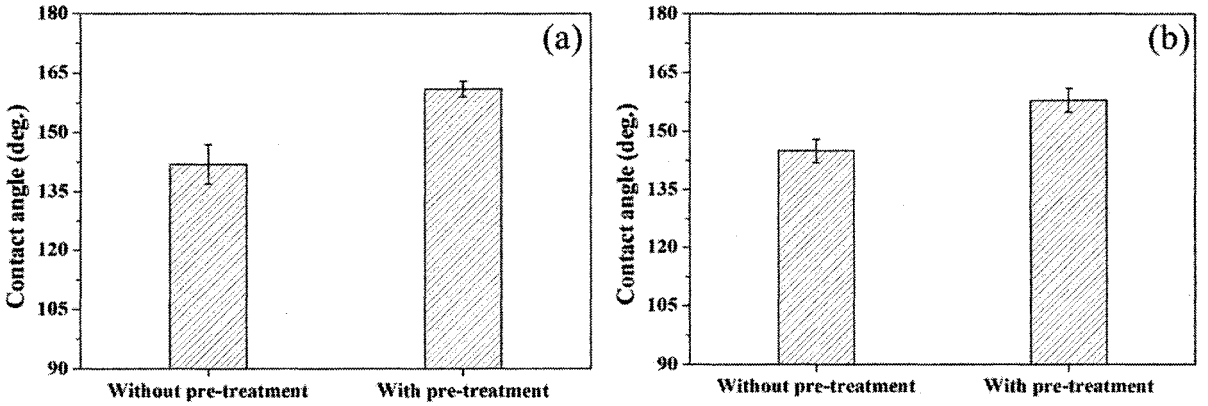

Figure IV.4: Evaluation of the contact angle of the PP-HMDSO coating deposited on a) a water-treated aluminum surface and b) an anodized aluminum with and without pre-treatment.

Table IV.1 presents the contact angle of different treated and untreated surfaces. The contact angle of the untreated aluminum surface was around ~ 90°. After the deposition coating of PP-HMDSO on the aluminum surface, the contact angle increased to around ~ 115°. It should be noticed that the maximum contact angle attainable on a flat surface by lowering the surface energy does not exceed 120° [14]. The results of wettability on

anodized aluminum and water-treated surfaces show that the water droplet was spread on the anodized and boiling water-treated aluminum surfaces, and the contact angles were about 12° and 17°, respectively. In fact, the presence of a polar group (such as –OH) on the water treated aluminum surfaces can facilitate the hydrogen bond or cause electrostatistic attraction between the water molecules and these surfaces [142]. Moreover, the 3-D capillary effect, due to the wicking and imbibitions in the broken sheets and nano-pores of the anodized aluminum surface, can lead to a quick spread of the water droplet on the surface [143]. As a result, the surfaces became hydrophilic after an anodizing and immersion in boiling water.

The contact angle of the PP-HMDSO coating deposited on anodized and water-treated aluminum surfaces showed superhydrophobic properties with a contact angle of about ~158° and ~161°, respectively. As a result, the presence of micro/nano structured roughness and low surface energy material on the surface caused the superhydrophobic characteristics of these surfaces.

Table IV.1: Comparison of wettability of untreated and treated aluminum surfaces.

Name	Contact angle	Figure
Untreated aluminum surface	90°	
PP-HMDSO film deposited on aluminum surface	115°	
Anodized aluminum surface	12°	
Water-treated aluminum surface	17°	
PP-HMDSO film deposited on anodized aluminum surface	158°	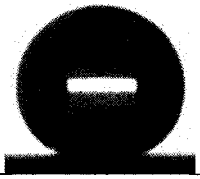
PP-HMDSO film deposited on water-treated aluminum surface	161°	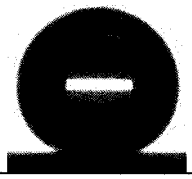

In order to study the chemical composition of the PP-HMDSO coating deposited on anodized and water treated aluminum surfaces, a FT-IR analysis was carried out. The FT-IR spectra of thin films of the PP-HMDSO coating deposited on anodized and water-treated aluminum surfaces are presented in Figures IV.5a-b.

The results show the presence of the peak corresponding to the CH_3 rocking in Si-$(CH_3)_2$ at 800 cm^{-1}, the Si-CH_3 rocking vibration in Si-$(CH_3)_3$ at 840 cm^{-1} and the Si-O-Si asymmetric stretching bonds occurring at around 1000-1150 cm^{-1}. In addition, the bands of the CH_3 symmetric bonding in Si-CH_3 present at 1260 cm^{-1} and the stretching of CH_x (x=1, 2, 3) symmetric and asymmetric occurred at around 2900–2960 cm^{-1} [43,76]. Furthermore,

the FTIR spectrum shows a broad absorption band at 3650-3200 cm-1 which can be attributed to O-H stretching mode of water molecules (Figure IV.5a). It also shows an Al-O stretching vibration band at 1700-1500 cm^{-1} (Figure IV.5b). These results confirm the presence of PP-HMDSO films on the surface of Al alloy.

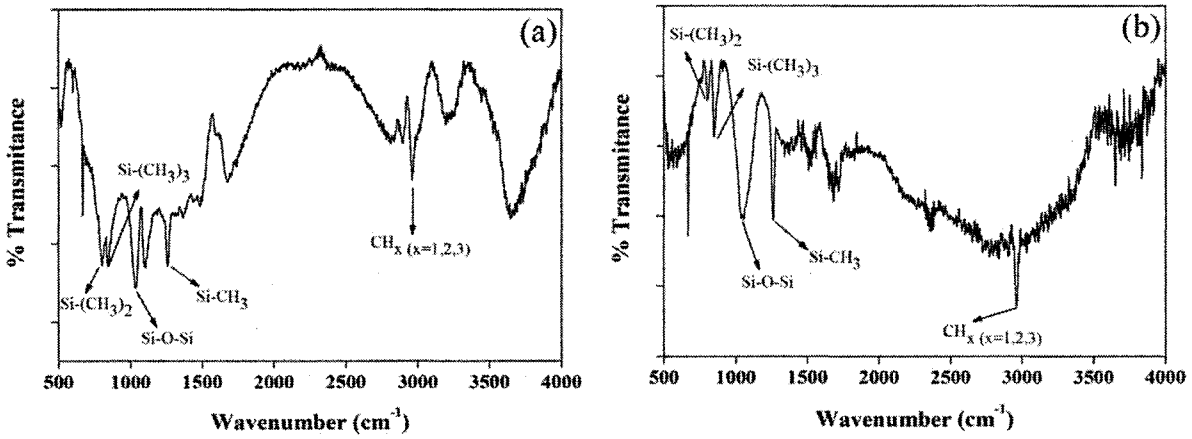

Figure IV.5: FT-IR spectrum of the PP-HMDSO coating on (a) water-treated aluminum surface and (b) anodized aluminum surface.

SEM analysis was used to study the surface morphology after coverage by the PP-HMDSO coating. SEM images of the anodized and water treated aluminum surfaces before and after the PP-HMDSO coating are presented in Figures IV.6a-d.

As shown in Figure IV.6a, the structure of the aluminum surface immersed in boiling water for 5 minutes exhibits a flower-like structure with a wide petal size and thick cell walls. After depositing the PP-HMDSO film on a water-treated aluminum surface the structure is significantly changed in that the surface was filled with a homogenous short fibrous structure (Figure IV.6b). On the anodized surface, the pores formed a "hexagonal

bird's nest" structure separated by thinner pore walls as shown in Figure IV.6c. After covering by PP-HMDSO coating on anodized aluminum, the presence of a coral-like nanostructure was observed (see Figure IV.6d). Furthermore, the presence of a white coating of PP-HMDSO film deposited on anodized and water-treated aluminum surfaces was also noted. The research work done by *Ji* et al. [43] also showed that the atmospheric pressure plasma polymerized HMDSO coating deposited on polyester fiber as a substrate leads to the presence of a white layer of a silicon component.

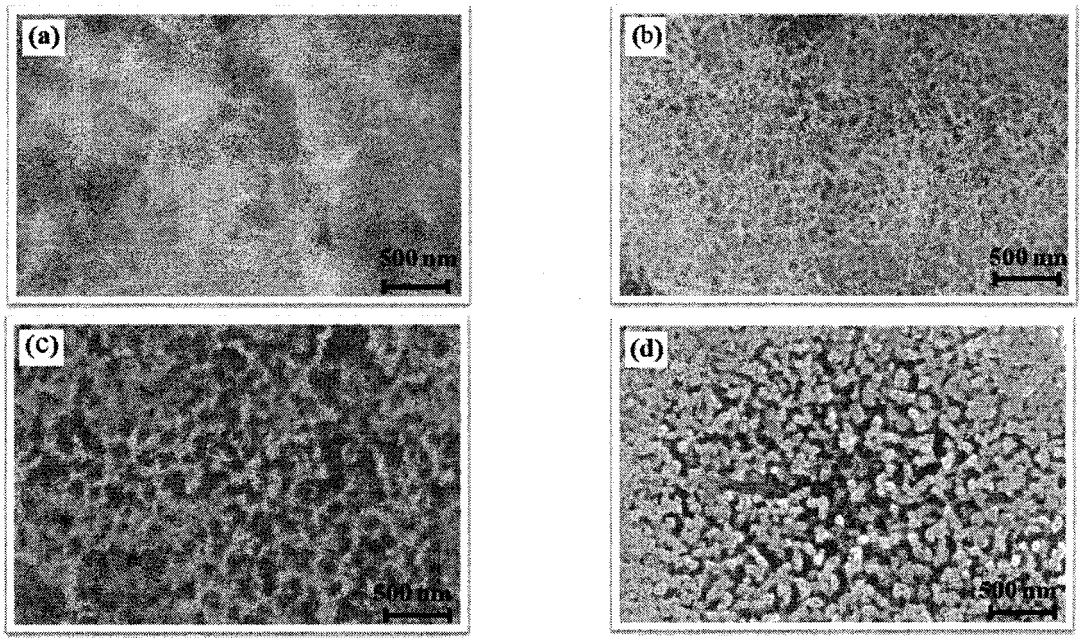

Figure IV.6: The SEM micrograph of a) aluminum immersed in boiling water, b) the PP-HMDSO coating deposited on a water-treated aluminum surface, c) anodized aluminum and d) PP-HMDSO coating deposited on an anodized aluminum surface.

Several plasma parameters can affect the chemistry of the resulting film, such as input power, distance from monomer inlet, deposition time, monomer flow rate, gas flow

rate, temperature, and pressure. Many studies report the influence of these individual on water-repellency of a coating [77,78,144,145]. In the present study, the influences of four plasma parameters are studied using the Grey-based Taguchi method in order to optimize the wettability of the resulting thin film.

IV-3- Optimization of plasma process parameters

In this section we will study the effect of the following plasma process parameters, at three levels; input power, deposition time; monomer flow rate, and distance from the monomer inlet. Their notations, unit and values at different levels are listed in Table IV.2.

It should be noted that, based on the full factorial experiments method in our present system, these four parameters and three levels would require $3^4 = 81$ tests. That represents a huge experimentation cost.

Table IV.2: Plasma process parameters and their levels.

Parameters	Notations	Units	Levels of factors		
			1	2	3
Input power	P	W	60	90	120
Monomer Flow rate	F	g/hr	10	15	20
Deposition time	T	min	5	15	25
Distance from monomer inlet	D	cm	8	13	17

Taguchi's factorial experiment approach reduces the number of experimental runs. For this system (four parameters at three levels), Taguchi's L9 orthogonal array consisting of 9 sets of data has been selected to optimize the multiple performance characteristics of

the high contact angle and the low contact angle hysteresis on the PP-HMDSO coating deposited on water treated and anodized surfaces (see Table IV.3 and Table IV.4).

Table IV.3. Orthogonal array L9 of the experimental runs and results of contact angle and contact angle hysteresis of the PP-HMDSO coating on a water-treated aluminum surface.

Test No.	P (W)	T (min)	F (g/hr)	D (cm)	Contact angle of the PP-HMDSO film on a water-treated aluminum surface (°)	Contact angle hysteresis of the PP-HMDSO film on a water-treated aluminum surface (°)
1	60	5	10	8	154 ± 3	24 ± 1
2	60	15	15	13	161 ± 4	32 ± 4
3	60	25	20	17	159 ± 3	13 ± 3
4	90	5	15	17	159 ± 2	35 ± 4
5	90	15	20	8	124 ± 2	47 ± 5
6	90	25	10	13	115 ± 3	49 ± 4
7	120	5	20	13	148 ± 3	46 ± 3
8	120	15	10	17	125 ± 2	55 ± 1
9	120	25	15	8	114 ± 2	33 ± 4

Table IV.4: Orthogonal array L9 of the experimental runs and results of the contact angle and contact angle hysteresis of a PP- HMDSO coating on an anodized aluminum surface.

Test No.	P (W)	T (min)	F (g/hr)	D (cm)	Contact angle of the PP-HMDSO film on an anodized aluminum surface (°)	Contact angle hysteresis of the PP-HMDSO film on an anodized aluminum surface (°)
1	60	5	10	8	155 ± 3	24 ± 5
2	60	15	15	13	159 ± 5	34 ± 3
3	60	25	20	17	162 ± 3	13 ± 3
4	90	5	15	17	158 ± 2	33 ± 4
5	90	15	20	8	120 ± 1	47 ± 2
6	90	25	10	13	116 ± 5	48 ± 2
7	120	5	20	13	138 ± 4	49 ± 1
8	120	15	10	17	118 ± 5	55 ± 2
9	120	25	15	8	115 ± 5	35 ± 4

Normally, the Taguchi method is used for optimizing a single response. In this study, the Grey-based Taguchi method is used to optimize multiple responses (the highest contact angle and the lowest contact angle hysteresis). The contact angle and the contact angle hysteresis have been normalized (between 0-1) to calculate the Grey relational generation. The normalized contact angle and contact angle hysteresis of the PP-HMDSO coating deposited on water treated and anodized aluminum surfaces for each set of the plasma process parameters are presented in Table IV.5. Then, the Grey relational coefficient for each response of a PP-HMDSO coating deposited on water-treated and anodized aluminum surfaces has been calculated by using Equation III.9 (see Table IV.6 and Table IV.7). Based on the literature [145], the value of ξ was set as 0.5. The grey relational grade can be calculated by using Equation III.10, which is the overall representative of both responses, as shown in Table IV.6 and Table IV.7.

Table IV.5: Normalized data of the experimental results for each performance characteristic of the PP-HMDSO coating deposited on boiling water treated and anodized aluminum surfaces.

Test No.	Normalized contact angle of the PP-HMDSO coating on		Normalized contact angle hysteresis of the PP-HMDSO coating on	
	Water-treated	Anodized	Water-treated	Anodized
1	0.85	0.85	0.26	0.26
2	1.00	0.94	0.45	0.50
3	0.96	1.00	0.00	0.00
4	0.96	0.91	0.52	0.48
5	0.21	0.11	0.81	0.81
6	0.02	0.02	0.86	0.83
7	0.72	0.49	0.79	0.86
8	0.23	0.06	1.00	1.00
9	0.00	0.00	0.48	0.52

Table IV.6: Pre-processing data of the experimental results for each performance characteristic of the PP-HMDSO coating deposited on a water treated aluminum surface.

Test No.	Grey relational coefficient of the PP-HMDSO coating on a water treated aluminum surface		Grey relational grade of the PP-HMDSO coating on a water treated aluminum surface
	First response (contact angle)	Second response (contact angle hysteresis)	
1	0.770	0.404	0.587
2	1.000	0.477	0.739
3	0.922	0.333	0.627
4	0.922	0.512	0.717
5	0.388	0.724	0.556
6	0.338	0.778	0.558
7	0.644	0.700	0.672
8	0.395	1.000	0.697
9	0.333	0.488	0.411

Table IV.7: Pre-processing data of the experimental results for each performance characteristic of the PP-HMDSO coating deposited on an anodized aluminum surface.

Test No.	Grey relational coefficient of the PP-HMDSO coating on an anodized aluminum surface		Grey relational grade of the PP-HMDSO coating on an anodized aluminum surface
	First response (contact angle)	Second response (contact angle hysteresis)	
1	0.770	0.404	0.568
2	0.887	0.500	0.665
3	1.000	0.333	0.667
4	0.855	0.488	0.658
5	0.359	0.724	0.541
6	0.338	0.750	0.544
7	0.495	0.778	0.646
8	0.348	1.000	0.674
9	0.333	0.512	0.423

Now, the multi response problem has been transformed into a single equivalent response. Therefore, the higher Grey relational grade means that the corresponding parameter combination is closer to the optimum [119,120]. Thus, Taguchi's method was

used to obtain the higher Grey relational grade with regard to robustness in signal-to-noise (S/N) ratio based on the larger-the-better criterion Equation III.2, as shown in Table IV.8.

The mean responses for S/N ratio of PP-HMDSO films on water-treated and anodized aluminum surfaces for each set of the plasma process parameters are shown in Table IV.9 and Table IV.10, and they are represented graphically in Figure IV.7a-b.

Table IV.8: The Signal-to-noise (S/N) ratio of Grey relational grade of the PP-HMDSO coating on water-treated and anodized aluminum surfaces.

Test No.	P (W)	T (min)	F (g/hr)	D (cm)	S/N ratio of the PP-HMDSO coating on	
					Water-treated surface	Anodized surface
1	60	5	10	8	-4.625	-4.625
2	60	15	15	13	-2.631	-3.180
3	60	25	20	17	-4.048	-3.522
4	90	5	15	17	-2.891	-3.460
5	90	15	20	8	-5.094	-5.329
6	90	25	10	13	-5.068	-5.287
7	120	5	20	13	-3.454	-3.927
8	120	15	10	17	-3.129	-3.426
9	120	25	15	8	-7.726	-7.478

Also, the difference between the highest and lowest values of the S/N ratio is an indicator with regard to the influence of a parameter. So, the rank of each parameter was determined by the difference between the highest and the lowest S/N ratio. From the results obtained, in Table IV.9 and Table IV.10, it is clear that D (i.e. the distance from monomer inlet) the greatest contributor to the overall water repellency (Max(S/N) - Min(S/N) = 2.46 and 2.34). The factors P (i.e. the plasma power) and T (i.e. deposition time) also provided a

fairly large contribution to the plasma polymer coating hydrophobicity. On the other hand, the monomer flow rate (F) played a minor role in the water repellency of the micro/nano-coating. Therefore, the order of importance of the controlling parameters on water repellency of PP-HMDSO coating was: D>T>P>F.

Table IV.9: The response effects of the S/N ratios and their ranking of the PP-HMDSO coating deposited on a water-treated aluminum surface.

Plasma Parameters	Means of S/N ratio of the PP-HMDSO coating on a water-treated surface			Max(S/N)-Min (S/N)	Ranking
	Level 1	Level 2	Level 3		
P (W)	-3.77	-4.35	-4.77	1	3
T (min)	-3.66	-3.62	-5.61	1.99	2
F (g/hr)	-4.27	-4.42	-4.20	0.22	4
D (cm)	-5.82	-3.72	-3.36	2.46	1

Table IV.10: The response effects of the S/N ratios and their ranking of the PP-HMDSO coating deposited on an anodized aluminum surface.

Plasma Parameters	Means of S/N ratio of the PP-HMDSO coating on an anodized surface			Max(S/N)-Min (S/N)	Ranking
	Level 1	Level 2	Level 3		
P (W)	-3.776	-4.692	-4.944	1.168	3
T (min)	-4.004	-3.978	-5.429	1.451	2
F (g/hr)	-4.446	-4.706	-4.259	0.447	4
D (cm)	-5.810	-4.132	-3.469	2.341	1

Figures IV.7a-b show the variation and the effect of coating parameters to S/N ratio. The factor levels with the largest S/N ratios are the optimum levels as they minimize the sensitivity over the range of noises. In order to have the optimal conditions (high contact angle and the low contact angle hysteresis), we are looking for the condition where the

highest S/N ratio exists. Therefore, the optimal conditions for the PP-HMDSO to obtain a superhydrophobic film according to their high S/N ratios correspond to P1T2F3D3 (see Figures IV.7 a-b). This condition corresponds to an input power of 60W, a deposition time of 15 min, a monomer flow rate of 20 g/hr, and a distance from monomer inlet of 17 cm.

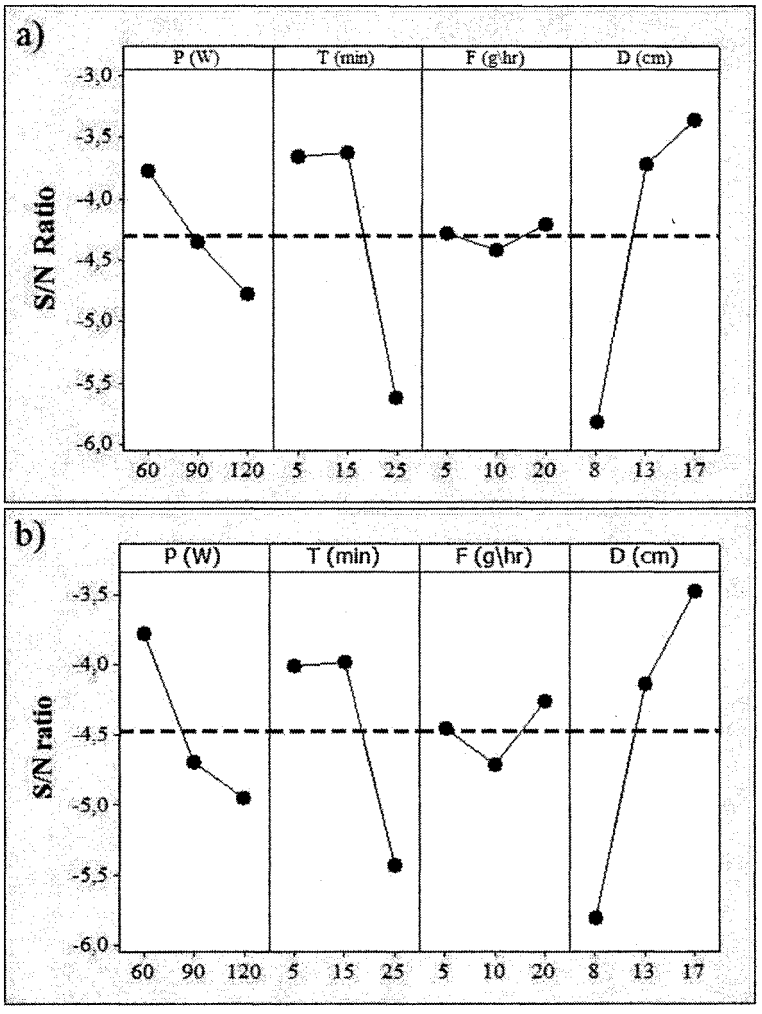

Figure IV.7: Variation of average S/N ratios with factor levels of the PP-HMDSO coating deposited on a) a water-treated aluminum surface and b) an anodized aluminum surface.

These results clearly show that the water repellency properties of a PP-HMDSO coating can be improved by decreasing the input power. It is generally believed that decreasing the input power causes a low ion bombardment. Likewise, a low ion bombardment can cause low precursor fragmentation; which yields a high concentration of retained methyl groups. The presence of a high concentration of methyl groups encourages the hydrophobic properties of the coating. Many studies have likewise observed a similar effect of power on wettability in a plasma polymerization process [65,146,147].

It is also observed that by increasing the distance from the monomer inlet, the hydrophobicity improves. It was shown that at a high distance, the density and the energy of electrons and ions are absent or negligible. Therefore, the absence of charged particles leads to orientation of the chains and networks of a coating characterized by a low surface energy [73]. *Butoi* et al [91] have also found that depositions performed at the farthest distance from the plasma glow discharge of Hexafluoropropylene oxide (HFPO) displayed a high degree of orientation. They showed that the free movement of undesired energetic species bombardment occurs simply at high distance because these species are lost through plasma recombination processes prior to reaching a substrate.

By increasing the monomer flow rate, or in other words the concentration of the methyl group, low significant effect on wettability was observed. *Kale* et al [31] have observed a similar effect of the monomer flow on wettability. They found that at primary deposition time, there is no variation in the surface energy when monomer concentration is increased. But at high deposition time, the surface energy is diminishes only slightly by

increasing the monomer flow rate.

Many studies showed that deposition time can lead to an increase in the thickness of the coating [77,78,89]. The results of 25 minute deposition time (contact angle and contact angle hysteresis) were satisfactory, however. In spite of this, in this study, 15 minutes is the optimum deposition time, considering the influence on other plasma parameters in order to create a superhydrophobic coating (high contact angle and low contact angle hysteresis).

Once the optimal process parameters have been determined, the final step is to verify the improvement of the contact angle and contact angle hysteresis at optimum conditions obtained by Grey-based Taguchi method. For this reason, an additional experiment was performed at optimum conditions (P1T2F3D3). The results of the contact angle at optimum condition showed an increase up to 161 ± 2° for the PP-HMDSO coating on a water-treated surface and 158 ± 3° for the PP-HMDSO film on anodized aluminum, respectively (see Figures IV.8a-b).

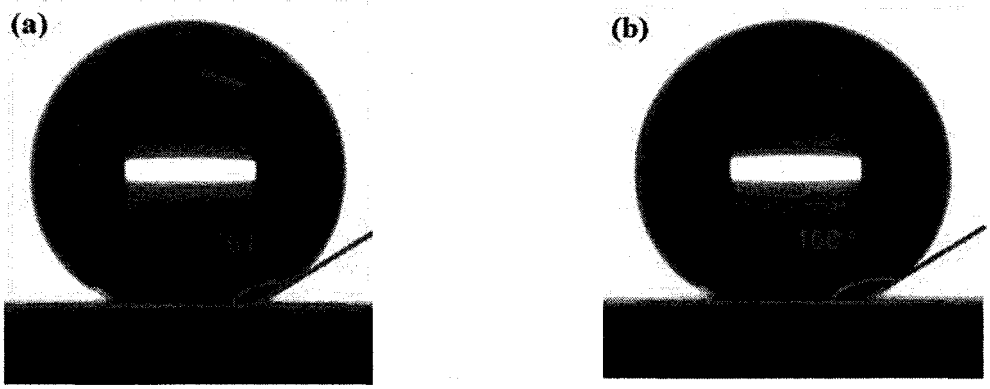

Figure IV.8: Contact angle of the PP-HMDSO coating deposited at optimum condition of plasma polymerization on a) a water-treated aluminum surface and b) an anodized aluminum surface.

Also, a contact angle hysteresis is 11 ± 2° and 13 ± 2° for PP-HMDSO coating deposited on water-treated and anodized aluminum surface, respectively. Based on Cassie-Baxter equation, which as explained in chapter II, the fraction of surface in contact with the water droplet is calculated (Table IV.11). It should be mentioned the contact angle of PP-HMDSO coating deposited on flat surface is around 100°.

Table IV.11, The surface area fraction (f) for PP-HMDSO coating deposited on treated surfaces

Name	Contact angle (°)	*f*
PP-HMDSO coating on anodized Al surface	158°	0.088
PP-HMDSO coating on water-treated Al surface	161°	0.066

The small value of *f* shows that the air is trapped under a drop interstice in the rough surface, and the water droplet can roll off easily. The very low value of sliding angle 2 ± 0.5° and 8 ± 0.4° for the PP-HMDSO deposited on water-treated aluminum and anodized aluminum surfaces also confirms the value of *f*. Furthermore, these results indicate that our analytic method provided a beneficial innovation, including a robust design and an ideal function for the water-repellency coating.

IV-4- Conclusion

The results presented here show that the superhydrophobic surfaces were derived by combining two surface roughening processes (anodization and boehmite methods) with the low surface energy coating (plasma polymerized HMDSO film). The result of SEM and contact angle analysis showed significant effects on voltage and time on the anodization

process as well as immersion time on the boehmite process.

In order to optimize plasma polymerization, four controlling parameters of the plasma process, namely input power, deposition time, monomer flow rate, and distance from the monomer inlet were considered. The Taguchi approach, followed by the Grey relational analysis, was applied to solve this multi-response optimization problem (high contact angle and low contact angle hysteresis). Through the Grey-based Taguchi method, it was found that the distance of the monomer inlet substrate and the plasma energy play the most significant role in affecting the coating's wettability.

The optimal condition proposed by this method has been verified through additional experiments which showed an increase in static contact angle up to 161° and 158 ° and a decrease in contact angle hysteresis up to 11° and 13° with sliding angle 2 ± 0.5° and 8 ± 0.4°, for a plasma polymerized HMDSO coating deposited on water treated and anodized aluminum surfaces, respectively.

CHAPTER V

STUDY OF THE STABILITY OF THE PLASMA POLYMERIZED HMDSO COATING

CHAPTER V

STUDY OF THE STABILITY OF THE PLASMA POLYMERIZED HMDSO COATING

Introduction

This chapter concerns the durability of a PP-HMDSO coatings deposited on anodized and water treated aluminum surfaces and obtained at the optimum conditions of plasma parameters from chapter IV. The aging of these coatings is studied under UV degradation, stability in various pH solutions, and consecutive icing/de-icing cycles. Their stability is evaluated by contact angle measurement, surface morphology analysis, and surface chemical composition. Here, we use the abbreviation *W15* for a PP-HMDSO deposited for 15 minutes on water-treated aluminum surface, and *A15* for a PP-HMDSO deposited for 15 minutes on an anodized aluminum surface.

V-1-Effect of UV radiations on HMDSO thin films

In order to simulate sunlight exposure, the surfaces are exposed to a UVA fluorescent lamp. The contact angle is measured after each eight-hour cycle of exposure. This section focuses on the stability of surfaces *A15* and *W15* against UV degradation.

V-1-1- Effect of UV exposure on a HMDSO coating deposited on an anodized aluminum surface

The stability of *A15* was studied after UV exposure by measuring the surface contact angle. Figure V.1 depicts the evaluation of the contact angle as a function of UV light exposure time. The results show that the contact angle rapidly decreases from 158° to 150° after 35 hours of UV exposure. The contact angle remains constant up to 150 hours and it is reduced to 145° after 240 hours of UV exposure.

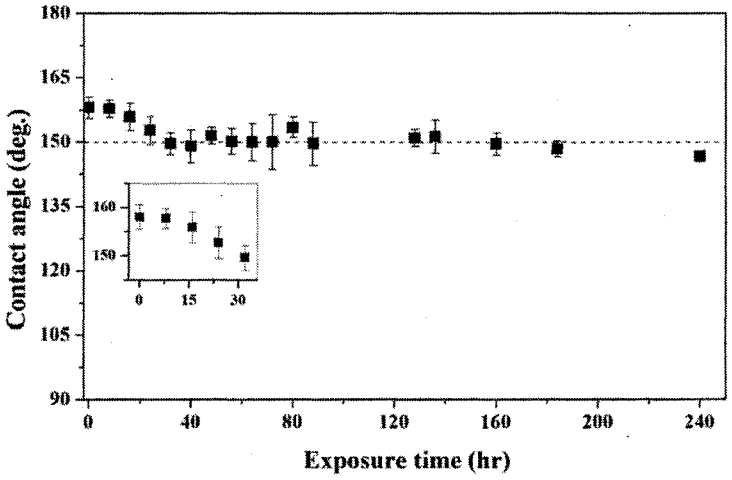

Figure V.1: Variation of contact angle versus exposure time of UV light on *A15*.

FT-IR analysis was used to demonstrate the effect of UV exposure on the chemical composition structure of the *A15*. Figures V.2a-b depict the FT-IR spectrum of the *A15* before and after 240 hours of UV exposure. It shows that the intensity of Si-$(CH_3)_2$, Si-$(CH_3)_3$, Si-CH_3, and CH_x (x = 1, 2, 3) groups decreased after UV exposure. Nevertheless, the presence of these groups represents the hydrophobic characteristic of *A15* after 240 hours of UV exposure. Therefore, the FT-IR analysis and the contact angle measurement confirm the stability of the superhydrophobic *A15* against UV degradation.

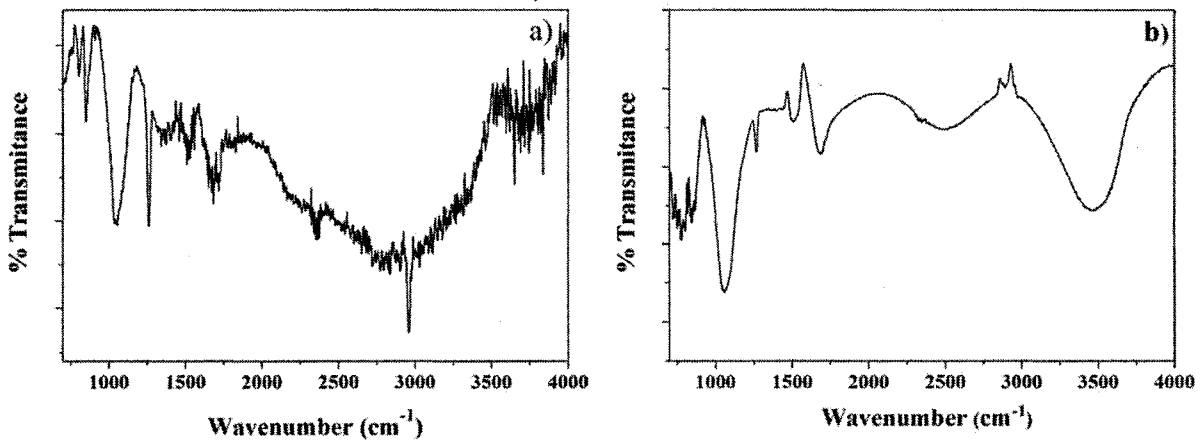

Figure V.2: FT-IR spectrum of the film deposition on *A15* a) before 240hr UV exposure and b) after 240 hr of UV exposure.

V-1-2- Effect of UV exposure on the HMDSO coating on a water-treated aluminum surface

The effect of UV exposure time on the contact angle is shown in Figure V.3, where the contact angle of *W15* rapidly decreases and reaches 150° in the first 15 hours of

exposure. After the initial fall, the contact angle remains constant around 150° for up to 100 hours of exposure and the contact angle is slightly decreased to 145° after 240 hours of UV exposure.

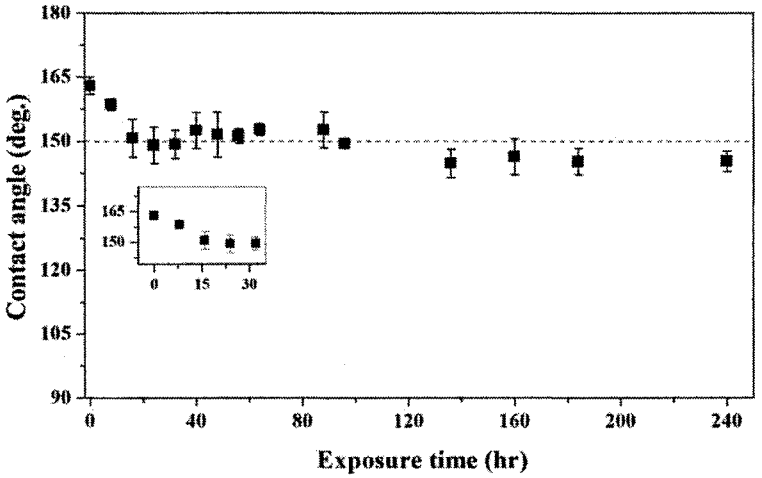

Figure V.3: Variation of contact angle versus exposure time of UV light of *W15*.

The similar FT-IR spectrum results for *W15* surface before and after 240 hours of UV exposure were achieved. Therefore, we concluded the PP-HMDSO coating deposited on anodized and water treated aluminum surfaces have a relatively good stability against UV degradation compared to other research work done by *Hugan* et al. [148] that showed the superhydrophobic coating had changed to hydrophilic coating after 8 hours of UV exposure. It should be noted that 240 hours of exposure in the mentioned apparatus is equivalent to about six months of natural exposure in Canada (see section III.3.6).

V-2- Effect of different pH solution and immersion in distilled water on wettability of HMDSO coating

Acidic rain is a common phenomenon in urban and industrial areas, and it can have harmful effects on outdoor infrastructure. Hence the study of the stability of a coating in acidic conditions is necessary. Furthermore, in order to apply the superhydrophobic surface to industrial fields, it is critical to reveal the chemical stability of the superhydrophobic film in different pH solutions [149]. In order to evaluate the stability of a coating against rainwater in outdoor conditions and other applications, superhydrophobic surfaces were exposed to different pH solutions (acidic, basic and neutral solutions), and the resistance of the coating against different pH levels was investigated. The *A15* and *W15* were immersed in acidic, basic and neutral solutions for 240min. Subsequently, all the surfaces were carefully blow-dried by N_2 and their contact angle was measured. Also, in order to evaluate the coating's stability as a function of immersion time in water, the surfaces were immersed for extended periods of time in the pH7 (distilled water) solution after which the contact angle of these surfaces was measured.

V-2-1- Stability of HMDSO coating on an anodized aluminum surface immersed in various pH solutions

A study of the stability of a HMDSO coating deposited on an anodized aluminum surface (Figure V.4) shows that the contact angle of *A15* decreased to 130° in a basic solution while the contact angle was near 150° in acidic and neutral solutions after

immersing for 240 min. The result shows that the coating is more stable in acidic and neutral than in basic solutions. *Isimjan* et al. [6] showed that the superhydrophobic coating was destroyed after 5 day immersion in acidic solution without affecting surface morphology. Their results showed that the structure of the chemical composition of the coating can be affected by different pH values.

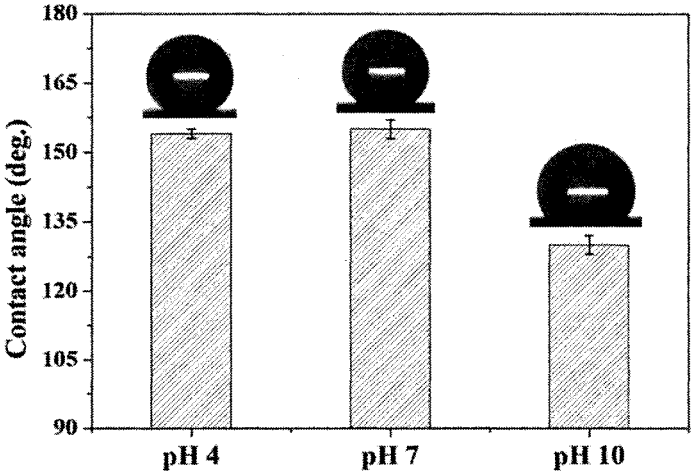

Figure V.4: Contact angle value of *A15* after 240 min immersion in different pH solutions.

The contact angle of *A15* as a function of immersion time in distilled water is shown in Figure V.5a. It can be seen that the contact angle decreased sharply from 158° to 140° after an immersion time of 20 hours. After that, the contact angle decreased continuously after 670 hours of immersion in water when it reached about 103°. As the immersion time increased to 740 hours, the contact angle suddenly decreased to 90°. Also, we compare the stability of *A15* in water with the stability of untreated surface. A study of the variation of contact angle of the untreated aluminum surface as a function of immersion time showed

that the contact angle decreased from 90 ± 2° to 20 ± 2.4° after 740 hours of immersion in water (Figure V.5b). Thus, the reduction of contact angle after 740 hours of immersion in water may be hypothesized as follows the coating is dissolved and corrosive sets in. Moreover, the reduction of the contact angle of untreated aluminum after 740 hours of immersion in distilled water may be related to the same chemical reaction (corrosion).

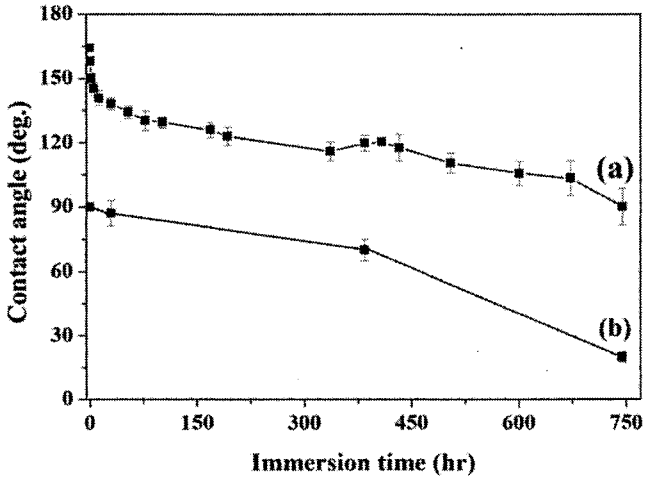

Figure V.5: Variation of contact angle versus immersion time in distilled water on a) *A15* and b) untreated aluminum.

V-2-2- Stability of a HMDSO coating on a water-treated aluminum surface immersed in various pH solutions

The variation of contact angle of *W15* as a function of pH values after 240 minutes of immersion is presented in Figure V.6. We can see the static water contact angle decreases to be in the ranges of 146 ± 1 to 158 ± 2° after 240 min immersion in each pH's solution (4, 7 and 10). These results indicate that the *W15* is a superhydrophobic surface relatively good

resistance in acidic, basic and neutral solutions.

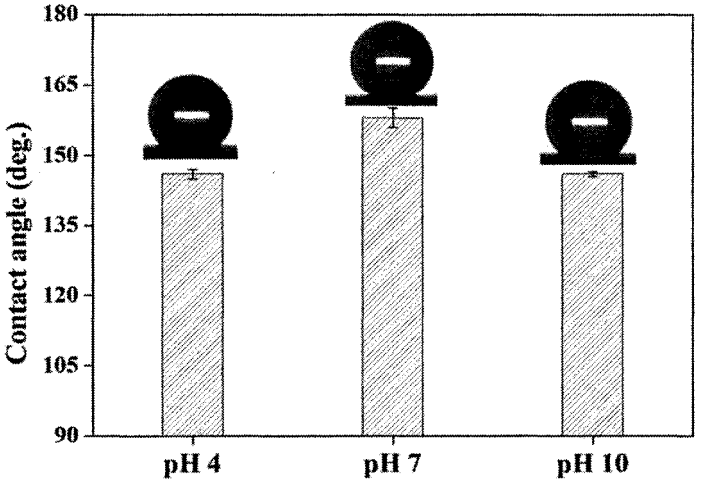

Figure V.6: The contact angle value of *W15* after 240 minutes immersion in different pH solution.

The variation of contact angle of *W15* as a function of immersion time in distilled water is shown in Figure V.7. A rapid decrease in contact angle value (near 150°) of *W15* can be seen at the beginning. After that, the surface keeps its superhydrophobicity (145 ± 5°) for up to 200 hours of immersion. The reduction in contact angle to around 120° is observed after 700 hours. By increasing the immersion time to 740 hours, the contact angle sharply decreases to 83°. *Gnanappa* et al. [104] showed that the superhydrophobic properties of a plasma polymerized fluorocarbon surface was decreased after 5 days of immersion in water due to the degradation of the coating. Immersion for a long time in water may either detach or dissolve the coating without damage to the surface morphology.

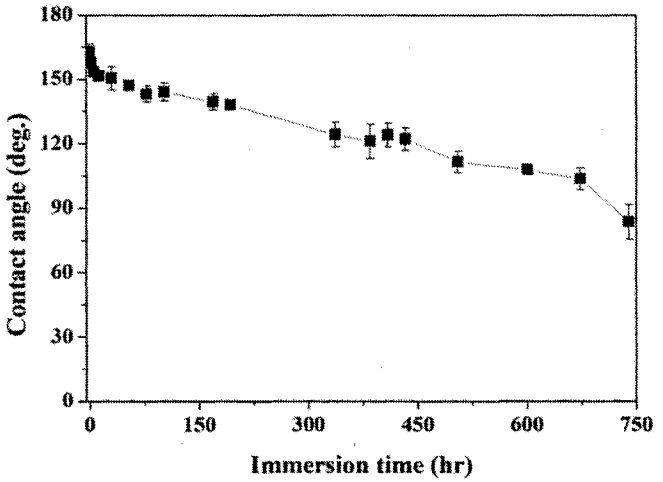

Figure V.7: Variation of contact angle of *W15* versus immersion time in distilled water.

If we compare the results of the stability of *W15* and *A15* immersed in different pH solutions, *W15* shows a greater stability than *A15* in a basic solution, while in acidic and neutral solutions, their stability is equal after 240 minutes. Also, the *A15* and *W15* surfaces have a relatively good stability after 740 hours (~ 30 days) of immersion in distilled water, and they have approximately the same hydrophobic properties.

V-3-Icephobicity

Many studies have further shown the good correlation between superhydrophobicity and icephobicity [52,150–152], although a few studies did not agree with this aspect and showed the inverse results [55,56]. In order to compare and come to conclusion regarding the relationship between hydrophobicity and icephobicity, several factors should be considered such as: the method of ice accumulating on a surface, type of the accumulated ice, and the morphology of the surface. In this work, the glaze ice accumulation on the

samples was performed by spraying the super cooled water droplets in a wind tunnel at sub-zero conditions after which the ice adhesion strength was measured by a centrifugal instrument. Also, in order to assess the durability of their ice-repellent properties over time, they were tested after several icing/de-icing cycles. The stability of the surfaces was evaluated by contact angle measurements and ice adhesion strength after several icing/de-icing cycles.

V-3-1- Ice adhesion measurement of a PP-HMDSO coating

Table V.1 compares the shear stress of an untreated aluminum surface, a PP-HMDSO coating on an aluminum surface, and PP-HMDSO deposited on anodized and water treated surfaces (*A15* and *W15*). It can be seen that the shear stress of untreated aluminum (contact angle ~ 90°) is 350 ± 25 kPa (ARF = 1), which is decreased to 250 ± 20 kPa (ARF = 1.4) for the PP-HMDSO film deposited on untreated aluminum (contact angle ~ 115°); it decreases even more, to 100 ± 9 kPa (ARF = 3.5) and 30 ± 8 kPa (ARF = 11.6) for the *A15* (contact angle ~ 158°) and *W15* (contact angle ~ 161°), respectively. These results indicate that reduction in ice adhesion strength is affected not only by the low surface material coating but also by the roughness of the surface resulting from anodization and immersion in boiling water.

Table V.1: Comparison of ice adhesion strength of untreated and treated aluminum substrates.

Name	Shear stress (kPa)	ARF
Untreated aluminum	350 ± 25	1
PP-HMDSO coating on aluminum	250 ± 10	1.4
A15	100 ± 9	3.5
W15	30 ± 8	11.6

Figures V.8a-c depicts images of accumulated ice on the untreated aluminum surface, PP-HMDSO coating on the aluminum surface as a hydrophobic surface, and *W15* as a superhydrophobic surface after 90 seconds. It is obvious that a thick homogeneous ice layer has accumulated on untreated aluminum surfaces (see Figure V.8a). A remarkable change in the form of accumulated ice on a hydrophobic surface is observed, as shown in Figure V.8b where the heterogeneous freezing of water droplets on the hydrophobic surface can be seen. Accumulated ice formed with difficultly on the superhydrophobic surface, and the quantity of ice was reduced (see Figure V.8c). These are in agreement with the work done by *Sarshar* et al. [53]. They also showed that a superhydrophobic surface (contact angle ~ 170° and contact angle hysteresis ~ 3°) with nano structured roughness can lead to an increase in the delay of ice accumulation on a surface.

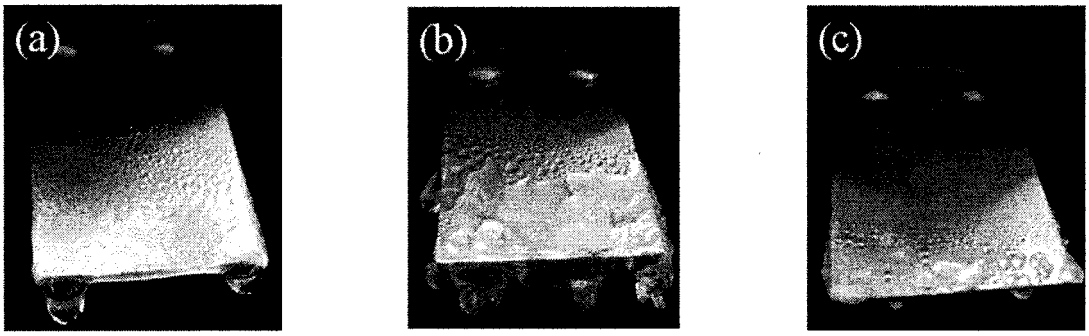

Figure V.8: Images of a) an untreated aluminum surface, b) a hydrophobic surface and c) a superhydrophobic surface after glaze ice accumulation in the wind tunnel for 90 seconds.

V-3-2- Study of the stability of a coating against several icing/de-icing cycles

In order to evaluate the longevity of such surfaces and to assess their potential outdoor applications, their durability is studied following several icing/de-icing cycles. It should be noted that in order to reduce extensive maintenance and operating costs, any developed surface should be stable enough to maintain its superhydrophobic and icephobic characteristics in various environments and weather conditions.

V-3-2-1-Ice adhesion of a HMDSO coating deposited on an anodized aluminum surface

Ice adhesion strength and contact angle of the *A15* sample were measured after several icing/de-icing cycles. Figure V.9 depicts that ice adhesion stress remains approximately constant at 100 ± 9 kPa (ARF = 3.5) for the first seven icing/de-icing cycles, after which it increased to 250 ± 25 kPa (ARF = 1.4). Although the shear stress increased after fifteen icing/de-icing cycles, it reached 250 kPa; however, the surface still retained its icephobic properties (ARF = 1.4).

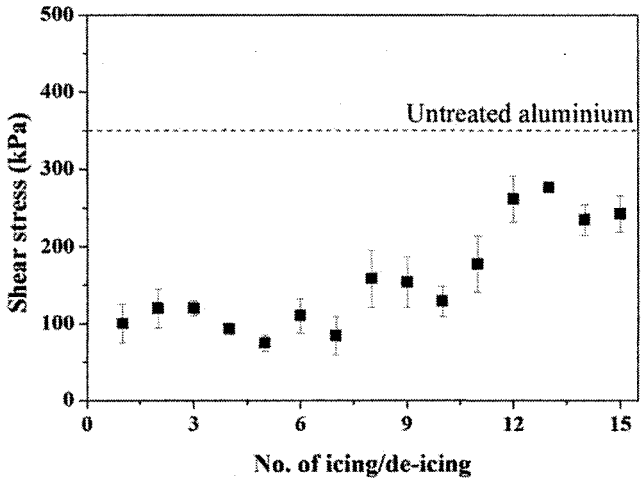

Figure V.9: Variation of shear stress of *A15* surface as a function of icing/de-icing cycles.

The evaluation of the contact angle as a function of icing/de-icing cycles is shown in Figure V.10. It can be observed that the contact angle of the *A15* sample decreased from 158 ± 2 ° to 145 ± 4° after fifteen icing/de-icing cycles. Even though the contact angle was still high, the increment of *f* value (from Cassie-Baxter equation) from 0.088 to 0.218 may be the reason why the water droplets were unable to move freely on the surface. These results show that a transition has occurred from Cassie-Baxter to Wenzel wetting regime after fifteen icing/de-icing cycles. Moreover, the increase of the sliding angle value of the surface from 8 ° to 25 ° after fifteen icing/de-icing cycles confirms this phenomenon.

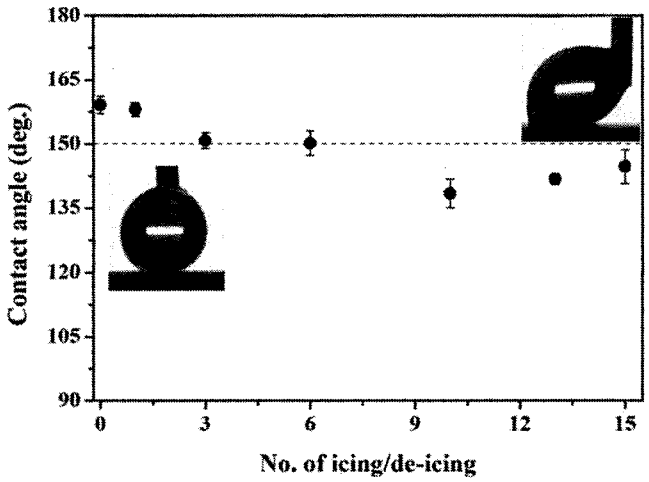

Figure V.10: Variation of contact angle of *A15* surface versus several icing/de-icing cycles and images of contact angle hysteresis before and after fifteen icing/de-icing cycles.

This variation in the icephobic behaviour of the surfaces after successive icing/de-icing cycles may be attributed to the following two phenomena: (1) modification or degradation of the surface roughness and/or (2) partial elimination of low surface energy coating on the surface.

The morphology of *A15* was studied with SEM images. Figure V.11a shows the presence of a spongy micro-structure on the surface before any icing/de-icing cycles. However, after fifteen icing/de-icing cycles, the morphology of the surface has been changed significantly by the presence of large pores on the surface (see Figure V.11b). This phenomenon may result from the collapse of the initial micro/nano-structured layer, creating larger roughness features.

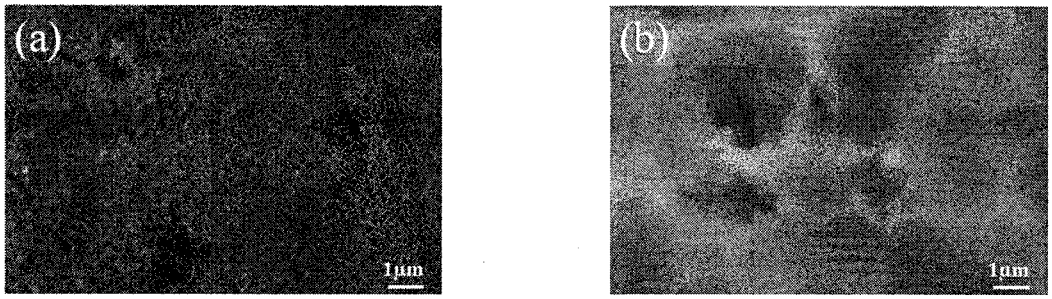

Figure V.11: SEM images of *A15* a) before the icing/de-icing cycles, and b) after fifteen icing/de-icing cycles.

Figures V. 12a-b depicts the AFM images of the *A15* before and after the icing/de-icing cycles. Figure V.12a exhibits the needle-like structure (Rms = 47 nm) on the PP-HMDSO thin films before any icing/de-icing. After fifteen icing/de-icing cycles, the needle-like structure has been removed from the surface (Rms = 99 nm) (Figure V.12b). Also, the small hills were transformed to big hills. Kurtosis value of the surface before the icing/de-icing cycles is around 4, indicating a spiky surface. This value decreases to around 2.5 after fifteen icing/de-icing cycles and consequently, the surface has lost its spiky characteristics [153].

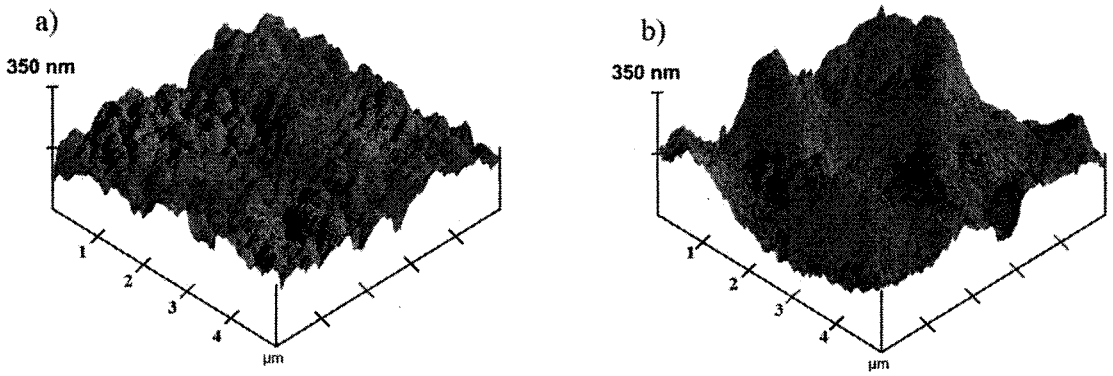

Figure V.12: AFM images of *A15* a) before the icing/de-icing cycles, and b) after fifteen icing/de-icing cycles.

XPS analysis was carried out to determine the chemical composition of the plasma polymerized HMDSO coating deposited on anodized aluminum before and after the icing/de-icing cycles. Table V.2 depicts the atomic percentage of Si_{2p} (at 103.1 eV), C_{1s} (at 285 eV), O_{1s} (at 533eV) and Al_{2P} (at 75.1eV) on the *A15* before and after fifteen icing/de-icing cycles. As evident from that Table, there is no significant variation in the chemical composition after fifteen icing/de-icing cycles, which shows that the coating is still present after several icing/de-icing cycles.

Table V.2: Elemental composition of the *A15* before and after fifteen icing/de-icing cycles.

	Binding energy (eV)	Atomic values (%)	
		Before icing/de-icing	After icing/de-icing
Si	103.1	14	13
C	285	21	21
O	533	52	51
Al	75	13	15

XPS spectra can be obtained at a high resolution, focusing on the specific binding energy of the C1s fitting components. Figures V. 13a-b depicts C_{1s} curve-fitting spectra of the *A15* before and after fifteen icing/de-icing cycles, respectively. The spectrum can be satisfactorily fitted with a combination of three distinct peaks: the peak at 284.6eV corresponds to $(CH_3)_x$-Si-O, the peak at 285.4eV to C–C and C-H species, and the peak at 287eV to C-O groups. The percentage of these functions before and after icing/de-icing cycles is 12 % $(CH_3)_x$-Si-O), 8% (C–C) and 1% (C-O), respectively. These results show that no significant variation in the concentration of these groups was observed after fifteen

icing/de-icing cycles.

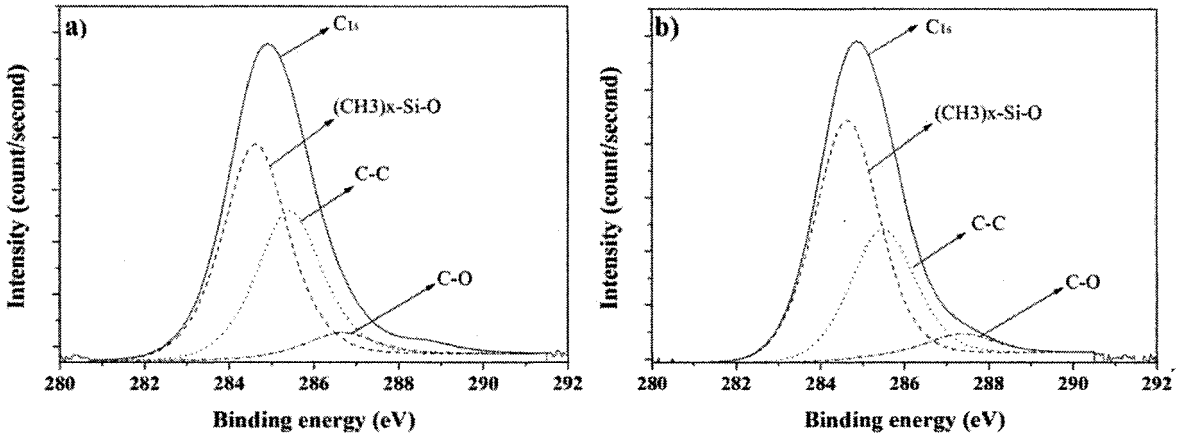

Figure V.13: C_{1s} spectra of *A15* a) before the icing/de-icing cycles, and b) after fifteen icing/de-icing cycles.

Hence these results show that the variation of surface roughness has been the dominant parameter in increasing the ice adhesion strength and decreasing the contact angle of surface *A15* after fifteen icing/de-icing cycles.

V-3-2-2-Ice adhesion of a HMDSO coating deposited on a water-treated aluminum surface

Ice adhesion strength and contact angle of the *W15* sample were measured after several icing/de-icing cycles. Figure V.14 depicts that ice adhesion strength is 30 ± 8 kPa (ARF = 11.6) for the first icing/de-icing cycle with a slight increase to 100 ± 40 kPa (ARF = 3.5) after fifteen successive icing/de-icing cycles. Although shear stress increases after fifteen icing/de-icing cycles, the surface is still icephobic (ARF = 3.5).

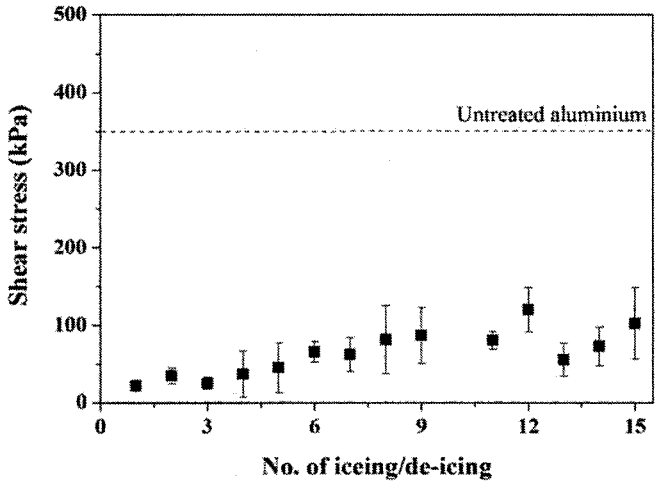

Figure V.14: Variation of shear stress of *W15* versus several icing/de-icing cycles.

The variation of contact angle of *W15* as a function of icing/de-icing cycles (Figure V.15) shows that the contact angle of *W15* slightly decreases from 161 ± 2° to 154 ± 4° after fifteen icing/de-icing cycles. This result confirms the stability of the superhydrophobic properties of the coating over time and through varying conditions. Even though, the *f* value is increased from 0.066 to 0.122, the water droplets can easily roll off the surface since the sliding angle value of the surface has remained constant around 2° before and after the fifteen icing/de-icing cycles. Consequently, it can be assumed that the Cassie-Baxter wetting regime is still dominant on this surface after fifteen icing/de-icing cycles.

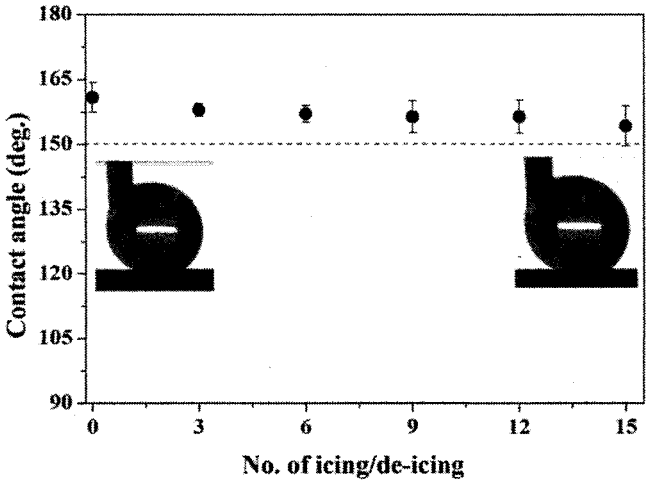

Figure V.15: Variation of contact angle and images of contact angle hysteresis of *W15* as a function of several icing/de-icing cycles.

The morphology of *W15* is studied with AFM (Figures V.16a-b) before and after the icing/de-icing cycles. Figure V.16a depicts the needle-like structure on the surface before any icing/de-icing (Rms = 35 nm). However, after fifteen icing/de-icing cycles, the surface roughness only slightly decreased to 28 nm despite the presence of a needle-like structure on the surface (see Figure V.16b). The Kurtosis value of the surface before and after fifteen icing/de-icing cycles is around 3, which indicates Gaussian distribution and a random surface. Also, the positive Kurtosis values indicate the enduring spiky characteristic of the surface [154].

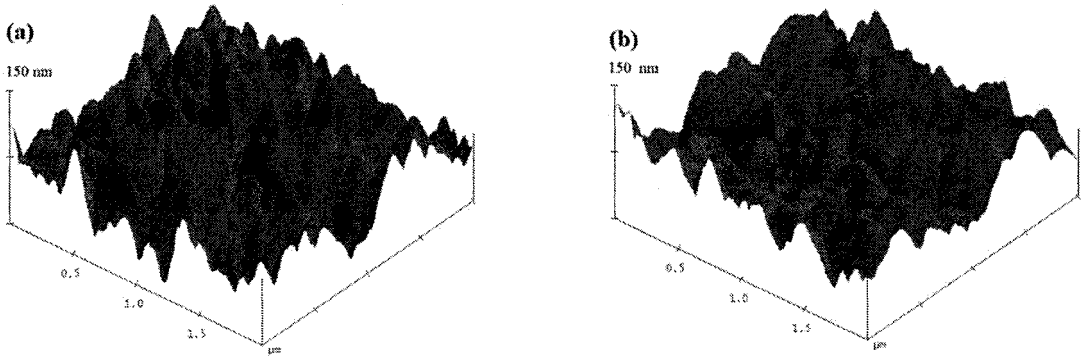

Figure V.16: AFM images of *W15* a) before the icing/de-icing cycles, and b) after fifteen icing/de-icing cycles.

Table V.3 depicts the atomic ratio of C/O and Al of *W15* before and after fifteen icing/de-icing cycles which are obtained by XPS analysis. As shown in Table V.3, there is no variation in the ratio of C/O and Al% of *W15* surface after fifteen icing/de-icing cycles which confirms the results of contact angle measurement and ice adhesion strength.

Table V.3: Atomic ratio of *W15* before and after fifteen icing/de-icing cycles.

Atomic ratio	Surface *W15*	
	Before icing/de-icing	After icing/de-icing
C/O	1.4	1.4
Al	11	11

Figure V.17 depicts the FT-IR spectrum of *W15* after fifteen icing/de-icing cycles. As mentioned before, the presence of methyl groups at bands 2960 cm^{-1}, 1260 cm^{-1}, 840 cm^{-1} and 800 cm^{-1}on the surface can be considered the result of the hydrophobic characteristic of the surface. Consequently, these results are confirmed by contact angle measurements and ice adhesion strength of *W15* after fifteen icing/de-icing cycles.

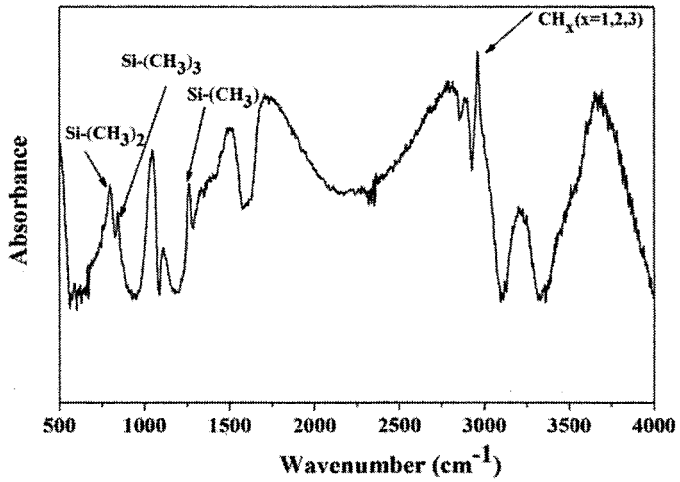

Figure V.17: FT-IR spectrum of *W15* after fifteen icing/de-icing cycles.

Although the coating conditions for *A15* and *W15* were the same, the stability of these surfaces is not similar after fifteen icing/de-icing cycles. Moreover, the presence of aluminum on the surfaces indicates that these surfaces are not fully covered by PP-HMDSO coatings. The difference in the underlying structure of the aluminum surfaces [anodized aluminum (Al_2O_3) and aluminum treated in boiling water (AlOOH)] can be a reason. By comparing the results of shear stress and contact angle of *A15* and *W15*, the stability of *W15* is more than that of *A15* after fifteen icing/de-icing cycles.

V-4-Conclusion

The durability of a PP-HMDSO coating on treated aluminum surfaces (*A15* and *W15*) was studied under a variety of conditions such as UV exposure, immersion in different pH solutions, and successive icing/de-icing cycles. These results indicate that *A15* and *W15* had good resistance to UV degradation. In addition, *A15* had low resistance in a basic solution,

although *W15* had good stability in different pH solutions. Likewise, after 740 hours immersion in distilled water, *A15* and *W15* both lost their hydrophobic properties and contact angle decreased to around 90° and 83°, respectively.

Under atmospheric icing conditions, *A15* and *W15* showed ice adhesion strength 3.5 times and 11.67 times lower than an untreated aluminum surface, respectively. Although *A15* lost some of its nano-structured roughness after fifteen icing/de-icing cycles, it still had superhydrophobic with icephobic properties (ARF = 1.4). XPS analyses showed that the amount of carbon content on *A15* (which determines the methyl groups on the coating) was constant after fifteen icing/de-icing cycles. SEM and AFM images showed that the needle-like structure of *A15* disappeared after fifteen icing/de-icing cycles. While, *W15* still had a good stability after fifteen icing/de-icing cycles. XPS analysis indicated that the atomic ratio of C/O before and after fifteen icing/de-icing cycles was approximately constant. The AFM images also showed that the surface kept its roughness.

CHAPTER VI

IMPROVEMENT OF THE STABILITY OF A PLASMA POLYMERIZED HMDSO COATING

CHAPTER VI

IMPROVEMENT OF THE STABILITY OF A PLASMA POLYMERIZED HMDSO COATING

Introduction

In the present chapter, in order to improve the stability of the PP-HMDSO coating, the deposition time of plasma polymerization is increased at constant conditions of input power (60W), distance from the monomer inlet (17cm) and the monomer flow rate (20g/hr). The durability of coatings is studied under the following conditions: UV degradation, stability in various pH solutions, and consecutive icing/de-icing cycles. The abbreviation of *W25* is used for 25 minutes PP-HMDSO coating deposited on water-immersed aluminum, and *A25* is used for 25 minutes PP-HMDSO coating deposited on anodized aluminum. Finally, the corrosion resistance of a superhydrophobic surface is

examined by using the Potentiodynamic polarization technique.

VI-1- Modification of the plasma parameters

The physico-chemical structures of plasma-polymerized films depend on many process parameters, such as input power, monomer flow rate as well as distance from the monomer inlet, and deposition time. At higher distances from the monomer inlet, the density of ions and electrons decreases and it leads to lower monomer fragmentation. Then, in this study, the maximum distance possible from a monomer inlet in our setup was used during the plasma polymerization. Moreover, it should be noted that at low power, due to a low fragmentation of the precursor in plasma phase, the highest percentage of the methyl groups on the coating is reached. The minimum possible input power was used for plasma initiation at constant pressure and a lower input power was impossible in this study. Results from chapter IV also indicated that the monomer flow rate had very little effect on the superhydrophobic properties of the deposited coating. Here, the only effective parameter that could improve the stability was deposition time.

VI-1-1- Influence of deposition time on the thickness of thin films

In order to study the effect of deposition time on the stability of the coating, the deposition time was varied from 5 to 25 minutes during the plasma polymerization process. An ellipsometry instrument was used to measure the thickness of the coating following the increase of the deposition time. The results show that by increasing the deposition time from 5 to 25 minutes, the thickness of the coating increased from 5 nm to 18 nm and the

refractive index decreased from 1.59 to 1.42 (see Table VI.1). The reduction of the refractive index while thickness increased may indicate the presence of a developing porosity on the coating [155,156].

Table VI.1: Comparison of thickness and reflective index of different deposition time of the PP-HMDSO coating on treated aluminum.

Deposition time (min)	Thickness (nm)	Reflective index
5	5	1.59
15	12	1.57
25	18	1.42

VI-1-2- Effect of deposition time on the chemical composition of coatings

The XPS analysis was carried out to study the effect of changing the increments of deposition time on the actual chemical composition of the PP-HMDSO coating. Figure VI.1 depicts high-resolution peaks of C_{1s} and Si_{2p}. The bonding energy of the C_{1s} peak is around 285 eV, and 103 eV for the Si_{2p} peak [157]. It can be seen that by extending deposition time, the percentage of carbon to silicon ratio (C/Si) increases from 1.5 for 15 minutes to 2.15 for 25 minutes. These results show that the concentration of the methyl group which represents the hydrophobic characteristic of PP-HMDSO coating is increased by rising the deposition time. Furthermore, the percentage of Al_{2P} (at 75 eV) and O_{1S} (at 533 eV) in the coating is decreased respectively from 11% to 4% and from 52% to 34% by extending the deposition time (from 15 to 25 minutes). These results indicate a more homogeneous covering of the surface by the PP-HMDSO coating when deposition time is increased.

However, further increase of deposition time can lead to the formation of thicker coatings which are more sensitive to delaminate.

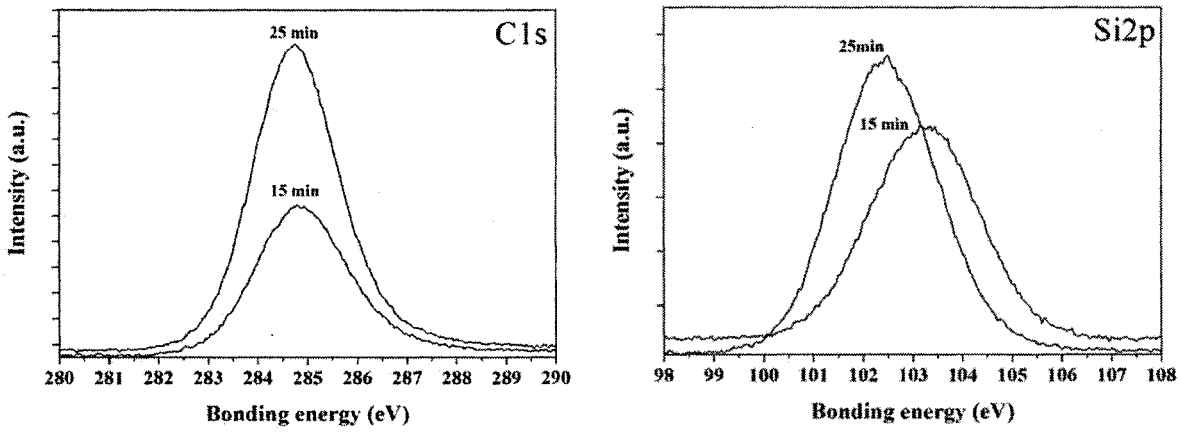

Figure VI.1: XPS high resolution of C_{1s} and Si_{2p} spectrums of PP-HMDSO coating on an anodized aluminum at two deposition times.

VI-1-3-Effect of deposition time on the wettability of PP-HMDSO coatings

As mentioned before, our aim is to improve the stability of the PP-HMDSO coating. The contact angle, the contact angle hysteresis and the sliding angle of different surfaces for different deposition times are given in Table VI.2. By increasing the deposition time from 15 minutes (*A15*) to 25 minutes (*A25*), the contact angle and the contact angle hysteresis are approximately constant, but the sliding angle decreases from 8° to 3° (*f* value from 0.088 to 0.059). Increasing the deposition time leads to higher coverage of PP-HMDSO coating on the anodized aluminum surface. However, increasing deposition time

does not have any significant effects on the contact angle, the contact angle hysteresis nor on the sliding angle of PP-HMDSO coating on water treated surface (*W15* and *W25*).

Table VI.2: Variation of contact angle, contact angle hysteresis, sliding angle of the PP-HMDSO coating at different deposition times on differently treated aluminum surfaces.

Name	Contact angle (°)	Contact angle hysteresis (°)	Sliding angle (°)
A15	158 ± 3	13 ± 2	8 ± 0.4
A25	162 ± 3	13± 3	3 ± 0.4
W15	161 ± 2	11 ± 2	2 ± 0.5
W25	159 ± 3	13 ± 3	2 ± 0.3

VI-2- Stability of the coating against UV degradation

In order to compare the effect of increment of the deposition time on the stability against UV degradation, *A25* and *W25* have been exposed to UV light for 537 hours. It should be noted that 537 hours of exposure in the mentioned apparatus are equivalent to approximately one year of natural exposure in Canada (see Chapter III.3.6).

VI-2-1-Effect of UV exposure on a PP-HMDSO coating on an anodized aluminum surface

Figure VI.2 indicates the variation of contact angle of *A25* after 537 hours of UV exposure. It shows that the contact angle of the surface decreased from 162° to 150° after 300 hours of exposure to UV light. Furthermore, by an increased exposure to UV light up to 537 hours, the contact angle of *A25* reached 140° (approximately superhydrophobic). As

a result, a rise of deposition time slightly improved the stability of the PP-HMDSO coating deposited on an anodized aluminum surface (see Figures VI.2 and V.1).

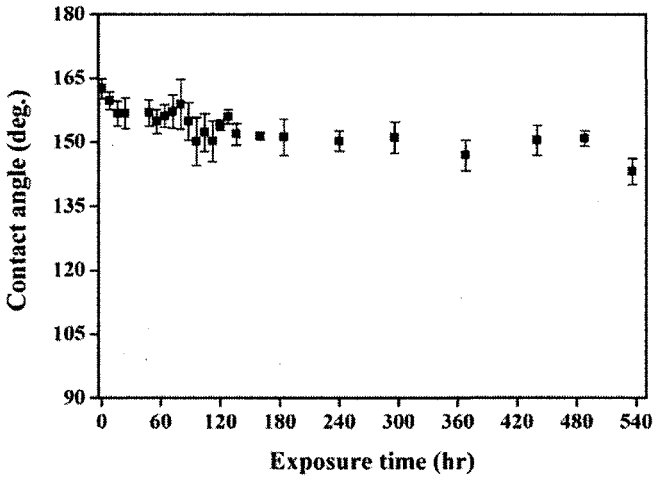

Figure VI.2: Variation of contact angle of *A25* as a function of UV exposure time.

VI-2-2-Effect of UV degradation of a PP-HMDSO thin film deposited on a water-treated aluminum surface

The evaluation of the contact angle of *W25* after 537 hours of exposure to UV is shown in Figure VI.3. The contact angle of the surface rapidly dropped to 150° after 15 hours of UV exposure. After the initial fall, the contact angle remained nearly constant (near 150°) for 180 hours at which point it still kept its superhydrophobicity. Then the contact angle underwent a minor decrease and reached 145° after 537 hours of UV exposure. Therefore, the increase of deposition time of PP-HMDSO coating on a water-treated aluminum surface has no effect on the stability against UV degradation after 537

hours (equal to one year exposure to sunlight).

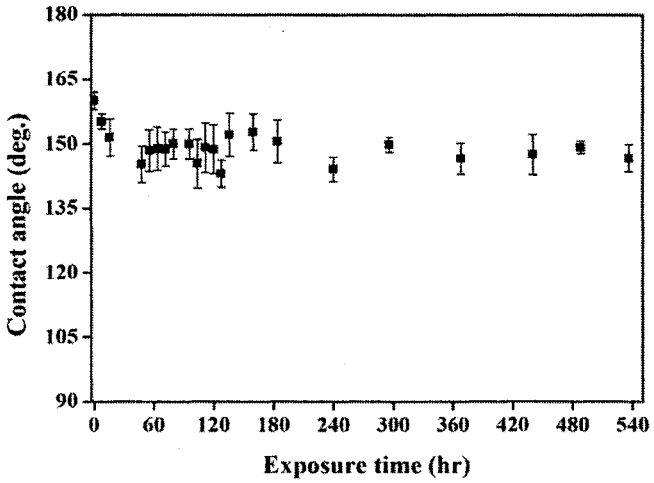

Figure VI.3: Variation of the contact angle of *W25* as a function of UV exposure time.

VI-3-Effect of various pH solutions and immersion in distilled water on the coating wettability

As we noticed in the previous chapter (see section V.2), in order to evaluate the stability of the coating, the surface is exposed to different pH values. In this section *A25* and *W25* are immersed in different pH solutions for a longer time (38 hours). The stability of the coatings is evaluated by measuring the contact angle. In addition, the durability of the coating is assessed as a function of immersion time in distilled water up to 1200 hours.

VI-3-1- Stability of an HMDSO thin film deposited on an anodized aluminum surface immersed in different pH solutions

The variation of the contact angle of *A25* during the 38 hours immersion period in

various pH solutions is shown in Figure VI.4. These results show that for the first 8 hours of immersion, pH values had little effect on the contact angle of *A25*. However, immersion in high acid or high base solutions can decrease the contact angle to 90°. However, the results of contact angle of the surface at higher immersion time (38 hours) presented good resistance in weak acid or base and neutral solutions. These results show that by increasing the deposition time, the stability of *A25* improved compared to the stability of *A15*.

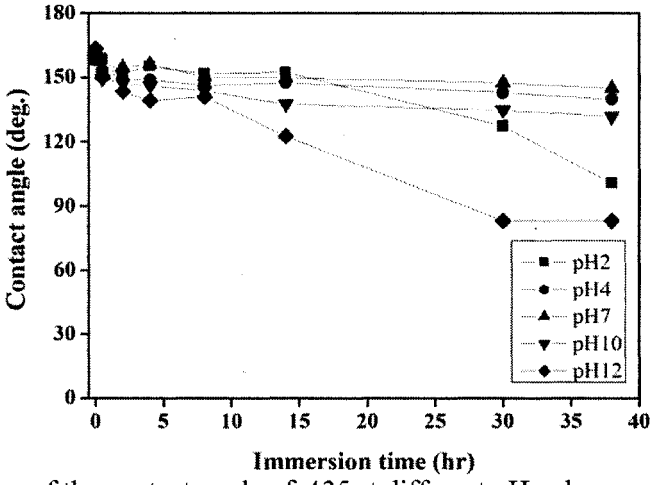

Figure VI.4: Variation of the contact angle of *A25* at different pH values versus immersion time.

In order to evaluate the stability of *A25* at pH = 7 (which corresponds to pure water) for extended time periods, in Figures VI.5, the variation of contact angle of *A25* after 1200 hours of immersion in water was studied. The contact angle decreased at three different time steps during the 1200 hours of immersion in water. In the first step (0 to 37 hours), the contact angle rapidly decreased from 162° to 140°. In the second step (37 to 525 hours), the contact angle remained approximately constant, around 140°. In the final step (525 to 1200

hours), the contact angle decreased linearly from 140° to 95°. Although a longer immersion time caused the contact angle to decrease, the surface still remained hydrophobic ($\theta > 90°$) after 1200 hours of immersion in water.

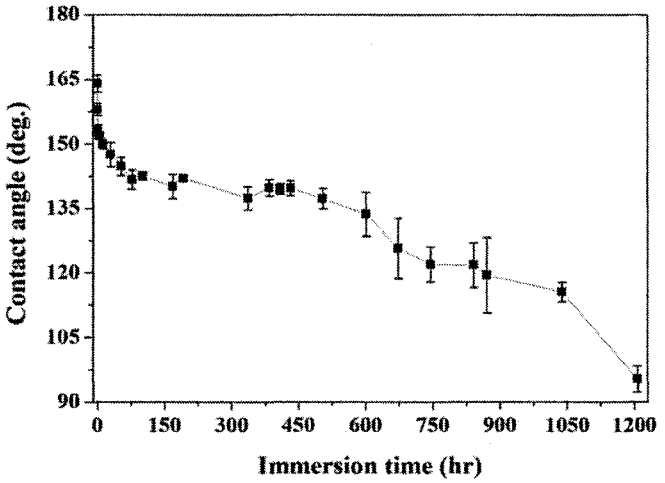

Figure VI.5: Variation of the contact angle of *A25* as a function of immersion time in distilled water.

VI-3-2-Stability of a HMDSO thin film deposited on a water-treated aluminum surface immersed in different pH solutions

Figure VI.6 presents the variation of the contact angle of *W25* during 38 hours of immersion in various pH solutions. In the first few hours, it was discovered that the different pH values have little effect on the contact angle of the surface. Besides, the surface showed a good resistance in weak acid and neutral solutions. However, at high and weak basic and at high acidic solutions, the contact angle decreased when the immersion time was lengthened.

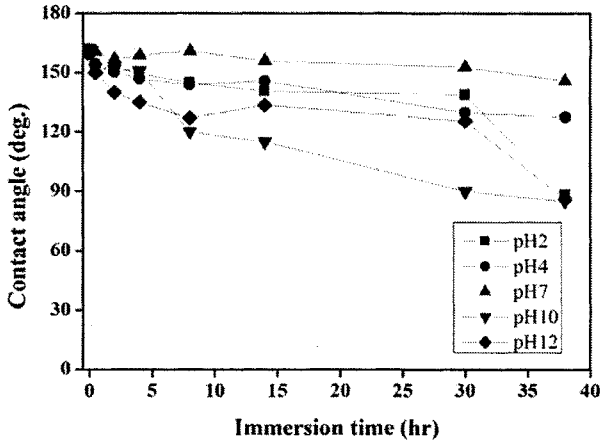

Figure VI.6: Variations of the contact angle of *W25* at different pH values versus immersion time.

The coating's stability of *W25* was studied as a function of immersion time in a pH7 solution for time periods beyond a day or two. Figure VI.7 shows that the contact angle decreased linearly from 161° to 100° after 700 hours. By increasing the immersion time up to 1200 hours, the contact angle reached 80°. Although the contact angle decreased after 1200 hours of immersion in water, the surface could still be considered hydrophobic.

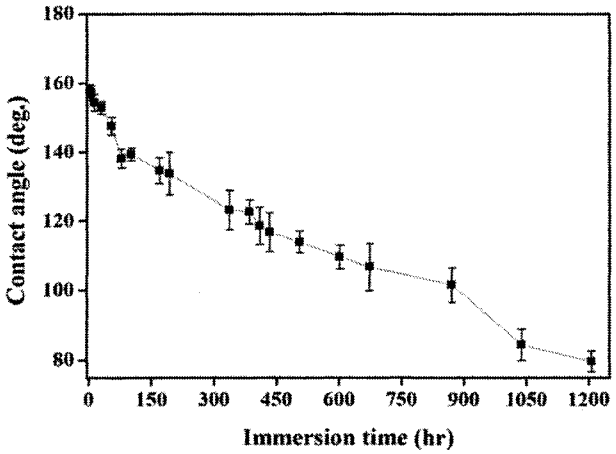

Figure VI.7: Variation of the contact angle of *W25*versus immersion time in distilled water.

VI-4-Ice adhesion strength results

The ice adhesion strength of different treated surfaces at different deposition time periods is compared in Table VI.3. The results show that *W25* and *A25* can be associated with reduction of the ice adhesion strength. It can be seen that by increasing plasma polymerization deposition time, the ice adhesion strength of *A15* was reduced from 100 kPa to 83 kPa for *A25*. The ice adhesion strength of *W15*, however, was increased from 30 kPa to 46 kPa for *W25* (25 minutes). These low variations are not significant, and it is concluded that the ice adhesion strength for both surfaces (*W15* and *W25*) remains the same.

Table VI.3: Comparison of ice adhesion strength of untreated and PP-HMDSO coated aluminum substrates.

Name	Ice adhesion strength (kPa)	ARF
Untreated aluminum	350 ± 25	1
W25	46 ± 6	7.6
A25	83 ± 5	4.2

VI-4-1-Stability of a PP-HMDSO coating against several icing/de-icing cycles

In order to evaluate the longevity of the surfaces and to assess their potential outdoor applications, their durability was studied following several icing/de-icing cycles. Ice adhesion strength and contact angle of *A25* and *W25* were measured after each successive

icing/de-icing cycle.

VI-4-1-1-Study of the stability of a PP-HMDSO thin film deposited on an anodized aluminum surface after several icing/de-icing cycles

The variation of ice adhesion strength of *A25* after several icing/de-icing cycles is shown in Figure VI.8. These results show that the ice adhesion stress of *A25* had a minor increment after fifteen icing/de-icing cycles. Ice adhesion strength started from 83 ± 5 and reached 130 ± 30 kPa. Also, it was noticed that the surface could keep its icephobic characteristic (ARF = 2.7). These results show that the ice adhesion strength of *A25* (130 kPa) is almost half that of *A15*'s ice adhesion strength (250 kPa) after fifteen icing/de-icing cycles. Therefore, by comparing the results of the shear stress value of *A25* after fifteen icing/de-icing cycles (ARF = 2.7) with the results obtained for *A15* (ARF = 1.4), a significant improvement of stability against several icing/de-icing cycles can be observed.

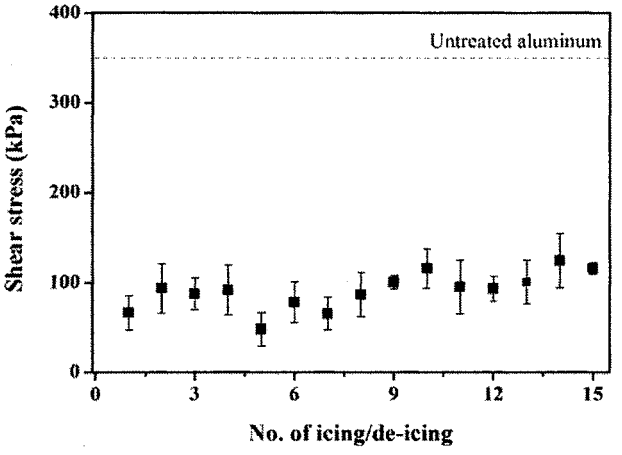

Figure VI.8: Variation of shear stress of *A25* versus several icing/de-icing cycles.

Figure VI.9 shows the variation of the contact angle on a superhydrophobic surface after several icing/de-icing cycles. The contact angle slightly decreased from 162 ± 3° to 156 ± 2° after fifteen icing/de-icing cycles. The water droplet can easily roll off the surface as the sliding angle has remained constant, around 3°, and the *f* value increased slightly from 0.059 to 0.104, after fifteen icing/de-icing cycles. It can also be assumed that the Cassie-Baxter wetting regime is still dominant after fifteen icing/de-icing cycles on the surface. Therefore, the increment of deposition time of a PP- HMDSO coating on an anodized aluminum surface leads to enhanced contact angle value of *A25* (156°) compared to the contact angle value of *A15* (145°) after fifteen icing/de-icing cycles.

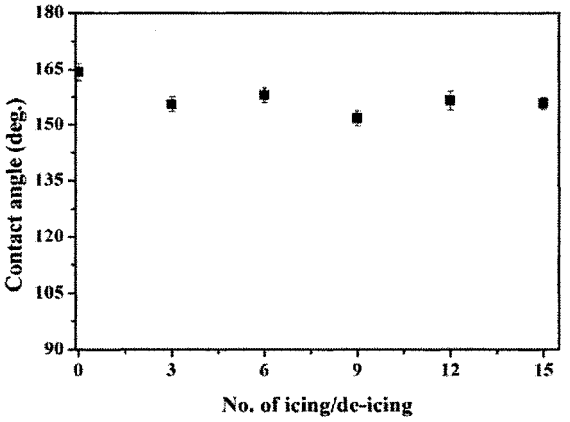

Figure VI.9: Variation of the contact angle versus icing/de-icing cycles for *A25*.

SEM images of *A25* before and after fifteen icing/de-icing cycles are presented in Figures VI.10a-b. A partial elimination of the coating is observed on some regions after fifteen icing/de-icing cycles, see Figure VI.10b; however, the surfaces have the same micro-structure before and after fifteen icing/de-icing cycles. The presence of micro-

structures after fifteen icing/de-icing cycles confirms the results of ice adhesion strength and the contact angle measurement.

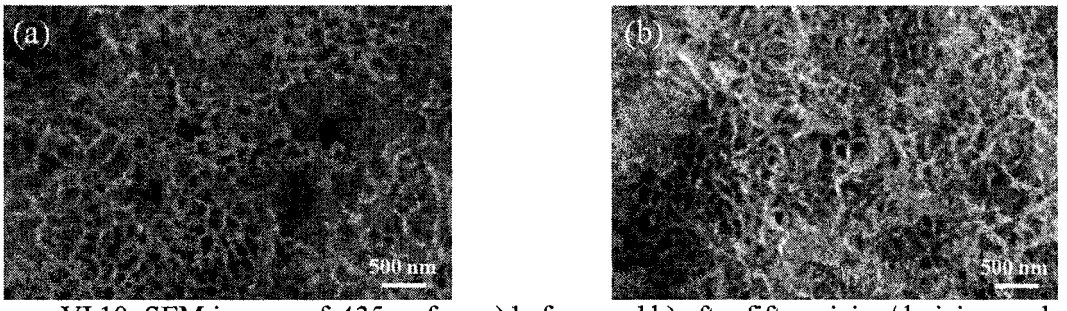

Figure VI.10: SEM images of *A25* surface a) before, and b) after fifteen icing/de-icing cycles.

The chemical composition results of *A25* before and after fifteen icing/de-icing cycles obtained by XPS analysis are summarized in Table VI.4. The presence of a carbon component of the coating before and after icing/de-icing showed the presence of an organic film on the surfaces. The amount of carbon and silicone groups decreased after fifteen icing/de-icing cycles. However, the ratio of C to Si (C/Si) as a concentration of organic to an inorganic function before and after icing/de-icing remained approximately constant (2.35 ± 0.25). The results indicate that the top layer of *A25* was probably removed after fifteen icing/de-icing cycles without affecting the structure. Despite the loss of coating of *A25* after fifteen icing/de-icing cycles, the percentage of carbon of *A25* over fifteen icing/de-icing cycles (26%) is more than its value of *A15* before fifteen icing/de-icing cycles (21%). Also, the amount of C/Si ratio of *A25* after fifteen icing/de-icing cycles (2.36) is more than *A15* before fifteen icing/de-icing cycles (1.5). The information obtained from the XPS analysis complements the results obtained from the SEM images, the contact

angle and ice adhesion strength measurement of *A25* after fifteen icing/de-icing cycles.

Table VI.4: The elemental composition of *A25* before and after fifteen icing/de-icing cycles by XPS measurements.

Surface *A25*	C	Si	O	Al
Before icing/de-icing	42	20	34	4
After icing/de-icing	26	11	43	20

In order to have a better understanding of the structure of C1s peak of *A25*, a high-resolution XPS measurement is carried out. Figures VI.11a-b shows the high resolution of C1s (285 eV) spectrum of *A25* before and after icing/de-icing cycles. It should be noted that the three peaks show the concentration of carbon groups on the surface ($(CH_3)_x$-Si-O, C-C, C-O). Figure VI.11a indicates a high concentration of methyl groups ($(CH_3)_x$-Si-O about 25%) on *A25* surface before fifteen icing/de-icing cycles. The percentage of the function decreased to 12% after fifteen icing/de-icing cycles, as shown in Figure 6.11b.

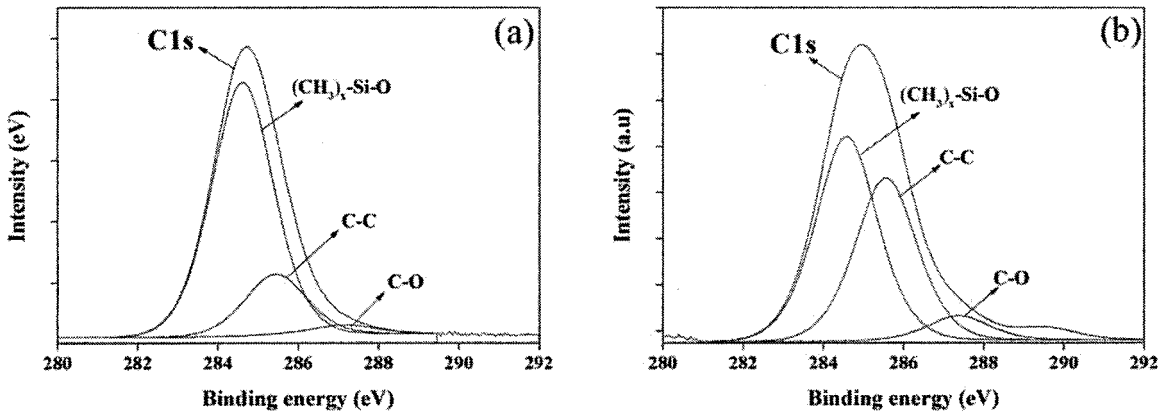

Figure VI.11: XPS High resolution spectrum of C1s of A25 a) before icing/de-icing cycles and b) after fifteen icing/de-icing cycles.

VI-4-1-2- Study of the stability of a PP-HMDSO coating deposited on a water-treated aluminum surface after several icing/de-icing cycles

In Figure VI.12, the shear stress of *W25* after fifteen icing/de-icing cycles shows an increase from 46 ± 6 kPa (ARF = 7.6) to 150 ± 26 kPa (ARF = 2.3), nonetheless it keeps its icephobic properties after fifteen icing/de-icing cycles. It should be noted that before the increase of the deposition time, the water-treated surface (*W15*) also had a good stability after several icing/de-icing cycles.

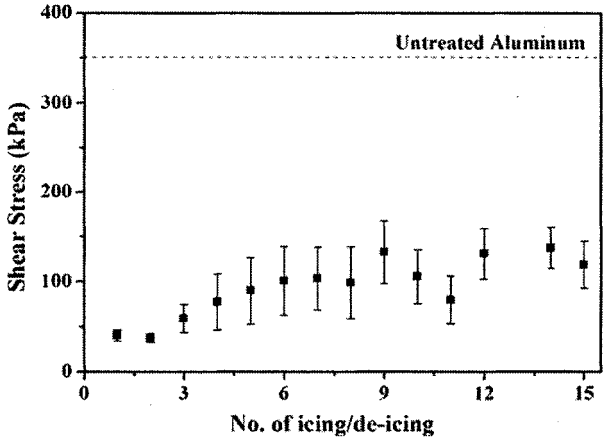

Figure VI.12: Variation of shear stress versus icing/de-icing cycles for *W25*.

The variation in contact angle of *W25* after several icing/de-icing cycles is shown in Figure VI.13. The results clearly demonstrate that the contact angle of *W25* varies little, from 161 ± 3° to 152 ± 4°, after fifteen icing/de-icing cycles. The water droplet can easily roll off the surface as the sliding angle has increased slightly from 2° to 3° and the f value

rises slowly from 0.080 to 0.141 after fifteen icing/de-icing cycles. It can also be assumed that Cassie-Baxter wetting regime is still dominant on the surface of *W25* after fifteen icing/de-icing cycles.

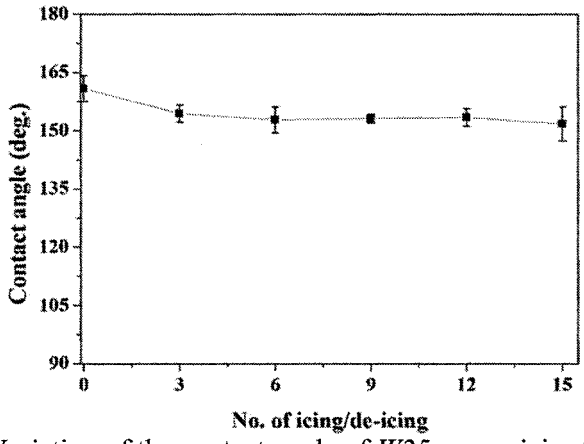

Figure VI.13: Variation of the contact angle of *W25* versus icing/de-icing cycles.

Figure VI.14a-b shows the chemical composition of *W25* before and after fifteen icing/de-icing cycles obtained by a FT-IR spectrum. The presence of methyl groups as a hydrophobic function of the surface was observed after fifteen icing/de-icing cycles. The FT-IR results confirm the results of the contact angle measurements and the adhesion strength of the superhydrophobic *W25* after fifteen icing/de-icing cycles.

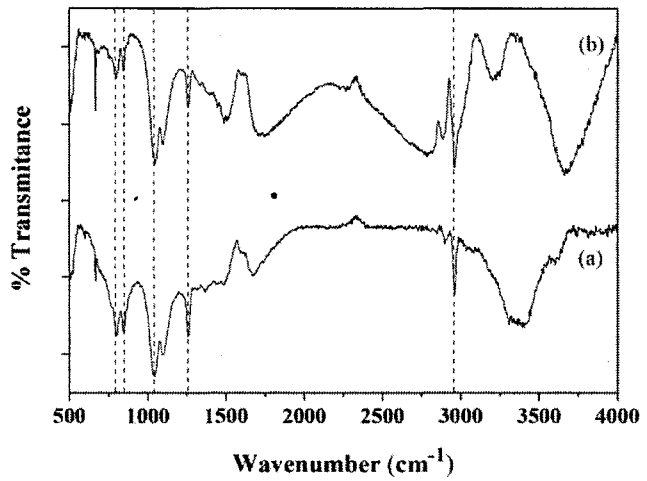

Figure VI.14: FT-IR spectrum of *W25* a) before and b) after fifteen icing/de-icing cycles.

VI-5- Study of anti-corrosion properties of superhydrophobic surfaces

Corrosion is considered a major problem in many industries. Since corrosion can lead to unexpected failures that can be costly in terms of repair costs, environmental damage, and potential harm to humans beings, many researchers have studied various techniques to improve corrosion resistance. Superhydrophobic coating is one of the methods used to protect the corrosion of surfaces. *Xu* et al. [158] showed that the polarization current of a superhydrophobic coating was reduced by two order of magnitude after one hour of immersion in 3.5% sodium chloride solution.

In this section, the corrosion behavior of the PP-HMDSO coating deposited on anodized aluminum is studied. The degree of corrosion resistance of a superhydrophobic surface was compared with aluminum alloy 6061 and anodized aluminum surfaces.

Potentiodynamic polarization was carried out to compare the corrosion behavior of

untreated aluminum, anodized aluminum, and superhydrophobic aluminum surfaces (Figure VI.15). Results show that the corrosion potential (E_{corr}) of untreated aluminum is around -756 mV with corrosion current of 1.48×10^{-6} A (Figure VI.15a). After anodizing the surface, the corrosion potential value has increased to -663 mV and current has decreased to 2.2×10^{-7} A, as displayed in Figure VI.15b. This result indicates that the anodization method leads to an improvement of corrosion resistance [106]. The PP-HMDSO coating deposited on anodized aluminum as a superhydrophobic coating leads to the potential corrosion shift in a positive direction at -225 mV with a low current of 1.2×10^{-7} A (see Figure VI.15c). These results show that the corrosion current density of a superhydrophobic coating decreased by one order of magnitude as compared to an untreated aluminum surface.

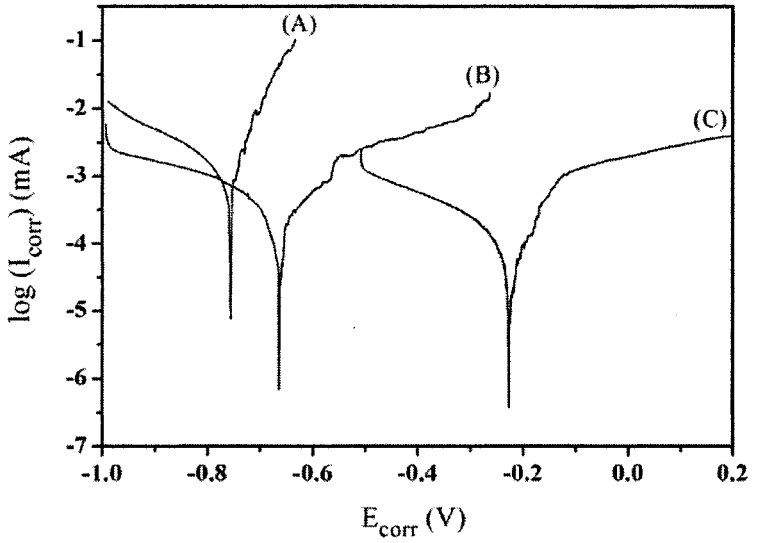

Figure. VI.15: Potentiodynamic polarization curves of a) aluminum alloy 6061, b) anodized aluminum and c) superhydrophobic surface for 24 h in 3.5% NaCl (seawater).

According to the results of the polarization resistance technique, the values of the corrosion potential (E_{corr}), corrosion current (I_{corr}), and polarization resistance (R_p) of untreated aluminum, anodized aluminum, and the PP-HMDSO coating on an anodized aluminum are summarized in Table VI.5.

Table VI.5: Comparison of corrosion parameters on aluminum alloy, anodized aluminum and superhydrophobic surface.

Type of surface	Ecorr (mV)	Icorr (A)	Rp (kΩ)
Aluminum alloy 6061	-756	1.48×10^{-6}	16
Anodized aluminum	-663	0.22×10^{-7}	159
Superhydrophobic surface	-225	0.12×10^{-7}	265

The results reveal that the polarization resistance of untreated aluminum is around 16 kΩ. By anodizing the aluminum surface, the polarization resistance has increased ten times more than on untreated aluminum. The polarization resistance of a superhydrophobic surface is 16 times more than that of untreated aluminum and 1.7 times more than anodized aluminum. Hence the PP-HMDSO coating is proven protection for the aluminum substrate.

VI-6-Conclusion

In order to improve the stability of the PP-HMDSO coating, deposition time was increased from 15 to 25 minutes. By increasing deposition time, the thickness of the coating was increased as well. The XPS analysis showed an increase in the hydrophobic functional group on the coated substrate. In addition, the wettability of *A25* remained approximately constant when compared to surface *A15*, whereas a sliding angle was improved from 8 ° to

3°. However, the wettability of *W25* is similar to that of *W15*.

The durability of *A25* and *W25* was studied under a variety of conditions such as UV exposure, immersion in different pH solutions, and successive icing/de-icing cycles. These results indicated that *A25* and *W25* have a good resistance for up to 537 hours of UV exposure. In addition, *A25* and *W25* kept their hydrophobicity after 740 hours of immersion in a pH7 solution.

Under atmospheric icing conditions, the icephobic properties of *A25* were improved by which the ARF is 4.2 times more than of untreated aluminum surface. Additionally, on *A25* there was some partial removal of PP-HMDSO coating as shown by the XPS analysis. After fifteen icing/de-icing cycles, it kept its surface morphology (SEM images) and it was still superhydrophobic with icephobic properties (ARF = 2.7). Besides, the result of ice adhesion on *W25* showed that it still had good stability after fifteen icing/de-icing cycles.

Finally, the corrosion measurement analysis showed that the anodization method improved the corrosion resistance of untreated aluminum up to 10 times, while the superhydrophobic surface improved corrosion resistance up to 16 times and 1.7 times more than for an untreated aluminum surface and anodized aluminum surface, respectively.

CHAPTER VII

CONCLUSIONS AND FUTURE WORKS

CHAPTER VII

CONCLUSIONS AND FUTURE WORKS

VII-1- Conclusions

The work described in this thesis concerned the development of a stable superhydrophobic coating with icephobic properties by using a low-pressure plasma polymerizing process. Superhydrophobic surfaces were achieved by the creation of a micro/nano rough surface, using anodization and boehmite methods followed by a coating of low surface energy materials. The influence of voltage and time in anodization technique as well as immersion time in boehmite technique was optimized by contact angle measurement.

Also, plasma processing parameters had been optimized by the Grey-based Taguchi method to minimize the number of experiments and, subsequently, optimize the conditions

in order to have high contact angle and low contact angle hysteresis. Additionally, the order of importance of the controlling parameters was obtained. The results indicated that the distance from the monomer inlet contributed the most to overall water repellency. The input plasma power and deposition time also provided a fairly large contribution to the plasma polymer coating hydrophobicity. On the other hand, the monomer flow played a minor role on the water repellency of the coating.

The durability of plasma-polymerized coatings was studied under natural conditions such as UV degradation, immersion in different pH solutions and, after several icing/de-icing cycles. The results showed that the stability of *A15* and *W15* were maintained against UV degradation after 240 hours, since they kept superhydrophobic properties (contact angle ~ 150°). Besides, the superhydrophobic coatings were stable after 740 hours of immersion in distilled water. Furthermore, the superhydrophobic coating can reduce the ice adhesion strength of an aluminum surface 3.5 and 11.6 times (*A15* and *W15* respectively), compared with a hydrophobic coating on which ice adhesion strength was reduced only 1.4 times more than untreated aluminum. The durability of *A15* and *W15* was studied after fifteen icing/de-icing cycles. Although the shear stress of *A15* increased after fifteen icing/de-icing cycles, it kept its icephobic properties (ARF = 1.4). The SEM and AFM images of *A15* after fifteen icing/de-icing cycles showed the important variation of surface morphology and the reduction of surface roughness. *W15* retained a good stability after fifteen icing/de-icing cycles. The XPS analysis and AFM images of *W15* confirmed the presence of CH_3 groups (as a hydrophobic function groups) and the same micro-nano structure of roughness after fifteen icing/de-icing cycles.

In order to improve the stability of the plasma polymerized HMDSO coating, the deposition time was increased. By increasing the deposition time, the thickness of the coating was increased from 5 to 18 nm. Also, the percentage of hydrophobic Si-CH_3 functional groups on the surface was increased through this extension the deposition time. The results of the contact angle and the sliding angle measurements showed that by increasing the deposition time, the sliding angle of *A25* was less than the sliding angle of *A15,* while they kept the same static contact angles. Superhydrophobic *A25* demonstrated good stability against UV degradation after 537 hour of UV exposure; it continued to show presence of hydrophobic properties (contact angle ~ 90°) of *A25* after 1200 hours of immersion in distilled water. The shear stress of *A25* increased slightly from 83 kPa to 130 kPa after fifteen icing/de-icing cycles. The superhydrophobic properties of *A25* (contact angle~156°) and its icephobic properties (ARF = 2.7) showed good stability after fifteen icing/de-icing cycles. *W25* had good stability after fifteen icing/de-icing cycles as, was confirmed by the results of contact angle measurement and FT-IR analysis.

Finally the plasma polymerized HMDSO coating as a superhydrophobic coating also improved the corrosion resistance of the aluminum surface in addition to improving its ice repellency.

VII-2- Future works

- Since that the fluorocarbon precursor has a good adhesion to different substrates with relatively inert surfaces that have extremely low free energy and the low friction

coefficient. Also the Polytetrafluoroethylene (PTFE) was shown as one of the best fluorocarbon polymers due to its low electrical permittivity of ~2.1, low surface energy and chemical stability. Therefore, the use of a fluorocarbon precursor is a worthy object of study in order to compare it with the results of the organosilicon precursor used in this thesis.

- Performing some tests under natural conditions would contribute great originality in this study, because of all experimental tests were conducted in the laboratory by controlling the different parameters;

- Study the physico-chemical variation of different surfaces: untreated aluminum, anodized aluminum, and water-treated aluminum, successive icing/de-icing cycles. In this study we found that the under-lying structure can affect the stability of coating.

- Study the influence of the liquid water content, temperature, wind speed and droplet size on adhesive ice on a surface in order to accumulated different type of ice.

- Make additional experimental tests to better understand the process of ice accretion on these surfaces subjected to an electric field. This study does not take into account the presence of an external electric field during the accumulation of ice on our different samples. However, it was found that the amount of ice accumulated and its density depend on the intensity and polarity of the applied voltage. Moreover, in the presence of an external electric field, additional charges will accumulate more proten fillers present in the glaze ice.

- According to the preliminary results obtained in the study of corrosion resistance of a PP-HMDSO coating, it is suggested to use the design of experiment technique to optimize plasma processing parameters to observe the effect of superhydrophobic properties and anti-corrosion of a plasma polymerization coating simultaneously.

- In this study, the durability of the superhydrophobic coating based on measuring the contact angle was studied against immersion in various pH solutions. Also, it was shown that the superhydrophobic surface, which was created by PP-HMDSO coating, led to improving the corrosion resistance of the aluminum surface. Therefore, advanced studies are proposed concerning the corrosive properties of different pH solutions on a superhydrophobic surface.

References

[1] Farzaneh M., ed., 2008, "Atmospheric Icing of Power", Springer, Berlin.

[2] Farzaneh M., 2000, "Ice Accretion on H.V. conductors and Insulators and Related Phenomena," Invited Paper, Philosophical Transactions, the Royal Society London, no. 358, pp. 1–35.

[3] Farzaneh M., and Kasaai M. R., "Analytical Evaluation of Existing Mechanisms of Ice Adhesion on Power Network Equipment," Proceedings of the 23rd International Conference on Offshore Mechanics and Arctic Engineering, American Society of Mechanical Engineers (ASME), New York, Vancouver, Canada, p. 51267.

[4] Farzaneh M., and Kasaai M. R., "A Critical Evaluation of the Existing Methods to Determine Ice Adhesion Strength," Proceedings of the 23rd International Conference on Offshore Mechanics and Arctic Engineering, American Society of Mechanical Engineers (ASME), New York, Vancouver, Canada, p. 51264.

[5] Farzaneh M., Volat C., and Leblond, 2008, "Anti-icing and De-icing Techniques for Overhead Lines," Atmospheric Icing of Power Networks, M. Farzaneh, ed., Elsevier, pp. 229–268.

[6] Menini R., Ghalmi Z., and Farzaneh M., 2011, "Highly resistant icephobic coatings on aluminum alloys," Cold Regions Science and Technology, 65(1), pp. 65–69.

[7] Jafari R., Menini R., and Farzaneh M., 2010, "Superhydrophobic and Icephobic Surfaces Prepared by RF-sputtered polytetrafluoroethylene coatings," Applied Surface Science, 257(5), pp. 1540–1543.

[8] Farhadi S., Farzaneh M., and Kulinich S. A., 2010, "Nanostructured Superhydrophobic Surfaces with Anti-Ice Properties," (387), pp. 4–6.

[9] Arianpour F., Farzaneh M., and Kulinich S. A., 2010, "Nanopowder-Doped Silicone Rubber Coatings for Anti-Ice Applications," Scanning Electron Microscopy, (497), pp. 4–6.

[10] Ma M., and Hill R. M., 2006, "Superhydrophobic surfaces," Current Opinion in Colloid & Interface Science, 11(4), pp. 193–202.

[11] Inagaki N., 1996, "Plasma Surface Modification and Plasma Polymerization", Technomic Publishing Company, Inc.

[12] D' Agostino R., 1990, Plasma Deposition, Treatment, and Etching of Polymers, Academic Press, Boston.

[13] Jafari R., Foroughi Mobarakeh L., and Farzaneh M., 2011, "Water-repellency enhancement of nanostructured plasma-polymerized HMDSO coatings," Nanoscience and Nanotechnology Letters, 4(3), pp. 369–374.

[14] Nakajima A., Hashimoto K., and Watanabe T., 2001, "Invited Review Recent Studies on Super-Hydrophobic Films," Langmuir, 41, pp. 31–41.

[15] Young T., 1805, "An Essay on the Cohesion of Fluids," Phil. Trans. R. Soc. Lond., 95, pp. 609–612.

[16] Fürstner R., Barthlott W., Neinhuis C., and Walzel P., 2005, "Wetting and self-cleaning properties of artificial superhydrophobic surfaces," Langmuir : the ACS Journal of Surfaces and Colloids, 21(3), pp. 956–61.

[17] Wikipedia, 2013, "http://en.wikipedia.org/wiki/Lotus_effect."

[18] Parkin I. P., and Palgrave R. G., 2005, "Self-cleaning coatings," Journal of Materials Chemistry, 15(17), p. 1689.

[19] Yuan Z., Chen H., Zhang J., Zhao D., Liu Y., Zhou X., Li S., Shi P., Tang J., and Chen X., 2008, "Preparation and characterization of self-cleaning stable superhydrophobic linear low-density polyethylene," Science and Technology of Advanced Materials, 9(4), pp. 1–5.

[20] Barraza H. J., Hwa M. J., Blakley K., O'Rear E. a., and Grady B. P., 2001, "Wetting Behavior of Elastomer-Modified Glass Fibers," Langmuir, 17(17), pp. 5288–5296.

[21] Nosonovsky M., and Bhushan B., 2008, "Multiscale Dissipative Mechanisms and Hierarchical Surfaces", Springer, Verlag Berlin Heidelberg.

[22] Cassie A. B. D., and Baxter S., 1944, "Wettability of porous surfaces," Transactions of the Faraday Society, 40, pp. 546–551.

[23] Jafari R., and Farzaneh M., 2012, "Development a simple method to create the superhydrophobic composite coatings," Journal of Composite Materials, pp. 1–5.

[24] Momen G., Farzaneh M., and Jafari R., 2011, "Wettability behaviour of RTV silicone rubber coated on nanostructured aluminium surface," Applied Surface Science, 257(15), pp. 6489–6493.

[25] Jafari R., and Farzaneh M., 2011, "Fabrication of superhydrophobic nanostructured surface on aluminum alloy," Applied Physics A, 102(1), pp. 195–199.

[26] Liao K.-S., Wan A., Batteas J. D., and Bergbreiter D. E., 2008, "Superhydrophobic surfaces formed using layer-by-layer self-assembly with aminated multiwall carbon nanotubes.," Langmuir.: the ACS journal of surfaces and colloids, 24(8), pp. 4245–53.

[27] Saleema N., Farzaneh M., and Paynter R. W., 2009, "Fabrication of TiO2 μ-donuts by sol–gel spin coating using a polymer mask," Applied Surface Science, 255(11), pp. 5837–5842.

[28] Nakajima a, 2000, "Preparation of hard super-hydrophobic films with visible light transmission," Thin Solid Films, 376(1-2), pp. 140–143.

[29] Li M., Zhai J., Liu H., Song Y., Jiang L., and Zhu D., 2009, "Electrochemical Deposition of Conductive Superhydrophobic Zinc Oxide Thin Films," Society, pp. 9954–9957.

[30] Ghalmi Z., Menini R., and Farzaneh M., 2009, "Theoritical Studies and Quantification of Ice Adhesion Mechanisms," Proceeding of the 13th International workshop on Atmospheric icing of structures, IWAIS, Andermatt.

[31] Kale K. H., and Palaskar S., 2010, "Atmospheric pressure plasma polymerization of hexamethyldisiloxane for imparting water repellency to cotton fabric," Textile Research Journal, 81(6), pp. 608–620.

[32] Jafari R., Asadollahi S., and Farzaneh M., 2012, "Applications of Plasma Technology in Development of Superhydrophobic Surfaces," Plasma Chemistry and Plasma Processing, 33(1), pp. 177–200.

[33] Laforte, C., Laforte, J.L., Carrier L. C., 2002, "How a solid coating can reduce the adhesion of ice on a structure," Proceedings of the International Workshop on Atmospheric Icing of Structures (IWAIS), p. 6.

[34] Roach P., Shirtcliffe N. J., and Newton M. I., 2008, "Progess in superhydrophobic surface development," Soft Matter, 4(2), pp. 224–240.

[35] Pulpytel J., Kumar V., Peng P., Micheli V., Laidani N., and Arefi-Khonsari F., 2011, "Deposition of Organosilicon Coatings by a Non-Equilibrium Atmospheric Pressure Plasma Jet: Design, Analysis and Macroscopic Scaling Law of the Process," Plasma Processes and Polymers, 8(7), pp. 664–675.

[36] Kako T., Nakajima A., Irie H., Kato Z., Uematsu K., Watanabe T., and Hashimoto

K., 2004, "Adhesion and sliding of wet snow on a super-hydrophobic surface with hydrophilic channels," Journal of Materials Science, 39(2), pp. 547–555.

[37] Zhang X., Shi F., Niu J., Jiang Y. G., and Wang Z. Q., 2008, "Superhydrophobic surfaces: from structural control to functional application," Journal of Materials Chemistry, 18(6), pp. 621–633.

[38] Menini R., and Farzaneh M., 2009, "Elaboration of Al2O3/PTFE icephobic coatings for protecting aluminum surfaces," Metal Finishing, 107(7-8), pp. 40–46.

[39] Safaee A., 2008, "Nanostructured Metal Surfaces and Their Passivation For Superhydrophobic and Antiicing Applications," University of Quebec at Chicoutimi.

[40] Rombaldoni F., Mossotti R., Montarsolo A., Songia M. B., Innocenti R., and Mazzuchetti G., 2008, "Thin film deposition by PECVD using HMDSO-O-2-Ar gas mixture on knitted wool fabrics in order to improve pilling resistance," Fibers and Polymers, 9(5), pp. 566–573.

[41] Ji Y., Kim S., Kwon O., and Lee S., 2009, "Easy fabrication of large-size superhydrophobic surfaces by atmospheric pressure plasma polymerization with non-polar aromatic hydrocarbon in an in-line process," Applied Surface Science, 255(8), pp. 4575–4578.

[42] Ku W.-L., Hung C.-L., Lee S.-M., and Han-Ming C., 2010, "Optimization in thermal friction drilling for SUS 304 stainless steel," The International Journal of Advanced Manufacturing Technology, 53(9-12), pp. 935–944.

[43] Ji Y. Y., Hong Y. C., Lee S. H., Kim S. D., and Kim S. S., 2008, "Formation of super-hydrophobic and water-repellency surface with hexamethyldisiloxane (HMDSO) coating on polyethyleneteraphtalate fiber by atmosperic pressure plasma polymerization," Surface & Coatings Technology, 202(22-23), pp. 5663–5667.

[44] Energy deregulation forces wide scale distributed energy, 2008, "Http://mgx.com/blogs/2008/03/30/energy-deregulation-forces-wide-scale-distributed-energy."

[45] ISO12494, 2001, International Standards of Atmospheric Icing on Structures, ISO12494.

[46] Noormohammed S., 2009, "Nanostructured Thin Films for Icephobic Applications," University of Quebec at Chicoutimi.

[47] Jafari R., and Farzaneh M., 2010, "Icephobic and superhydrophobic surfaces

prepared on micro-nano structured aluminium oxyde by RF-sputtered polytetrafluoroethylene coatings," Proceedings of the International Conference on Nanotechnology: Fundamentals and Applications, Ottawa, Ontario, Canada.

[48] Menini R., and Farzaneh M., 2009, "Elaboration of Al2o3/PTFE Icephobic Coatings for Protecting Aluminum Surfaces," Surface & Coatings Technology, 203, pp. 1941–1946.

[49] Kulinich S. A., and Farzaneh M., 2011, "On ice-releasing properties of rough hydrophobic coatings," Cold Regions Science and Technology, 65(1), pp. 60–64.

[50] Sarkar D. . K., and Farzaneh M., 2009, "Superhydrophobic Coatings with Reduced Ice Adhesion," Journal of Adhesion Science and Technology, 23(9), pp. 1215–1237.

[51] Guo P., Zheng Y., Wen M., Song C., Lin Y., and Jiang L., 2012, "Icephobic/anti-icing properties of micro/nanostructured surfaces.," Advanced materials (Deerfield Beach, Fla.), 24(19), pp. 2642–8.

[52] Huang Y., Hu M., Yi S., Liu X., Li H., Huang C., Luo Y., and Li Y., 2012, "Preparation and characterization of silica/fluorinated acrylate copolymers hybrid films and the investigation of their icephobicity," Thin Solid Films, 520(17), pp. 5644–5651.

[53] Sarshar M. A., Swarctz C., Hunter S., Simpson J., and Choi C.-H., 2012, "Effects of contact angle hysteresis on ice adhesion and growth on superhydrophobic surfaces under dynamic flow conditions," Colloid and Polymer Science, 291(2), pp. 427–435.

[54] Wang F., Li C., Lv Y., Lv F., and Du Y., 2010, "Ice accretion on superhydrophobic aluminum surfaces under low-temperature conditions," Cold Regions Science and Technology, 62(1), pp. 29–33.

[55] Chen J., Liu J., He M., Li K., Cui D., Zhang Q., Zeng X., Zhang Y., Wang J., and Song Y., 2012, "Superhydrophobic surfaces cannot reduce ice adhesion," Applied Physics Letters, 101(11), p. 111603.

[56] Jung S., Dorrestijn M., Raps D., Das A., Megaridis C. M., and Poulikakos D., 2011, "Are Superhydrophobic Surfaces Best for Icephobicity?," Langmuir : the ACS journal of surfaces and colloids, pp. 3059–3066.

[57] Hare E., Shafrin E., and Zisman W., 1954, "Properties of films of adsorbed fluorinated acids," The Journal of Physical Chemistry, 58(3), pp. 236–239.

[58] Terlingen J. G. A., 1993, "Introduction of funtional groups at polymer surfaces by Glow discharge techniques," Universiteit Twente.

[59] Tendero C., Tixier C., Tristant P., Desmaison J., and Leprince P., 2006, "Atmospheric pressure plasmas: A review," Spectrochimica Acta Part B-Atomic Spectroscopy, 61(1), pp. 2–30.

[60] Yasuda H., and Matsuzawa Y., 2005, "Economical Advantages of Low-Pressure Plasma Polymerization Coating," Plasma Processes and Polymers, 2(6), pp. 507–512.

[61] Yasuda H. K., 1985, "Plasma Polymerization", Academic Press, Orlando, Florida 32887.

[62] Service M. T., "Plasma polymerized coatings," www.tungsten.com.

[63] Mukhopadhyay S. M., Joshi P., Datta S., and Macdaniel J., 2002, "Plasma assisted surface coating of porous solids," Applied Surface Science, 201(1-4), pp. 219–226.

[64] Prat R., Koh Y. J., Babukutty Y., Kogoma M., Okazaki S., and Kodama M., 2000, "Polymer deposition using atmospheric pressure plasma glow (APG) discharge," Polymer, 41(20), pp. 7355–7360.

[65] Zhang J., Van Ooij W., France P., Datta S., Radomyselskiy A., and Xie H. Q., 2001, "Investigation of deposition rate and structure of pulse DC plasma polymers," Thin Solid Films, 390(1-2), pp. 123–129.

[66] Hozumi Sekoguchi, H., Kakinoki, N., Takai, O. A., 1997, "Preparation of transparent water-repellent films by radio-frequency plasma-enhanced chemical vapour deposition," Journal of Materials Science 32(16), pp. 4253–4259.

[67] Takai O., Hozumi A., and Sugimoto N., 1997, "Coating of transparent water-repellent thin films by plasma-enhanced CVD," Journal of Non-Crystalline Solids, 218, pp. 280–285.

[68] Visser S. A., Hewitt C. E., Fornalik J., Braunstein G., Srividya C., and Babu S. V, 1997, "Compositions and surface energies of plasma-deposited multilayer fluorocarbon thin films," Surface & Coatings Technology, 96(2-3), pp. 210–222.

[69] Gilman A. B., Potapov V. K., and Dvornikova K. V, 2004, "On Glow Discharge Polymerizations of Polyfluoroarenes," Chemistry for Sustainable Development 12, 12, pp. 595–600.

[70] Mccord M. G., Hwang Y. J., Qiu Y., Hughes L. K., Bourham M. A., and Carolina N., 2002, "Surface Analysis of Cotton Fabrics Fluorinated in Radio- Frequency Plasma," Polymer, pp. 6 – 8.

[71] Yang G. H., Zhang Y., Kang E. T., Neoh K. G., Huan a. C. H., and Lai D. M. Y., 2002, "Plasma polymerization of allylpentafluorobenzene on copper surfaces," Journal of Materials Chemistry, 12(3), pp. 426–431.

[72] Zhang Y., Kang E. T., Neoh K. G., Huang W., Huan A. C. H., Zhang H., and Lamb R. N., 2002, "Surface modification of polyimide films via plasma polymerization and deposition of allylpentafluorobenzene," Polymer, 43(26), pp. 7279–7288.

[73] Intranuovo F., Sardella E., Rossini P., d'Agostino R., and Favia P., 2009, "PECVD of Fluorocarbon Coatings from Hexafluoropropylene Oxide: Glow vs. Afterglow," Chemical Vapor Deposition, 15(4-6), pp. 95–100.

[74] Kumar V., Pulpytel J., Rauscher H., Mannelli I., Rossi F., and Arefi-Khonsari F., 2010, "Fluorocarbon Coatings Via Plasma Enhanced Chemical Vapor Deposition of 1H,1H,2H,2H-perfluorodecyl Acrylate - 2, Morphology, Wettability and Antifouling Characterization," Plasma Processes and Polymers, 7(11), pp. 926–938.

[75] Zanini S., Riccardi C., Orlandi M., Esena P., Tontini M., Milani M., and Cassio V., 2005, "Surface properties of HMDSO plasma treated polyethylene terephthalate," Surface & Coatings Technology, 200(1-4), pp. 953–957.

[76] Zanini S., Riccardi C., Orlandi M., Fornara V., Colombini M. P., Donato D. I., Legnaioli S., and Palleschi V., 2008, "Wood coated with plasma-polymer for water repellence," Wood Science and Technology, 42(2), pp. 149–160.

[77] Grimoldi E., Zanini S., Siliprandi R. A., and Riccardi C., 2009, "AFM and contact angle investigation of growth and structure of pp-HMDSO thin films," European Physical Journal D, 54(2), pp. 165–172.

[78] Behnisch J., Tyczkowski J., Gazicki M., Pela I., Hollander A., and Ledzion R., 1998, "Formation of hydrophobic layers on biologically degradable polymeric foils by plasma polymerization," Surface & Coatings Technology 98(1-3), pp. 872–874.

[79] Hegemann D., Brunner H., and Oehr C., 2002, "Plasma Treatment of Polymers to Generate Stable , Hydrophobic Surfaces," 6(4), pp. 221–235.

[80] Hegemann D., 2008, "Macroscopic control of plasma polymerization processes," Pure and Applied Chemistry, 80(9), pp. 1893–1900.

[81] Schwarz J., Schmidt M., and Ohl A., 1998, "Synthesis of plasma-polymerized hexamethyldisiloxane (HMDSO) films by microwave discharge," Surface & Coatings Technology, 98(1-3), pp. 859–864.

[82] Hirotsu T., Castillo M., Nakayama K., Tsuruta S., and Suzuki H., 2007, "Surface wetting phenomena of plasma polymer-coated sheets of poly(L-lactic acid)/poly(butylene succinate)," Thin Solid Films, 515(9), pp. 4125–4129.

[83] Taylor P., Kale K. H., and Palaskar S. S., 2012, "Structural studies of plasma polymers obtained in pulsed dielectric barrier discharge of TEOS and HMDSO on nylon 66 fabrics," (February 2013), pp. 37–41.

[84] Kale K. H., and Palaskar S. S., 2012, "Plasma Enhanced Chemical Vapor Deposition of Tetraethylorthosilicate and Hexamethyldisiloxane on Polyester Fabrics Under Pulsed and Continuous Wave Discharge," 125(5), pp. 3996–4006.

[85] Siliprandi R. a., Zanini S., Grimoldi E., Fumagalli F. S., Barni R., and Riccardi C., 2011, "Atmospheric Pressure Plasma Discharge for Polysiloxane Thin Films Deposition and Comparison with Low Pressure Process," Plasma Chemistry and Plasma Processing, 31(2), pp. 353–372.

[86] Palaskar S., Kale K. H., Nadiger G. S., and Desai A. N., 2011, "Dielectric Barrier Discharge Plasma Induced Surface Modification of Polyester / Cotton Blended Fabrics to Impart Water Repellency Using HMDSO," Journal of Applied Polymer Science, 122(2), pp. 1092–1100.

[87] Yeping L., 2001, "Study of plasma-polymerization deposition of C2H2/CO2/H2 onto ethylene-co-propylene rubber membranes," Radiation Physics and Chemistry, 60(6), pp. 637–642.

[88] McCord Hwang, Y. J., Qiu, Y., Hughes, L. K., & Bourham, M. A. M. G., 2003, "Surface analysis of cotton fabrics fluorinated in radio-frequency plasma," Journal of Applied Polymer Science 88(8), pp. 2038–2047.

[89] Morent R., De Geyter N., Jacobs T., Van Vlierberghe S., Dubruel P., Leys C., and Schacht E., 2009, "Plasma-Polymerization of HMDSO Using an Atmospheric Pressure Dielectric Barrier Discharge," Plasma Processes and Polymers, 6, pp. S537–S542.

[90] Yajima Kuroda, T., Okabe, Y., Sugiyama, K. T., 2003, "Dynamic plasma CVD and preparation of functional organic thin films," Journal of Photopolymer Science and Technology 16(1), pp. 61–65.

[91] Butoi C. I., Mackie N. M., Gamble L. J., Castner D. G., Barnd J., Miller A. M., and Fisher E. R., 2000, "Deposition of highly ordered CF2-rich films using continuous wave and pulsed hexafluoropropylene oxide plasmas," Chemistry of Materials, 12(7), pp. 2014–2024.

[92] Hozumi A., Cheng D. F., and Yagihashi M., 2011, "Hydrophobic/superhydrophobic oxidized metal surfaces showing negligible contact angle hysteresis.," Journal of colloid and interface science, 353(2), pp. 582–7.

[93] Hozumi A., and McCarthy T. J., 2010, "Ultralyophobic oxidized aluminum surfaces exhibiting negligible contact angle hysteresis.," Langmuir : the ACS journal of surfaces and colloids, 26(4), pp. 2567–73.

[94] Hozumi A., and McCarthy T. J., 2010, "Ultralyophobic oxidized aluminum surfaces exhibiting negligible contact angle hysteresis.," Langmuir : the ACS journal of surfaces and colloids, 26(4), pp. 2567–2573.

[95] Momen G., and Farzaneh M., 2012, "A ZnO-based nanocomposite coating with ultra water repellent properties," Applied Surface Science, 258(15), pp. 5723–5728.

[96] Lúcia M., Raymond N., Eletrônicos D. D. S., Politécnica E., Paulo U. D. S., Prof A., Gualberto L., Sala A., and Sp S. P., 2006, "Hydrophobic Plasma Polymerized Hexamethyldisilazane Thin Films : Characterization and Uses," 9(1), pp. 9–13.

[97] Isimjan T. T., Wang T., and Rohani S., 2012, "A novel method to prepare superhydrophobic, UV resistance and anti-corrosion steel surface," Chemical Engineering Journal, 210, pp. 182–187.

[98] Irzh A., Ghindes L., and Gedanken A., 2011, "Rapid deposition of transparent super-hydrophobic layers on various surfaces using microwave plasma.," ACS applied materials & interfaces, 3(12), pp. 4566–72.

[99] Huang C., Pan C.-H., and Liu C.-H., 2010, "Deposition of hydrophobic nano-coatings with low-pressure radio frequency CH2F2/Ar plasma processing," Thin Solid Films, 518(13), pp. 3570–3574.

[100] Ishizaki T., Masuda Y., and Sakamoto M., 2011, "Corrosion resistance and durability of superhydrophobic surface formed on magnesium alloy coated with nanostructured cerium oxide film and fluoroalkylsilane molecules in corrosive NaCl aqueous solution.," Langmuir : the ACS journal of surfaces and colloids, 27(8), pp. 4780–4788.

[101] Xu X., Zhang Z., Guo F., Yang J., Zhu X., Zhou X., and Xue Q., 2012, "Superamphiphobic self-assembled monolayer of thiol on the structured Zn surface," Colloids and Surfaces A: Physicochemical and Engineering Aspects, 396, pp. 90–95.

[102] Zanini S., Grimoldi E., and Riccardi C., 2013, "Development of controlled releasing surfaces by plasma deposited multilayers," pp. 1–6.

[103] Parker J. L., Claesson P. M., Wang J.-H., and Yasuda H. K., 1994, "Surface Forces between Plasma Polymer Films," Langmuir, 10(8), pp. 2766–2773.

[104] Gnanappa A. K., O'Murchu C., Slattery O., Peters F., Aszalós-Kiss B., and Tofail S. a. M., 2008, "Effect of annealing on hydrophobic stability of plasma deposited fluoropolymer coatings," Polymer Degradation and Stability, 93(12), pp. 2119–2126.

[105] Touzin M., Chevallier P., Lewis F., Turgeon S., Holvoet S., Laroche G., and Mantovani D., 2008, "Study on the stability of plasma-polymerized fluorocarbon ultra-thin coatings on stainless steel in water," Surface and Coatings Technology, 202(19), pp. 4884–4891.

[106] Yin Y., Liu T., Chen S., and Cheng S., 2008, "Structure stability and corrosion inhibition of super-hydrophobic film on aluminum in seawater," Applied Surface Science, 255(5), pp. 2978–2984.

[107] "http://www.corrosion-club.com/costs.htm."

[108] Huang Y., Sarkar D. K., Gallant D., and Chen X.-G., 2013, "Corrosion resistance properties of superhydrophobic copper surfaces fabricated by one-step electrochemical modification process," Applied surface science, 282, pp. 689–694.

[109] "http://asm.matweb.com."

[110] Hennesthal C., 2003, Application Report NanoWizard.

[111] Kelly R. G., Scully J. R., Shoesmith D. W., and Buchheit R. G., 2003, "'Electrochemical Techniques in Corrosion Science and Engineering'," Electrochemical Techniques in Corrosion Science and Engineering, P.E. Philip A. Schweitzer, ed., Marcel Dekker, Inc. TM New, Basel, p. 436.

[112] Vargel C., 2004, The Corrosion of Aluminium, Elsevier.

[113] Petrovic J., and Thomas G., 2008, Reaction of Aluminum with Water to Produce Hydrogen.

[114] Tadanaga K., Katata N., and Minami T., 1997, "Formation Process of Super-Water-Repellent Al2O3 Coating Films with High Transparency by the Sol – Gel Method," 16, pp. 3213–3216.

[115] Nikaido N., Shirai S., Iihashi M., and Umemoto S., 1978, "Process for Treating the surface of aluminium or aluminium alloy."

[116] "http://www.sigmaaldrich.com."

[117] Jafari R., Tatoulian M., and Arefi-Khonsari F., 2011, "Improvement of the Stability of Plasma Polymerized Acrylic Acid Coating Deposited on Ps Beads in a Fluidized Bed Reactor," Reactive and Functional Polymers, 71(4), pp. 520–524.

[118] Issa B., 2007, Six Sigma Statistics with EXCEL and MINITAB, McGraw-Hill Professional.

[119] Lin J. L., and Lin C. L., 2002, "The use of the orthogonal array with Grey relational analysis to optimize the electrical discharge machining process with multiple performance characteristics," International Journal of Machine Tools and Manufacture, 42(2), pp. 237–244.

[120] Datta S., Bandyopadhyay A., and Pal P. K., 2008, "Grey-based Taguchi method for optimization of bead geometry in submerged arc bead-on-plate welding," International Journal of Advanced Manufacturing Technology, 39(11/12), p. 1136.

[121] Nosonovsky M., and Bhushan B., 2007, "Hierarchical roughness optimization for biomimetic superhydrophobic surfaces.," Ultramicroscopy, 107(10-11), pp. 969–79.

[122] Callies M., Chen Y., Marty F., Pépin A., and Quéré D., 2005, "Microfabricated textured surfaces for super-hydrophobicity investigations," Microelectronic Engineering, 78-79, pp. 100–105.

[123] Bhushan B., and Chae Jung Y., 2007, "Wetting study of patterned surfaces for superhydrophobicity.," Ultramicroscopy, 107(10-11), pp. 1033–41.

[124] Miwa M., Nakajima A., Fujishima A., Hashimoto K., and Watanabe T., 2000, "Effects of the Surface Roughness on Sliding Angles of Water Droplets on Superhydrophobic Surfaces," Langmuir, 16(13), pp. 5754–5760.

[125] Banitalebi Dehkordi H., Kollar L., Farzaneh M., Camirand P., and Damours C., 2009, Introduction, Instrumentation and Calibration of CIGELE Atmospheric Icing Research Wind Tunnel (CAIRWT).

[126] Laforte C., and Beisswenger A., 2005, "Icephobic Material Centrifuge Adhesion Test," (June).

[127] Solution Material Testing, "http://atlas-mts.com/services/natural-weathering-testing/natural-weathering-testing-sites/north-america/."

[128] Mission T. A., 2001, "What is the network of weathering?," Weathering Testing

Guidebook, p. 108.

[129] Ghali E., 2010, "Corrosion Resistance of Aluminum and Magnesium Alloys Understanding, Performance, and Testing", John Wiley & Sons, Inc., Hoboken, New Jersey.

[130] Kumar V., Jolivalt C., Pulpytel J., Jafari R., and Arefi-Khonsari F., 2012, "Development of silver nanoparticle loaded antibacterial polymer mesh using plasma polymerization process.," Journal of biomedical materials research. Part A, pp. 1–12.

[131] Kumar V., Pulpytel J., Giudetti G., Rauscher H., Rossi F., and Arefi-Khonsari F., 2011, "Amphiphilic Copolymer Coatings via Plasma Polymerisation Process: Switching and Anti-Biofouling Characteristics," Plasma Processes and Polymers, 8(5), pp. 373–385.

[132] Iriyama Y., and Noda M., 1998, "Plasma polymerization of fluoromethanes," Journal of Polymer Science Part A: Polymer Chemistry, 36(12), pp. 2043–2050.

[133] Foroughi Mobarakeh L., Jafari R., and Farzaneh M., 2011, "Superhydrophobic Surface Elaboration Using Plasma Polymerization of Hexamethyldisiloxane (HMDSO)," Advanced Materials Research, 409, pp. 783–787.

[134] Gustafsson S., 2011, "Corrosion properties of aluminium alloys and surface treated alloys in tap water treated alloys in tap water."

[135] Madaeni S. S., and Ghaemi N., 2007, "Transformation of a hydrophilic membrane into semi-super-hydrophobic based on self-assembly of stearic acid monolayer over induced nanostructures on the membrane surface," Applied Surface Science, 254(2), pp. 627–632.

[136] Cho J.-S., Kim K.-H., Han S., Beag Y.-W., and Koh S.-K., 2003, "Hydrophilic surface formation on polymers by ion-assisted reaction," Progress in Organic Coatings, 48(2-4), pp. 251–258.

[137] Rider A., and Arnott D., 2000, "Boiling water and silane pre-treatment of aluminium alloys for durable adhesive bonding," International Journal of Adhesion and Adhesives, 20(3), pp. 209–220.

[138] Jafari R., Tatoulian M., Morscheidt W., and Arefi-Khonsari F., 2006, "Stable plasma polymerized acrylic acid coating deposited on polyethylene (PE) films in a low frequency discharge (70 kHz)," Reactive & Functional Polymers, 66(12), pp. 1757–1765.

[139] Gandhiraman R. P., Muniyappa M. K., Dudek M., Coyle C., Volcke C., Killard A. J., Burham P., Daniels S., Barron N., Clynes M., and Cameron D. C., 2010, "Interaction of

Plasma Deposited HMDSO-Based Coatings with Fibrinogen and Human Blood Plasma: The Correlation between Bulk Plasma, Surface Characteristics and Biomolecule Interaction," Plasma Processes and Polymers, 7(5), pp. 411–421.

[140] Fernandes J. C. S., Ferreira M. G. S., Haddow D. B., Goruppa A., Short R., and Dixon D. G., 2002, "Plasma-polymerised coatings used as pre-treatment for aluminium alloys," Surface & Coatings Technology, 154(1), pp. 8–13.

[141] Barbier V., Tatoulian M., Li H., Arefi-Khonsari F., Ajdari A., and Tabeling P., 2006, "Stable modification of PDMS surface properties by plasma polymerization: application to the formation of double emulsions in microfluidic systems.," Langmuir : the ACS journal of surfaces and colloids, 22(12), pp. 5230–2.

[142] "http://chemed.chem.wisc.edu/chempaths/GenChem-Textbook/Fats-and-Lipids-706.html."

[143] Ye J., Yin Q., and Zhou Y., 2009, "Superhydrophilicity of anodic aluminum oxide films: From 'honeycomb' to 'bird's nest'," Thin Solid Films, 517(21), pp. 6012–6015.

[144] Laguardia L., Ricci D., Vassallo E., Cremona A., Mesto E., Grezzi F., and Dellera F., 2007, "Deposition of super-hydrophobic and oleophobic fluorocarbon films in radio frequency glow discharges," Macromolecular Symposia, 247, pp. 295–302.

[145] Yang Y.-S., Huang W., and Huang W.-Y., 2011, "Mechanical and hydrophobic properties of chromium carbide films via a multi-objective optimization approach," Thin Solid Films, 519(15), pp. 4899–4905.

[146] Hegemann D., Hossain M. M., Körner E., and Balazs D. J., 2007, "Macroscopic Description of Plasma Polymerization," Plasma Processes and Polymers, 4(3), pp. 229–238.

[147] Hegemann D., Brunner H., and Oehr C., 2001, "Deposition rate and three-dimensional uniformity of RF plasma deposited SiOx films," Surface and Coatings Technology, 142-144, pp. 849–855.

[148] Huang L., Lau S. P., Yang H. Y., Leong E. S. P., Yu S. F., and Prawer S., 2005, "Stable superhydrophobic surface via carbon nanotubes coated with a ZnO thin film.," The journal of physical chemistry. B, 109(16), pp. 7746–8.

[149] Ishizaki T., Lee S., and Teshima K., 2010, "High Functionalization of Magnesium Alloy Surface by Superhydrophobic Treatment."

[150] Zheng L., Li Z., Bourdo S., Khedir K. R., Asar M. P., Ryerson C. C., and Biris A.

S., 2011, "Exceptional superhydrophobicity and low velocity impact icephobicity of acetone-functionalized carbon nanotube films.," Langmuir : the ACS journal of surfaces and colloids, 27(16), pp. 9936–43.

[151] Nwankire C. E., Favaro G., Duong Q.-H., and Dowling D. P., 2011, "Enhancing the Mechanical Properties of Superhydrophobic Atmospheric Pressure Plasma Deposited Siloxane Coatings," Plasma Processes and Polymers, 8(4), pp. 305–315.

[152] Petrenko V. F., and Peng S., 2003, "Reduction of ice adhesion to metal by using self-assembling monolayers (SAMs)," Canadian Journal of Physics, 81(1-2), pp. 387–393.

[153] Kumar B. R., and Rao T. S., 2012, "AFM studies on surface morphology, topography and texture of nanostructured zinc aluminum oxide thin films," Digest Journal of Nanomaterials and Biostructures Vol., 7(4), pp. 1881–1889.

[154] Pham H., ed., 2006, Engineering Statistical Handbook, Springer London.

[155] Lommatzsch U., and Ihde J., 2009, "Plasma Polymerization of HMDSO with an Atmospheric Pressure Plasma Jet for Corrosion Protection of Aluminum and Low-Adhesion Surfaces," Plasma Processes and Polymers, 6(10), pp. 642–648.

[156] Morent R., De Geyter N., Van Vlierberghe S., Dubruel P., Leys C., and Schacht E., 2009, "Organic-inorganic behaviour of HMDSO films plasma-polymerized at atmospheric pressure ," Surface and Coatings Technology, - 203(- 10-11), pp. 1366–1372.

[157] Barreto M. C., Borris J., Thomas M., Hänsel R., Stoll M., and Klages C.-P., 2012, "Reduction of Plasticizer Leaching from PVC by Barrier Coatings Deposited Using DBD Processes at Atmospheric Pressure," Plasma Processes and Polymers, 9(11-12), pp. 1208–1214.

[158] Xu X. H., Zhang Z. Z., Yang J., and Zhu X., 2011, "Study of the corrosion resistance and loading capacity of superhydrophobic meshes fabricated by spraying method," Colloids and Surfaces A: Physicochemical and Engineering Aspects, 377(1-3), pp. 70–75.